LYMPHATIC FLUID MECHANICS: AN IN SITU AND COMPUTATIONAL ANALYSIS OF LYMPH FLOW

A Dissertation

by

ELAHEH RAHBAR

Submitted to the Office of Graduate Studies of
Texas A&M University
in partial fulfillment of the requirements for the degree of

DOCTOR OF PHILOSOPHY

August 2011

Major Subject: Biomedical Engineering

Lymphatic Fluid Mechanics: An In Situ and Computational Analysis of Lymph Flow

LYMPHATIC FLUID MECHANICS: AN IN SITU AND COMPUTATIONAL ANALYSIS OF LYMPH FLOW

A Dissertation

by

ELAHEH RAHBAR

Submitted to the Office of Graduate Studies of
Texas A&M University
in partial fulfillment of the requirements for the degree of

DOCTOR OF PHILOSOPHY

Approved by:

Chair of Committee,	James E. Moore Jr.
Committee Members,	David C. Zawieja
	Gerard L. Coté
	Wonmuk Hwang
Head of Department,	Gerard L. Coté

August 2011

Major Subject: Biomedical Engineering

ABSTRACT

Lymphatic Fluid Mechanics: An In Situ and Computational Analysis of Lymph Flow.

(August 2011)

Elaheh Rahbar, B.S., Michigan State University

Chair of Advisory Committee: Dr. James E. Moore Jr.

The lymphatic system is an extensive vascular network responsible for the transport of fluid, immune cells, proteins and lipids. It is composed of thin-walled vessels, valves, nodes and ducts, which work together to collect fluid, approximately 4 L/day, from the interstitium transporting it back to the systemic network via the great veins. The failure to transport lymph fluid results in a number of disorders and diseases. Lymphedema, for example, is a pathology characterized by the retention of fluid in limbs creating extreme discomfort, reduced mobility and impaired immunity. In general, there are two types of edema: primary edema, being those cases that are inherited (i.e. genetic predisposition), and secondary edema, which develop post-trauma or injury of the lymphatic vessels. With the onset of breast cancer and radiation therapies, the prevalence of secondary edema is on the rise. Clinical studies show that up to 80% of women who undergo nodal-dissection surgery develop lymphedema in their arms within 3-5 years of the surgery. Unfortunately, there is no cure or remedy for lymphedema stemming from our lack of understanding of the lymphatic system.

The goal of this study is to evaluate lymph flow both experimentally and analytically to better understand the mechanisms regulating lymph transport. In particular we investigate the effects of pressure, volume loads and valve resistance on lymphatic function in the rat mesentery. Our experimental results are then used to develop computational and constitutive models to emulate the dynamic behavior of lymph transport. Collectively, the data illustrate the mechanics of lymphatic contractility and lymph flow. In particular, lymph flow and pumping significantly increase post edemagenic stress in the rat model. Furthermore, lymphangions exhibit highly nonlinear pressure-diameter responses at low pressures between 3-5 cmH_2O. These experimental results strongly suggest the regulation of lymph flow via changes in pressure, shear stress and vessel diameter. Furthermore, the computational and constitutive models from this study provide great insight into lymphatic function characterizing the mechanical properties of a single pumping unit (i.e. lymphangion). These models serve as valuable tools to further lymphatic research.

DEDICATION

To my parents and extended family who have loved and supported me from afar

ACKNOWLEDGEMENTS

This Ph.D. has taken me on an incredible journey and I have many people to thank for the lessons I have learned and my growth as an individual. First and foremost, I would like to thank my family for their endless support and encouragement over the years and instilling the belief that you can achieve anything with persistence and hard work. I would especially like to thank my dad for inspiring me to pursue a career in academia and research and my mom for her patience and positive outlook on life; she has now supported two "Rahbars" through their taxing doctoral years.

I would like to express my deepest gratitude to my advisor, Dr. James E. Moore, Jr. who has been a great mentor and friend. I first met Dr. Moore in the summer of 2004 as an undergraduate research intern and was quickly impressed by the amount of work he entrusted to me. Needless to say I learned a lot that summer about engineering and research. He continued to guide me and convinced me to return to Texas A&M University as a Ph.D. student. It has been truly an honor and privilege to work for Dr. Moore and I am indebted to him for believing in me and pushing me to new heights during this challenging doctoral project. A special thanks goes out to his wife, Peggy, for treating me as a member of her extended family in College Station.

I also owe a sincerest thanks to Dr. David C. Zawieja at the Texas A&M Health Science Center who has been an incredible mentor throughout my graduate studies. I never thought I could work with animals, let alone perform surgeries on rats. Working in his lab has made me more appreciative of experimental biologists and has made me a

stronger researcher by gaining valuable skills with respect to animal preparations. Above all, he taught me the true fundamentals of experimental research and lymphatic biology and for that I am grateful. In addition, I would like to thank members of his department for their gracious support. These include: Dr. Anatoliy Gashev, Dr. Mariappan Muthuchammy, Dr. Wei Wang, Dr. Zhanna Nepiyushchikh, Dr. Sanjukta Chakraborty, Dr. Eric Bridenbaugh, Dr. Patrick Dougherty, Dr. Andrea Foskett, Dr. Olga Gasheva, and Scott Zawieja.

I want to thank and acknowledge the rest of my committee members (Dr. Gerard L. Coté and Dr. Wonmuk Hwang) for their guidance and critical insight on the work presented herein. In particular, I would like to acknowledge the significant contributions of Dr. Coté's student, Tony Akl, who aided in the optimization of the image acquisition and processing algorithm for my experimental data.

Additionally, I am very appreciative of my collaborators who have aided in my research endeavors and provided thoughtful insights of the research field. Dr. Daisuke Mori assisted me in my first project at Texas A&M University on vena cava filters; Dr. Duncan Maitland provided access to StarCCM+, commercial CFD software, which aided the development of my computational model for lymph flow and Dr. Michael Davis hosted me in Missouri where we engaged in long days running experiments and had in-depth discussions over methods of characterizing lymphatic valves.

Many thanks go to the biomedical engineering department staff that took care of my finances, paperwork and computer issues at Texas A&M. I would also like to extend

my gratitude to the National Science Foundation for awarding me a three-year fellowship to support me during my graduate studies.

Last but not least, I'd like to thank my boyfriend, José Franck Diaz, for his continuous support in completing this work. He has been the voice of reason and source of calmness when I wanted to throw something at the computer! I am grateful for his patience and keeping me motivated to do my best work; he has definitely given me renewed strength and purpose in life. I feel blessed to have him and know that I could not have finished this work without his love and devotion.

Finally, I would like to thank my former and current peers whom I have had the pleasure of working with and learning from, both in and out of the lab. Thanks also go to my friends and roommates for making my time at Texas A&M an unforgettable experience. In no particular order: William Richardson, Dr. Lucas Timmins, Dr. Clark Meyer, Dr. João Silva Soares, Shiva Bozorgchami, Rebecca Dahlin, Beth Placette, Andrew Peters, Ryan Bishop, John Wilson, Jon Weimer, Hallie Wagner, Dr. Arturo Valentin, Dr. Ryan Pedrigi, Alex Abraham, Dr. Jason Hirshburg, Holly Gibbs, Po-Feng Lee, Benjamin Hughes, James Monroe, Veronica Vasquez, and Roxana Naderi. Thank you all for taking this journey with me!

NOMENCLATURE

APSS	Albumin physiologic saline solution
CFD	Computational fluid dynamics
C:E	Collagen:Elastin Ratio
Dd	Diastolic diameter
Ds	Systolic diameter
EC	Endothelial cell
eNOS	Endothelial nitric oxide synthase
f	Frequency
GMP	Guanosine monophosphate
KPSS	Potassium physiologic saline solution
MLC	Myosin light chain
MW	Molecular weight
NLOM	Nonlinear optical microscopy
NO	Nitric oxide
P	Pressure
PBS	Phosphate buffered solution
PSS	Physiologic saline solution
Q	Flow rate
RBC	Red blood cell
Re	Reynolds Number

SMC	Smooth muscle cell
T	Time period
v	Velocity
WSS	Wall shear stress

TABLE OF CONTENTS

CHAPTER Page

LIST OF FIGURES

FIGURE Page

LIST OF TABLES

CHAPTER I

INTRODUCTION: THE LYMPHATIC SYSTEM AND A HISTORICAL REVIEW OF COMPUTATIONAL MODELING

The Lymphatic System

The lymphatic system is an extensive vascular network responsible for the transport of fluid, namely lymph, from the interstitial tissue beds to the venous circulation. It also includes a number of lymphoid organs such as the lymph nodes, tonsils, Peyer's patches, spleen, and thymus. Lymphatic vessels are generally not present in avascular structures such as the epidermis, hair, nails, cartilage, and cornea, nor are they present in the brain or retina (Oliver, 2004). The system has two dumping sites, the left and right lymph ducts which drain into their respective subclavian veins, as illustrated in Figure 1.1. The right duct is much smaller, collecting fluid only from the head, neck, thorax and right arm. The left lymph duct, or better known as the thoracic duct, collects lymph from the rest of the body. All together, the network transports approximately 4-6 liters of fluid per day. In addition to fluid circulation, the lymphatics are intimately involved in macromolecular homeostasis, lipid absorption, metastasis, and immune function (Zawieja et al., 2011). All of these functions rely on the generation and regulation of lymph flow. An impaired or dysfunctional lymphatic system can pose serious health problems, such as lymphedema, filariasis, elephantiasis, lymphangitis, ly-

---

This dissertation follows the style of the Journal of Biomechanics.

-mphangioma, and cancer metastasis (Rockson, 2006; Rockson, 2008; Rockson, 2010; Szuba and Rockson, 1998). These lymphatic maladies are a consequence of genetic mutations, developmental malformations, post-surgery insults, and damage from radiation therapies. Lymphedema, in particular, results from the accumulation of lymph in the interstitial tissue bed resulting in the swelling of the affected tissues. With the prevalence of cancer and nodal dissection surgeries on the rise, lymphedema is becoming a growing concern; up to 25-50% of patients who undergo nodal dissection experience some level of lymphedema (Rockson, 2006; Rockson, 2008; Rockson, 2010; Stanton et al., 2009; Szuba and Rockson, 1998). However, there is a lack of treatments for these lymphatic diseases. This is primarily due to our rudimentary knowledge of the lymphatic system and its basic function.

The first documented study of the lymphatic system was performed by Italian physician Gasparo Aselli in the early 17th century. He identified lymphatic vessels in the intestines of dogs and called them “venae alba et lactea”, which translates to “the milky white veins” or better known as “lacteals” (Aselli, 1627). This was followed by the investigations of Jean Pecquet, Olaus Rudbeck and Thomas Bartholin who published complete descriptions of the lymphatic system in animals and humans, from 1650-1653 (Barrowman, 1978). About a century later, these anatomical investigations were translated to understanding lymphatic function. The works of John Hunter from 1758-1759 proved the absorption of intestinal contents into the lacteals (Hunter, 1837). He further demonstrated the network of lymphangions connected to lymph nodes by injecting mercury into lymphatic vessels; a specimen of a breast injected with mercury

can be found at the Hunterian Museum (Pathological Series No. K 481.1) (Nohl-Oser, 1972). Despite these early findings, lymphatic investigations did not really take off until the 20th century resulting in a great disparity between our understanding of the blood and lymph vasculatures.

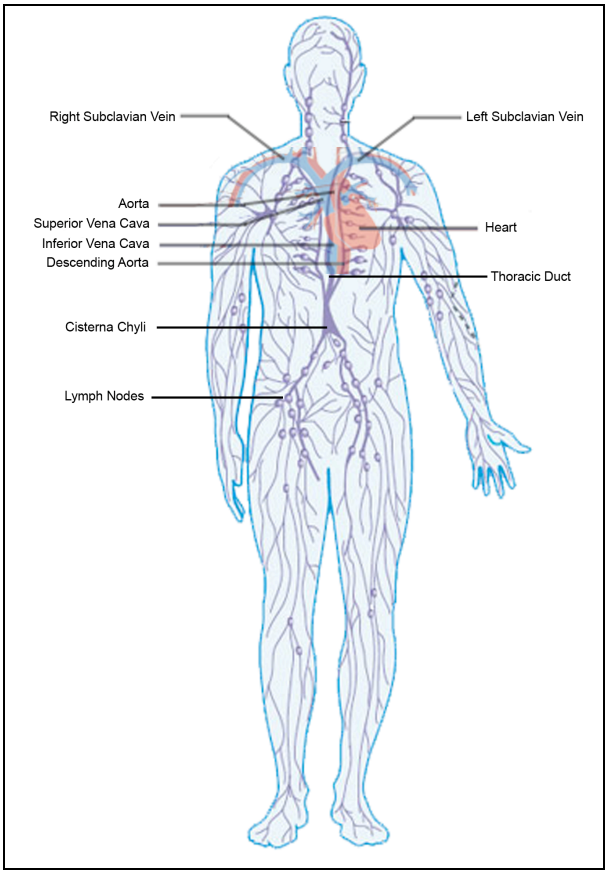

Figure 1.1. Illustration of the lymphatic system. Adapted from Brown (2005).

The 20th century was the beginning of in-depth analysis of the lymphatic system, both for the discovery of lymphatic origin and assessment of lymphatic behavior. The blood vasculature is the first functional network formed during embryonic development.

In vertebrates, the lymphatic vasculature develops in parallel, but secondary to the blood vascular system (Oliver, 2004; Oliver and Alitalo, 2005). In 1902, Florence Sabin proposed a model for lymphatic development suggesting that lymphatic vessels had a venous origin based on her investigations with pig embryos. She injected dye into pig embryos and observed endothelial cells (EC) bud from veins to form isolated primary lymphatic sacs. From these primary sacs, budding cells would then, centrifugally sprout towards the periphery, forming capillaries in the surrounding tissues and organs (Sabin, 1902; Sabin, 1904; Sabin, 1913). In 1910, Huntington and McClure proposed an alternative model for lymphangiogenesis, suggesting that the initial lymph sacs arise in the mesenchyme, independent of the venous system, and subsequently establish venous connections as they sprout (Huntington and McClure, 1910). Recent work, however, has supported Sabin's model for lymphangiogenesis and there continues to be a tremendous effort to advance our knowledge of lymphatic development, specifically in identifying lymphatic markers, genes and signaling proteins that regulate lymphangiogenesis (Oliver, 2004; Oliver and Alitalo, 2005).

In addition to the research on lymphatic development, a number of studies were conducted to evaluate structural and functional characteristics of lymphatic vessels. Structurally, the system is composed of initial lymphatics, collecting lymphatics, valves, nodes, and collecting ducts. The initial lymphatics, also referred to as terminal lymphatics or lymphatic capillaries, are the most distal structures of the lymphatic system. They are typically blind-ended tubes that anastomose with other initial or collecting lymphatics (Casley-Smith and Florey, 1961; Zawieja et al. 2011). The vessels

are thin-walled, comprised of a single layer of non-fenestrated endothelial cells, which have cytoplasmic extensions that overlap at the cell junctions (Casley-Smith, 1968; Azzali and Arcari, 2000; Zawieja et al., 2011). The vessels lack smooth muscle cells or pericytes and possess an incomplete basement membrane. These loose junctions allow for the absorption of lymph, white blood cells and proteins from the interstitial space into the lymphatic vessel (Casley-Smith and Florey, 1961; Casley-Smith, 1972; Zawieja et al. 2011).

There are two proposed mechanisms for the formation and uptake of lymph; namely the hydrostatic and oncotic theories, which are both based on Starling's principle of fluid exchange (Levick, 2003). The oncotic mechanism, proposed by Casley-Smith, relies on a protein concentration gradient between the interstitium and initial lymphatic (Casley-Smith, 1972). In general, the normal selective permeability of the capillaries affects protein concentrations in lymph, although typically lymph has protein concentrations lower than that of serum. Therefore, for the oncotic mechanism to hold true, a significant dilution of interstitial fluid (50-70%) is necessary so that the oncotic pressure differential is greater than the hydrostatic pressure differential. During lymphatic relaxation the protein concentration in the initial lymphatic would have to be up to three times greater than the protein concentration in the interstitium to allow interstitial fluid to enter the initial lymphatic through the open intercellular junctions. However, physiological evidence supporting this theory is minimal.

On the other hand, the hydrostatic mechanism for lymph formation has received more physiologic evidence. The hydrostatic theory claims that hydrostatic pressure

differences between the interstitium and the lumen of the initial lymphatic are responsible for lymph formation. Normally, the interstitial space has an average pressure near zero or can be slightly negative with respect to atmospheric pressure, and most initial lymphatics have positive pressures, so at first glance, the net pressure gradient is not in favor of lymph formation. However, recent work has revealed the presence of transient pressure gradients causing the untethered inner endothelial cells to deflect while the outer cells remain fixed, thereby allowing fluid and particles to move into the vessel lumen as illustrated in Figure 1.2 (Mendoza and Schmid-Schonbein, 2003). This behavior of the endothelial cells in the primary lymphatics is described as a primary valve allowing lymph to enter the lymphatic network. Recent work by various research groups has provided strong and growing support for the hydrostatic pressure theory and the role of these primary valves in lymph formation (Galie and Spilker, 2009; Mendoza and Schmid-Schonbein, 2003; Negrini et al., 1994; Negrini et al., 1999; Negrini et al., 2004).

Once lymph has entered the lymphatic system it must be transported a long distance “uphill” towards the dumping site in the subclavian veins. Unlike the cardiovascular system where the heart serves as the central pumping source for blood flow; the lymphatics have two types of lymph pumps namely, the intrinsic and extrinsic pumps. The intrinsic pump refers to individual lymphangions, which have the ability to contract and propel fluid forward. A lymphangion is defined to be the functional unit of a lymphatic vessel between consecutive valves. Since these vessels must pump and serve as conduits for flow, they have characteristics similar to the heart and blood vessels.

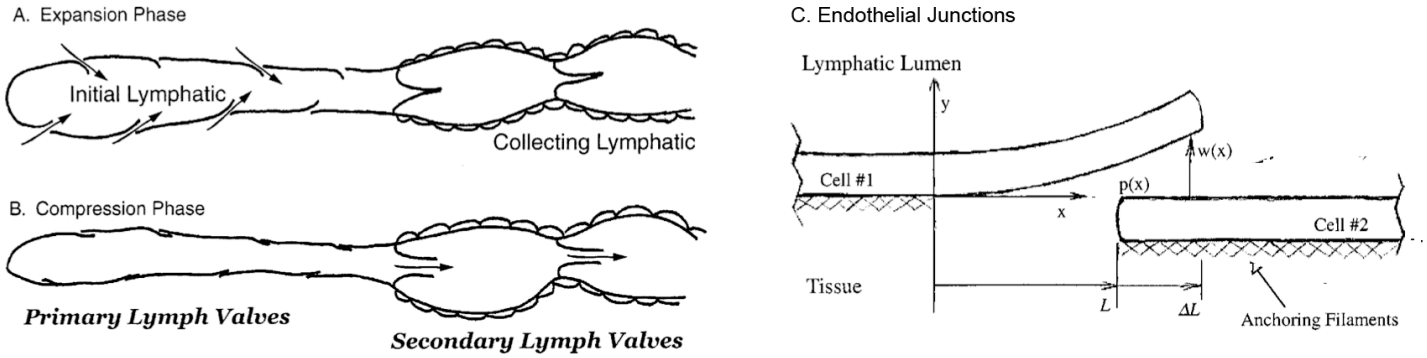

Figure 1.2. Initial lymphatics and primary valves. A) Drawings of initial and collecting lymphatics during the expansion phase. Primary valves are open and secondary valves are closed. B) During the compression phase, primary valves close and secondary valves are open to facilitate lymph flow. C) A schematic of the primary valves (i.e. loose endothelial junctions). (Mendoza and Schmid-Schonbein, 2003).

Anatomically, the vessels have three layers: a monolayer of endothelial cells surrounded by the basement membrane (intima), one to three layers of smooth muscle cells with collagen and elastin fibers (media) and a layer of connective tissue with fibroblasts and nerves (adventitia) (Yoffey and Courtice, 1970; Zawieja et al., 2011). Additionally, pacemaker cells have been shown to be present in the muscular walls but their exact location within the layers remains unknown (Gashev, 2002). In terms of pumping, these vessels exhibit phasic (rapid, brisk) and tonic (slow, long-lasting) contractions; with normal contraction frequencies of 4-5 per minute. Coordinated phasic contractions are initiated by the pacemaker activity and result in the depolarization and spread of action potentials from one cell to the next along the lymphangion producing an increase in intracellular calcium thereby causing the contraction of smooth muscle cells (Gashev, 2002; Zawieja, 2009). The contraction continues to propagate from one lymphangion to the next and causes a pulse in lymph flow. Numerous studies have shown the propagation of peristaltic-like contractions along a series of lymphangions (Gashev et al., 2004; Gashev et al., 2007; Zawieja et al., 1993). In this manner, they pump fluid from one lymphangion to the next and the lymphatic valves prevent backflow. Most studies have illustrated synchronized contractions (although irregularities do exist) from one lymphangion to the next, but there remain uncertainties in our knowledge of the mechanisms regulating valve opening and closure. It is strongly believed that mechanical factors such as, changes in pressure and flow affect the pumping characteristics of a lymphangion; further investigations must be performed to elucidate these mechanisms.

The extrinsic pump refers to the external forces from the surrounding tissue, pulsating arterioles and skeletal muscle, which facilitate lymph flow. Thus, lymph flow in the lymphatics of the heart, gut wall and skeletal muscle are strongly regulated by the extrinsic pump. Furthermore, lymphatic tone tends to play a more crucial role in regulating lymph flow in areas where the extrinsic pump is more dominant. These tonic constrictions produce alterations in the outflow resistance and are often modulated by pressure, flow, neural, and humoral influences (Oliver, 2004; Zawieja et al., 2011). Recent studies have shown flow and shear may also influence lymphatic tone (Dixon et al., 2006). Altogether, lymph flow is modulated by the dynamic interplay between the intrinsic and extrinsic pumps.

Given that lymph flow is highly dynamic and potentially bi-directional, the lymphatic valves play a crucial role in the prevention of reverse flow throughout the network. There have been several anatomical investigations on lymphatic valves and most of them conclude that valves are bicuspid in nature and are fully lined with endothelial cells as shown in Figure 1.3 (Albertine et al., 1982). Moreover, the valve leaflets (i.e. semi-lunar cusps) are flexible and extend from the vessel wall along an arc, often funnel shaped. They have been shown to be composed predominantly of endothelial cells with some collagen fibrils and fibroblasts (Albertine et al. 1982; Skalak et al., 1984). Bannykh et al. (1995) showed that ostial valves had marginal thickenings and prominent buttresses anchoring the valve leaflets to the vessel wall. Additionally, the sinus bulb around the valve leaflets has been observed to be more distensible and lacking of smooth muscle cells compared to the rest of the lymphangion wall.

Altogether, valve and sinus structure contribute significantly to lymph flow regulation, however the literature remains limited in this area. Some studies speculate that small changes in viscous pressure gradients in the lumen result in larger pressure drops across the valve leaflets and thus aid in the closure of the valve. Clearly, more investigations are necessary to characterize lymphatic valves and their role in flow regulation.

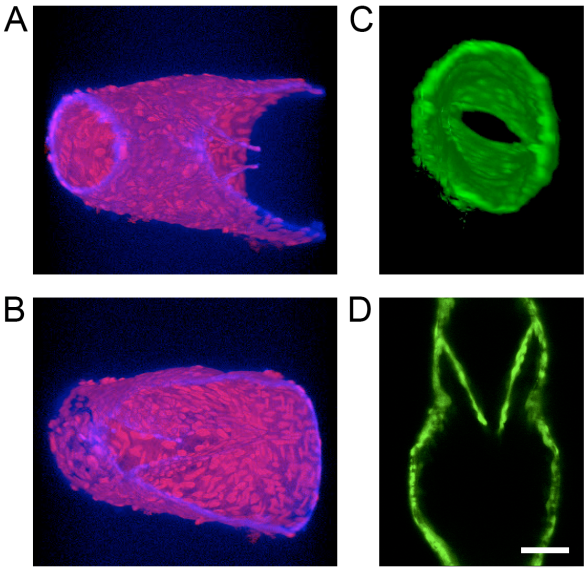

Figure 1.3. Confocal images of a lymphatic valve. A-B) Endothelial cells line the lymphatic vessel wall and valve leaflets. Cell nuclei stained red, cytoplasm stained blue. C) CellTracker Green was used to stain the lymphatic vessel. 3-D reconstruction shows the funnel shaped opening of the valve. D) Individual slice of lymphangion illustrating leaflets and sinus bulb region. Scale bar ~50 μm.

As the awareness of the lymphatic system continues to spread, more research is conducted in the field. There remain a lot of gaps in our knowledge of the basic functions and regulatory mechanisms dictating lymph flow, lymphatic contractility and valve function. New experimental and computational approaches must be adopted to

investigate these unknown processes.

History of Computational Modeling

Modeling of physiological systems became popular in the early 1970s. Models served as conceptual constructs, which allowed for numerous hypothesis testing and stimulated research. The power of mathematical models over experimental work gave the ability to predict unknown properties of a biological system. The models allowed for idealization of the physiologic process and isolation of sub-systems from the parent network. They were also, generally, less time consuming and inexpensive than their respective experimental setup. Many models for the arterial circulation were developed in the 1970s and these aided in improving designs for implantable devices to alleviate pathological conditions. Since then technology has grown tremendously and computational power has significantly increased. In fact, most recent computational frameworks tend towards multi-scale modeling where one mimics biological behavior at molecular, cellular, whole organ and network levels.

The first computational model for the lymphatic vasculature was developed in 1977 using the tools of continuum mechanics and lymphology (Reddy et al., 1977). The model consisted of 296 lymphangions, 15 organs and 1510 equations to be solved. Each lymphangion was a single computational node and the fluid mechanics were described by the Navier-Stokes equation. Given the assumption of laminar flow, the Navier-Stokes equation was reduced to Poiseuille flow. Results were simulated on a digital computer to yield pressure and flow patterns along the lymphatic network. The network model showed a weak dependence of the overall flow rate on the systolic and diastolic flow

rates, individually. However, when the contraction flow rate was assumed to depend on the degree of vessel distention during filling, the overall flow rate increased dramatically. Zweifach and Intaglietta (1968) summarized a model of the microcirculation that included terminal lymphatic vessels and highlighted the role of lymphatics on maintaining fluid balance. Fluid exchange was noted to depend heavily on lymphatic endothelial lining permeability. In a more elaborate model of microvascular networks, Pries et al. (2000) demonstrated the importance of wall shear stress in vessel-to-vessel communication under varying levels of tissue oxygenation. Furthermore, Mendoza and Schmid-Schonbein (2003) were the first to describe the mechanics of primary lymphatic valves and their relation to lymph formation. Their 1-D model illustrated the deflection of the loose endothelial cells when lymphatic pressure drops below interstitial fluid pressure allowing the entrance of lymph into the lumen of the initial lymphatics. The gaps consequently close upon the rise of lymphatic pressure to values greater than interstitial pressure. Since then, Galie and Spilker (2009) have further investigated lymph transport across these primary valves with a 2-D computational model that incorporates the porous nature of the interstitium. They observe attenuated cell deflections and flow rates for a given transmural pressure. While the modeling is more sophisticated, there is a lack of experimental data to support these new findings.

Considering a different approach, others have developed mathematical models which account for vessel resistance, inertial effects and compliance using a circuit-theory analog adapted from arterial flow models; each lymphangion is bounded by valves and inlet and outlet resistances are assumed (Macdonald et al., 2008; Stewart and

Laine, 2001; Quick et al., 2007). In particular, they have been able to describe the transition from “pump to conduit” behavior of lymphangions when the outlet pressures fall below inlet pressures with this model; and further observe that lymphatic contractions do not facilitate flow when vessels are in the “conduit” phase (Quick et al., 2007). Moreover, Venugopal et al. (2007) have investigated the coordination of contractile events on mean lymph flow. The model revealed that coordination of contractions did not significantly affect the average flow rate. In addition, contractile propagations in opposite directions had the similar effect on flow. This finding suggests that lymphangions operate individually and can independently adapt to local conditions. Similarly, MacDonald et al. (2008) investigated effects of wall compliance and contractile wave propagations on lymph flow. The model indicated that lymphangions would pump most efficiently when all sections of the wall contracted simultaneously, and there were minimal differences between forward and reverse propagating contractile waves. Alternatively, on a larger scale, Bertram et al. (2011) showed that sequential contractions in a short series chain of 5 lymphangions were more efficient than synchronized ones. The model presented by Bertram et al. (2011) is an oversimplified network of lymphangions and can be improved by performing experiments that will provide the necessary boundary conditions for a more physiologically relevant model. For example, experiments on isolated lymphatic vessels can be performed to characterize force-length and shear-dependent tension of lymphatic vessels and valve resistance. Elucidating such behaviors will aid in the development of better models.

While these models provide first order approximations of lymph flow and

lymphatic function, they do not take advantage of current computational capabilities. Furthermore, the assumption of Poiseuille flow in vessels that experience a dynamic range of diameters is concerning. A recent review by Grotberg and Jensen (2004) summarized the research on flexible tube artery models. Since the Reynolds number for flow in arteries is much higher (on the order of tens or hundreds) than in lymphangions (< 3) and arteries experience smaller changes in radius than lymphangions (which regularly undergo a 50% change in radius during the phasic contractile cycle), modeling techniques must be adapted for lymph flow. Blyth et al. (2003) combined theoretical/computational study of flow in pulsating cylindrical tubes with driven wall motion. The vessel radius was specified to vary as a function of time only. Additionally, a sinusoidal function for radius was specified, and solutions were pursued only for that special case. At low Reynolds number, flow was synchronous with wall motion whereas at higher Reynolds number (Re~650), a bifurcation takes place and chaotic oscillations were observed. The study, however, focused on chaotic behavior and not on small Reynolds number flows with large, arbitrary radius variations as encountered in lymphatics. Johnson et al. (1992) constructed a similar computational model of axisymmetric flow in a tube whose radius varied only with time in a sinusoidal manner. Pressure in the tube was assumed to vary only with axial position and time; an assumption that may not always be valid for flows in lymphatic vessels. Despite limiting the variation in radius to 20%, the wall motion had a strong influence on mean and peak values of wall shear rate and flow rate, relative to the rigid tube case. It was also noted that varying the phase relationship between pressure and wall motion had an effect on

the wall shear rate and flow rate. A study of terminal bronchial tube flow (Uchida and Aoki, 1977) allowed for finite variations in radius, but one end of the tube was assumed to be closed, with all fluid motion resulting from wall motion. This approach allowed for a semi-analytical similarity solution to be pursued. While flow in lymphatics is different than the models presented above, several potentially important flow phenomena were observed, including flow separation in expanding tubes at Reynolds number as low as 1.6. The results of these previous studies confirm the importance of accurately modeling wall deformations observed in lymphatics.

Moreover, appropriate modeling of wall deformation is crucial to understanding of the mechanical environment of lymphatic vessels. In particular, the production of nitric oxide (NO), a common vasodilator produced by endothelial cells, has been shown to depend on shear stress (Bohlen et al., 2009; Gasheva et al., 2006; Hagendoorn et al., 2004; Zawieja, 2009; Zawieja et al., 2011). Specifically, fluid shear stress activates endothelial nitric oxide synthase (eNOS) thereby increasing the production of NO, which diffuses into the smooth muscle activating soluble guanylate cyclase consequently forming cyclic guanosine monophosphate (GMP). Cyclic GMP stimulates protein kinase G followed by the phosphorylation of myosin light chain (MLC) phosphatase resulting in the dephosphorylation of MLC and ultimately relaxation of the smooth muscle. Hence, it is important develop a model that can incorporate this shear-dependent behavior of vessel diameter.

Additionally, we are not limited to simple geometries and can investigate the role of vessel geometry on flow patterns. This is important, particularly, for the modeling of

lymphatic valves. New imaging modalities such as fast scan confocal microscopy allow us to generate dynamic, realistic geometries of lymphangions which can then be converted into computational domains for 4-D computational flow models.

In summary, computational modeling has reached new heights and with the growth of technology and imaging modalities, much more sophisticated modeling can be adopted to study the lymphatic vasculature.

Dissertation Synopsis

The dissertation presented herein can be split into two parts, both of which constitute efforts in the field of lymphatic biology and fluid mechanics. The first section (Chapters II – IV) presents work that discusses the fluid mechanics of lymph flow in rat mesenteric lymphatic vessels. In particular, the investigation of edemagenic stress via saline infusion on lymphatic function *in situ* (Chapter II), the assessment of microparticles as flow tracers for isolated lymphatic experiments (pressure controlled) *in vitro* (Chapter III), and the development of a computational flow model for a lymphangion using the results from the *in situ* experiments (Chapter IV) are presented. Collectively, these works provide insight into the role of mechanical stimuli on lymphatic contractile function and regulation of lymph flow. The second section (Chapter V) characterizes passive properties and lymphatic structure at three axial locations along a lymphangion. Specifically, a constitutive model is developed to describe the passive pressure-diameter response of lymphatic vessels in terms of lymph flow regulation using a function of pressure and diameter, and correlate this behavior with the microstructure of the vessel using nonlinear optical microscopy techniques. The

results from this dissertation will greatly enhance our understanding of lymphatic behavior and will serve as the platform for future computational and multi-scale modeling of lymph flow regulation and lymphatic contractility in the lymphatic system.

CHAPTER II

LYMPH TRANSPORT IN RAT MESENTERIC LYMPHATICS EXPERIENCING EDEMAGENIC STRESS

Overview

Lymphedema has become a growing concern with the prevalence of breast cancer and nodal dissection surgeries. The goal of this study was to assess lymphatic system adaptations to increased fluid-volume loads *in situ*. Twelve rats were infused with saline at a rate of 0.2 mL/min/100g body weight via the femoral vein to induce edemagenic stress. We measured mesenteric lymphatic vessel diameter, lymphocyte velocity, lymphocyte density, and contraction frequency before, during and after saline infusion using an intravital microscope. Longitudinal statistical analysis was performed to evaluate significant changes over time (α=0.05). A ten, and six-fold increase in lymph velocity (0.1-1 mm/s) and flow rate (0.1-0.6 μL/min), were observed post-infusion, respectively (p-value<0.05). There were also statistically significant increases in contraction frequency and fractional pump flow 1-minute post-infusion (p-value<0.05). Time-averaged wall shear stress values increased 10X post-infusion to nearly 1.5 dynes/cm^2 (p-value<0.05). Similarly, maximum shear stress rose from 5 dynes/cm^2 to 40 dynes/cm^2. Mesenteric lymphatic vessel diameter, however, did not change significantly over the duration of the experiment. Lymphatic vessels adapted to edemagenic stress by increasing lymph transport. Specifically, increases in lymphatic contraction frequency, lymph velocity, and shear stress were statistically significant. Although the changes in

lymphatic diameter were not statistically significant, lymph pumping increased post-infusion. These results suggest that edemagenic conditions stimulate lymph transport via increases in lymphatic contraction frequency, lymph velocity and flow. These changes, consequently, resulted in large increases in wall shear stress, which will activate NO pathways and modulate lymphatic transport function.

Introduction

The lymphatic system transports fluid from the interstitium through a series of valves, nodes and pre- and post-nodal ducts that eventually empty into the great veins of the thorax at the juncture of the subclavian and internal jugular veins. This system is a key component in fluid balance, macromolecular homeostasis, lipid absorption, and immune function. All of these functions rely on the generation and regulation of lymph flow along the collecting lymphatic vessels. Therefore, in healthy individuals, there is a balance between the lymphatic load (i.e., the quantity of lymph produced/unit time) and the ability of the lymphatic vessels to transport lymph (Benoit et al., 1989; Levick, 2003; Rockson, 2006; Rockson 2010; Zawieja et al., 2011). An imbalance between load and transport capacity results in the accumulation of fluid in the interstitial tissue compartment, commonly known as lymphedema. Lymphedema occurs with a pathological increased in load, impaired lymphatic vasculature (either anatomically or functionally deranged), or in situations where there is a relative distortion of both factors (Rockson, 2006; Rockson, 2010). Edema has become a growing concern amongst breast cancer patients; up to 25% of women develop lymphedema in their arms within 3 years of nodal dissection surgery (Rockson, 2006; Rockson, 2010; Stanton et al., 2009).

Chronically, in addition to fluid accumulation, there is an increase in protein concentration, inflammation, recurrent infection, fibrosis and adipose content which causes pain, swelling and immobility for the individual. Despite widespread recognition of these serious health problems, there is a poor understanding of the mechanisms involved and a lack of effective treatments for lymphedema.

Lymph formation occurs in the interstitium; when water, solutes, and plasma proteins escape from the blood capillaries into the interstitial compartment. Flow across the capillary wall is a process of plasma ultrafiltration through a semi-permeable membrane. The primary driving force for ultrafiltration is capillary blood pressure (P_c), whereas the oncotic pressure of plasma proteins (π_p) opposes filtration. Starling's principle for fluid exchange states that the rate and direction of fluid movement across any particular segment of capillary wall depends on the local hydraulic pressure difference across the wall minus the opposing colloid oncotic pressure difference as shown by Equation 1, below (Levick, 2003; Renkin, 1986).

$$J_v = K_f\left(\left[P_c - P_i\right] - \sigma\left[\pi_p - \pi_i\right]\right) \qquad \text{(Equation 2.1)}$$

where, J_v is the volume flow across the capillary wall, K_f is the filtration coefficient for capillary wall, P_i is the interstitial fluid pressure, σ is oncotic reflection coefficient, and π_i is the colloid oncotic pressure of interstitial fluid.

While there is some debate on the exact mechanism regulating the transport of lymph into the initial lymphatics, it is generally believed that the average prevailing pressure gradient between the interstitial fluid and initial lymphatic changes periodically to allow lymph to enter the initial lymphatics (Schmid-Schonbein, 1990; Stanton et al.,

2009). In humans, approximately 4-8 liters of fluid is transported by the lymphatics per day (Olszewski, 2002). Thus, an imbalance between filtration and lymph drainage has the potential to cause edema relatively quickly. Once interstitial fluid enters the lymphatic system, it needs to be propelled "uphill" towards the return point in the great veins. Studies have shown that the lymphatic system relies on two pumps to transport lymph, namely the intrinsic and extrinsic pumps (Gashev, 2002; Gashev et al., 2007; Gashev, 2008; Zawieja et al., 1993; Zawieja, 2009; Zawieja et al., 2011). Collecting lymphangions, in particular, possess smooth muscle cells and therefore have the ability to contract intrinsically and actively pump lymph forward. The extrinsic pump refers to the pumping from contraction/relaxation cycles induced by adjacent structures acting upon the lymphatic (i.e. pulsating arteries, respiratory activities, GI peristalsis and skeletal muscle contractions). Conditions that are edemagenic will stimulate the lymph pump to increase its lymph transport (Benoit et al., 1989).

This study seeks to investigate lymphatic function under normal and edemagenic conditions in situ, using our previously established high speed imaging system (Akl et al., 2010; Dixon et al., 2006). Edemagenic stress will be induced by the administration of a saline infusion via the femoral vein in rats. This volume infusion will induce an increase in blood pressure, thereby increasing the pressure gradient across the capillary wall and resulting in an increased volume load on the initial lymphatics. We hypothesize that lymphatic vessels will accommodate the increased load by increasing one or more indicators of pumping function such as lymphatic diameter, lymph pump contraction frequency, lymph pump stroke volume and lymph flow rate. Thus, we propose to

quantify these quantities in rat mesenteric lymphatics under normal and edemagenic conditions.

Materials & Methods

Animals: Twelve male Sprague Dawley rats weighing 200-300 g were used for this study. All animals were housed in an environmentally controlled vivarium, approved by the American Association for Accreditation of Laboratory Animal Care, and allowed access to a standard pellet diet and water. Rats were fasted 15-20 hours before experimentation with water available ad libitum.

Surgical Preparation: The rats were anesthetized with intramuscular injections of fentanyl-droperidol (0.3 mL/kg) and diazepam (2.5 mg/kg). Supplemental doses of the anesthetic were provided as necessary. The right femoral vein was cannulated with PE-50 tubing for intravenous fluid (saline) administration. The cannula was connected to a syringe with a 23-gauge adapter. Saline (0.9% NaCl) was prepared and sterile filtered for all experiments. To prevent clotting of the cannula, 0.05 ml of heparin was diluted in 1 ml of saline and a small volume (0.1-0.5 ml) was perfused into the femoral vein. Once the cannula was firmly in place, the rat was transported to the preparation board. To gain access to the mesentery, a midline abdominal incision was made and a loop of small intestine was exteriorized. The mesentery was draped over a glass semi-circular viewing pedestal (12.5x25 mm), and with the aid of a dissecting microscope, a muscular collecting lymphatic was centered on the viewing pedestal. The exposed tissue was constantly suffused with warm albumin physiologic saline solution (in mM: 145.00 NaCl, 4.7 KCl, 2.0 $CaCl_2$, 1.17 $MgSO_4$, 1.2NaH_2PO_4 , 5.0 dextrose, 2.0 sodium

pyruvate, 0.02 EDTA, 3.0 MOPS, and 10 g/L bovine serum albumin). The solution was pre-warmed to 37°C and had the pH adjusted to 7.4. This suffusion prevented the lymphatic vessel and mesentery bed from drying up and further kept the animal's core and tissue temperature at 36-38°C for the entire duration of the experiment. In addition to monitoring body temperature, a pulse oximeter, attached to the rat's foot, was used to monitor blood oxygen levels and heart rate. The preparation was then transferred to a Zeiss intravital microscope for imaging.

Saline Infusion & Image Acquisition: Using a 80mm projective lens and 10x water immersion objective we were able to view the lymphatic vessels with a depth of field of approximately 14µm. The microscope was connected to a high resolution, high speed CCD camera (Phantom V5.2 1152x896,Vision Research Inc.) which captured images at 500 fps. The camera was triggered to capture a burst of 8 images at 500 fps then wait for 34 ms to take another burst of images (Akl et al., 2010). This allowed us to extend the imaging time to capture multiple contraction cycles. To extend the imaging time even further, the camera's field of view was reduced as much as possible to cover only the area occupied by the vessel during all times and to reduce the capture of unnecessary data. Data were recorded in intervals long enough to acquire at least 2 contractile cycles. Only lymphatics that exhibited spontaneous rhythmic contractile patterns were selected for this study. An initial acquisition was taken before any volume infusion at the beginning of the experiment to serve as the control. Thereby, we administered a slow constant perfusion of saline at 0.004 ml/min/100g body weight for 10 minutes using a syringe pump to account for insensible water loss that could affect lymph flow. This

flow rate has been estimated to be equal to the normal urine flow and respiratory water losses in rats (Benoit et al., 1989). Sequences of images were taken during this slow infusion (usually 1-2 sets). Once the slow infusion was stopped another brief acquisition was taken to ensure flow was normal. To induce hyperdynamic conditions, the infusion rate was increased to 0.2 ml/min/100g body weight for 10 minutes. This produces a significant hypotonic volume load, which we have shown in the past to increase lymph pumping (Benoit et al., 1989). Images were captured both during and after the high infusion, up to 25 minutes post fast infusion. In total, 7-12 sets of images were taken from each animal over the span of the entire experiment. Upon completion of the experiment, rats were euthanized with pentobarbital (120 mg/kg of body weight IP).

Image Processing: Images acquired from the experiments were processed with an in-house program, written in Matlab (version 2009b, MathWorks Inc. Natick, MA), to obtain values for lymphatic vessel diameter, lymphocyte velocity and lymphocyte density. Vessel diameter and lymphocyte velocities were continuously recorded using a correlation-based pattern-tracking algorithm described previously by Akl et al. (2010). Briefly, each set of 4 consecutive images were used to filter out background noise and create one image with enhanced particles to background contrast. Immune cells, presumably the majority of which are lymphocytes, in the filtered images were tracked to measure their velocity. Edge detection was used to measure vessel diameter, cell density and cell position. Lymphocyte density was calculated to ensure that we did not induce an inflammatory response. Further analysis involved calculating lymph pump contraction frequency, fractional pump flow, lymph flow rate, and wall shear stress from

the obtained velocity and diameter measurements, using general methods we used previously (Dixon et al., 2006).

Statistical Analysis: Data from the twelve rats were organized into eight time categories; namely, control (time=0, N=12), slow infusion (time=0-10 minutes experimental time, N=11), fast infusion (time=10-20 minutes experimental time, N=12), 1 minute post infusion (time = minute 21 experimental time, N=4), 3-5 minutes post infusion (time=23-25 minutes experimental time, N=11), 10-12 minutes post infusion (time=30-32 minutes experimental time, N=11), 13-19 minutes post infusion (time=33-39 minutes experimental time, N=6) and greater than 20 minutes post infusion (time >40 minutes experimental time, N=4). The shaded boxes and time axes in the figures represent these eight categories. All data are expressed as means ± standard error (SE). A generalized estimating equation (GEE) model, with compound symmetry covariance structure was used to compare each outcome variable to its respective control set, with a 95% confidence interval (α=0.05). This type of longitudinal analysis was chosen over repeated measures ANOVA due to its robustness in handling unequal sample sizes over time.

Results

Vessel Diameter: Average lymphatic diameter was greatest 13-19 minutes post infusion ($\bar{d}$=116.7 μm) but this increase in vessel diameter was not statistically significant. Diastolic diameters (D_d) ranged from 50-178 μm and systolic diameters (D_s) ranged from 20-169 μm throughout the experiment. When we normalized the data to the corresponding control diastolic diameter for each vessel, there was a slight increase in

diastolic diameter and decrease in systolic diameter both during fast infusion and one minute post infusion, but differences remained statistically insignificant (p-value >0.05) as shown in Figure 2.1a. There was a modest albeit non-significant increase in the normalized diastolic (~18%) and systolic (~35%) lymphatic diameters 13-19 minutes after infusion. However, it should be noted that p-value was lowest (p-value<0.1) during the last time point (i.e. >20 minutes post-infusion) for average diameter, diastolic diameter and systolic diameter suggesting that there could be a slight increase in vessel diameter at the end of the experiment. The pulse diameter (i.e. difference between diastolic and systolic diameter) began to increase and reached its maximum at one minute post infusion, but this increase was statistically insignificant (p-value = 0.453, Figure 2.1b). It is important to note that the standard deviation at each time point gradually increased as the mean pulse diameter increased meaning that there was a greater variation in the vessel diameter response to edemagenic stress, which may explain why statistical significance was not observed.

Lymphocyte Velocity and Flow Rate: Average lymphocyte velocity was 0.1 mm/s under control conditions and increased steadily upon administration of the fast saline infusion. Average velocity increased up to 10X and sustained velocities greater than 1 mm/s at 20 minutes post-infusion. Average lymph velocities increased throughout the entire infusion periods and were significantly higher at all time points following 3 minutes post-infusion (p-value<0.05, Figure 2.2). Similarly, changes in average flow rate were statistically significant at one minute post-infusion, 3-5 minutes post infusion, and 13-19 minutes post-infusion reaching a maximum value of 0.6 μL/min (p-value<0.05, Figure 2.2).

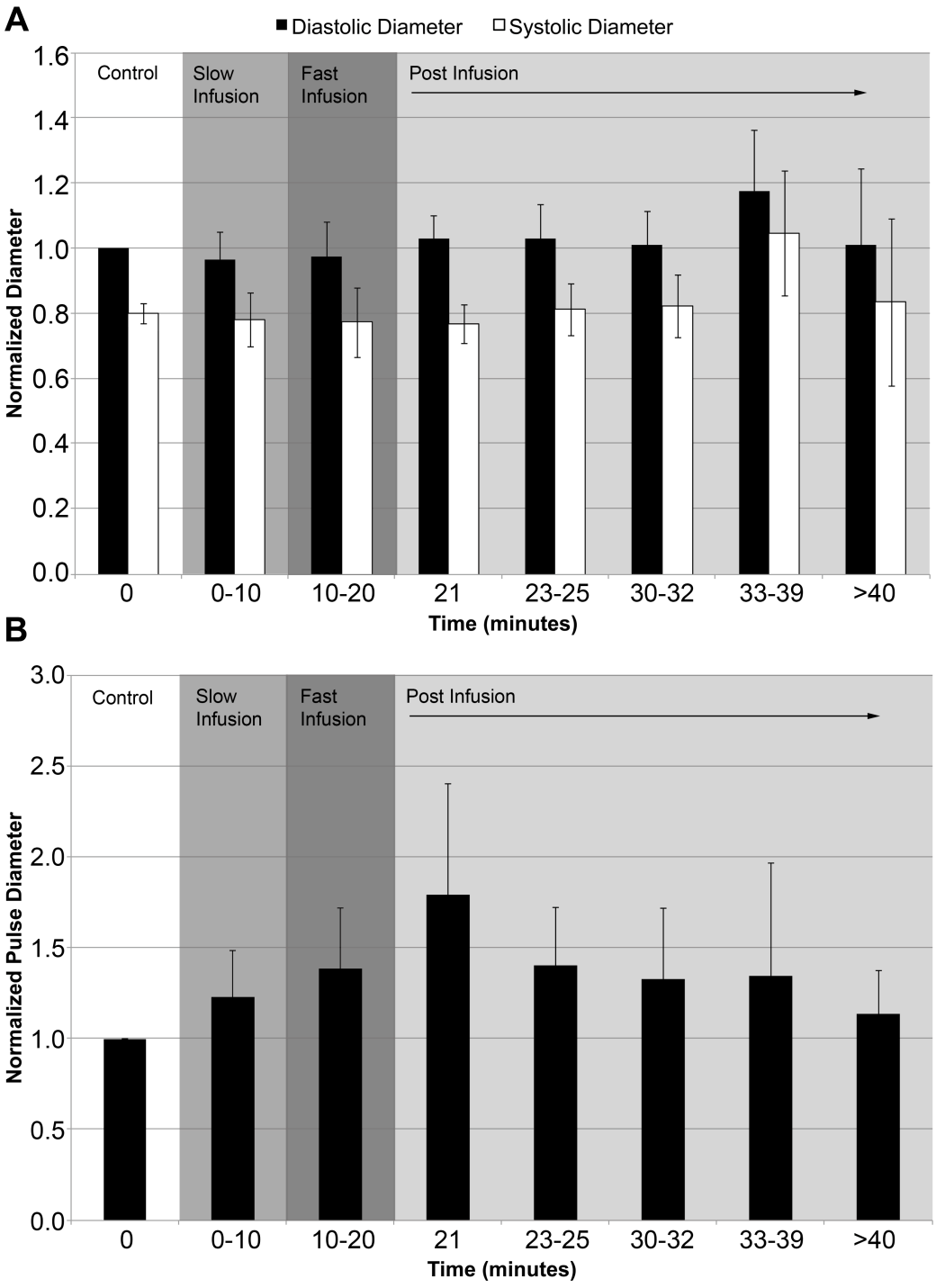

Figure 2.1. Plots of normalized Dd, Ds and pulse diameter. (A) Diastolic (black) and systolic (white) diameters were normalized to the control diastolic diameter. (B) Normalized pulse diameter over the entire duration of the experiment. Changes in diameter were not statistically significant (p-value>0.05).

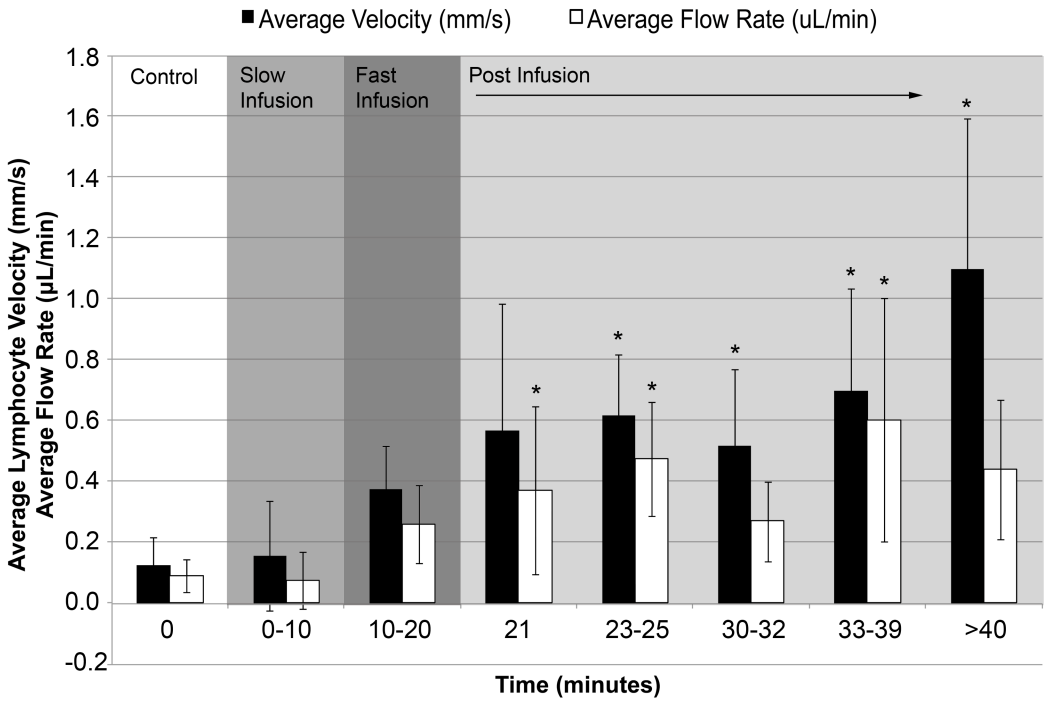

Figure 2.2. Plots of average lymphocyte velocity and flow rate. Average lymphocyte velocity and flow rate were measured throughout the experiment up to 50 minutes from the start of the experiment. Asterisks indicate a statistical increase compared to control values at time=0 (p-value<0.05).

Contraction Frequency and Fractional Pump Flow: There was over a 50% increase in contraction frequency at one-minute post infusion. In fact, contraction frequency significantly increased both during fast infusion and one minute post-infusion (p-value<0.05, Figure 2.3). Ejection fraction was determined from diastolic and systolic diameters and used to calculate fractional pump flow, which is defined as the product of ejection fraction and frequency. The data showed a significant increase in fractional pump flow during fast infusion, one-minute post infusion and 10-12 minutes post-infusion (Figure 2.3).

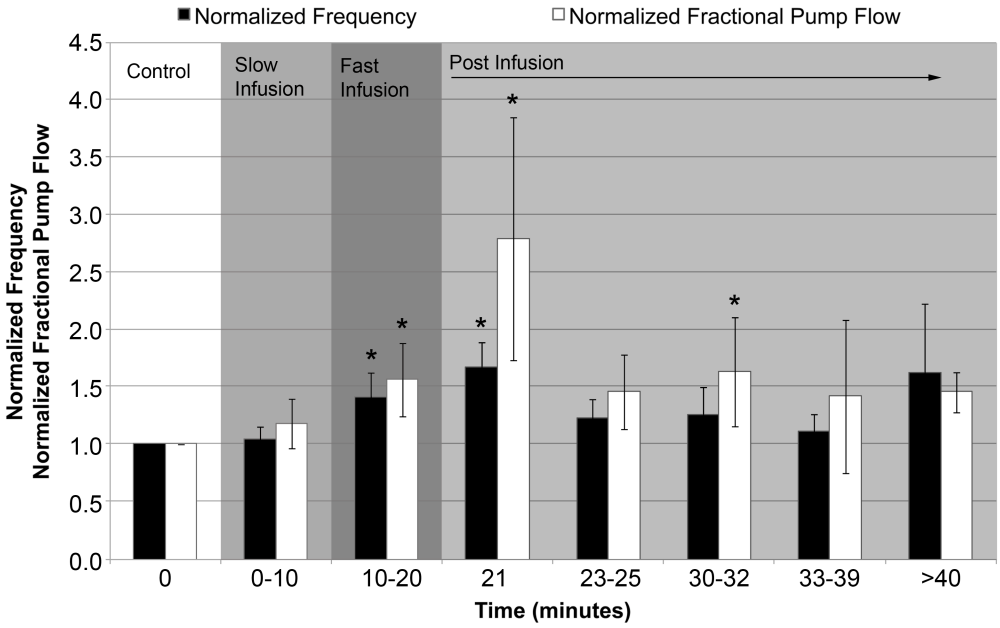

Figure 2.3. Plots of normalized contraction frequency and fractional pump flow. Contraction frequency and fractional pump flow were normalized to control values. Asterisks indicate a statistically significant increase in each parameter with respect to the control value at time=0 (p-value<0.05).

Wall Shear Stress: Average wall shear stress for control was 0.12 dynes/cm^2 with a maximum shear stress of 5 dynes/cm^2. As the experiment progressed, average wall shear stress increased by an order of magnitude to nearly 1.5 dynes/cm^2. The increases in average wall shear stress were statistically significant at all time points post-infusion with the exception of the 13-19 minute mark (Figure 2.4a). Maximum wall shear stress rose to 40 dynes/cm^2 during fast saline infusion; 8X higher than the control maximum value for shear stress. A larger increase (up to 13X) was observed at one minute post-infusion. Due to the large variation in maximum shear stress values amongst animals, we normalized the max shear stress with respect to the control value for max shear stress. There were statistically significant increases in normalized maximum wall shear stress

during fast infusion and one minute post-infusion (p-value <0.05, Figure 2.4b). Wall shear stress remained elevated at the end of the experiment.

Lymphocyte Density: To ensure that the saline infusion did not elicit an inflammatory response, we quantified cell density. Average cell density observed during our experiments was about 150,000 cells/mL. Our data shows that cell density decreased 15% from control over the duration of the experiment, which was expected, as the saline infusion would cause some dilution of the lymph. However this decrease in lymphocyte density was not statistically significant (p-value>0.05, Figure 2.5). Given that lymphocyte tracking is crucial to our velocity measurements, we captured high-speed video when the cells were observed, not continuously throughout the experiment. It is, therefore, possible that actual time averaged lymphocyte densities may be somewhat different than our reported values.

Discussion

The most common cause of lymphedema in the western world is the result of cancer surgery/therapies. With the prevalence of cancer and secondary lymphedema on the rise, characterizing lymphatic function and its response to an edemagenic stress is crucial to the understanding of these pathologies. Our knowledge of the mechanisms regulating transport of fluid and lymphatic contractility remains fairly rudimentary. In this study we evaluated lymphatic function and for the first time, measured lymph pump

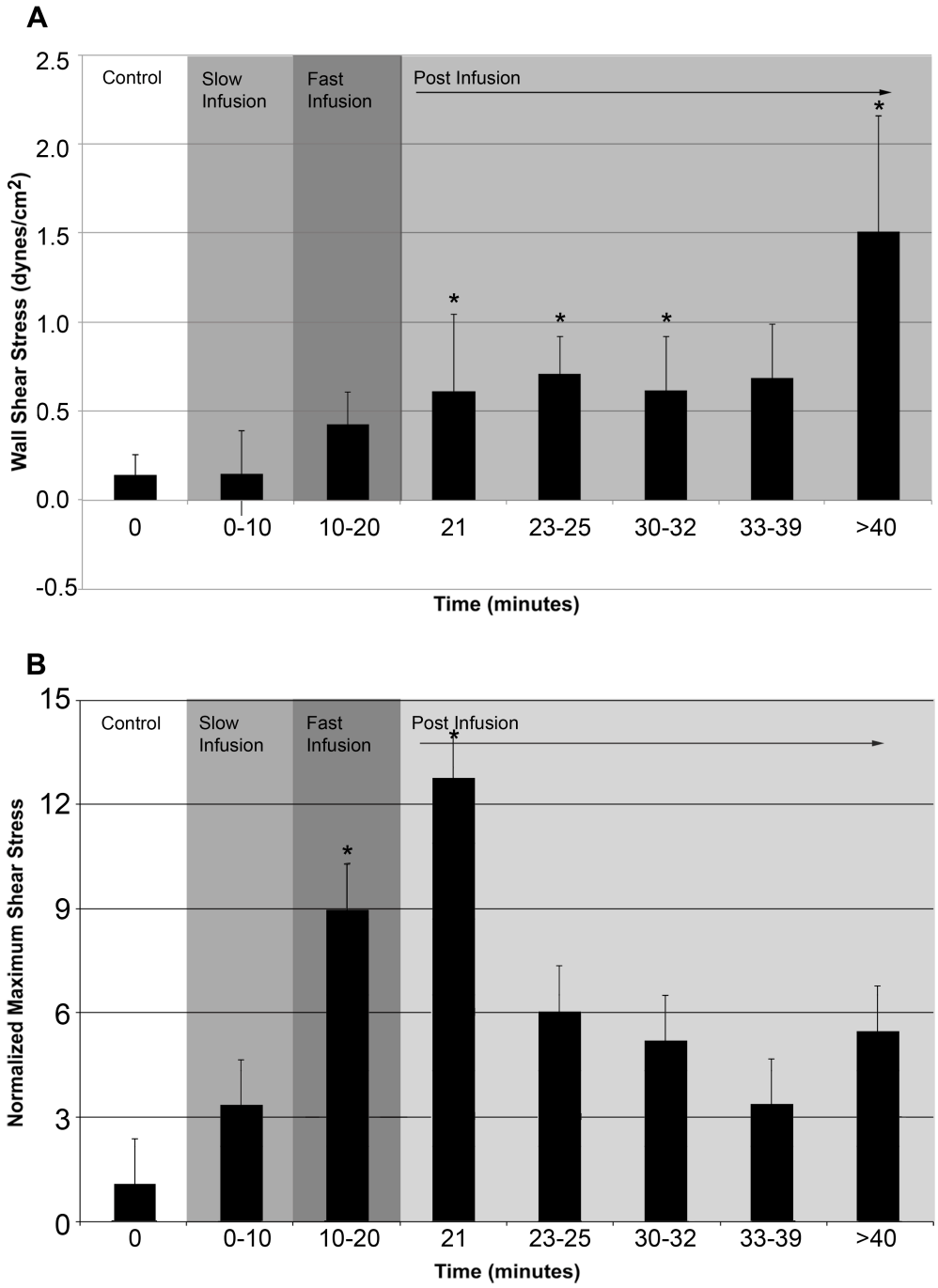

Figure 2.4. Plots of average wall shear stress and normalized maximum wall shear stress. (A) Average wall shear stress calculated assuming Poiseuille flow. (B) Maximum wall shear stress normalized to control. Asterisks indicate a statistically significant increase in shear stress (p-value<0.05). Note that shear stress was immediately affected with the induction of the fast infusion.

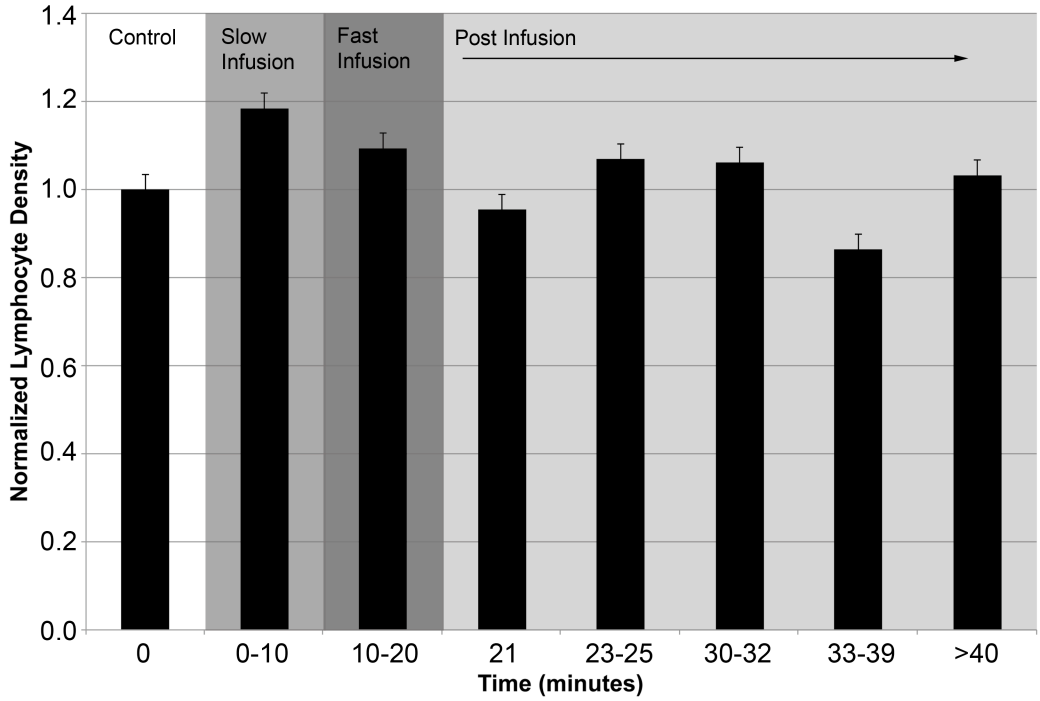

Figure 2.5. Plots of normalized lymphocyte density. No statistically significant change in density was observed (p-value>0.05). However, a 15% reduction in cells was observed post-infusion (33-39 minutes) as was expected by the dilution of lymph via the saline infusion.

activity simultaneously with lymph flow, lymph velocity and lymphatic wall shear stress under normal and edemagenic conditions in the rat mesentery *in situ*. Our results showed a significant increase in lymph flow rate, lymph velocity, lymphatic wall shear stress, lymphatic contraction frequency and fractional pump flow, while average lymphatic diameter remained relatively unchanged. These results strongly suggest the mechanosensing nature of lymphatic vessels where lymph pressure and shear stress play a role in modulating lymphatic contractility, the lymph pump and thus lymph transport.

Healthy lymphatic vessels from the rat mesentery were shown to quickly adapt to the increased fluid volume load induced by the saline infusion. The increase in lymph flow rate, lymphatic contraction frequency and the fractional pump flow clearly indicate increased lymphatic contractile activity. These results closely parallel the work by Benoit et al. (1989) who performed a similar experiment but did not measure actual lymph flow rate or velocity. As soon as one minute post-infusion lymph flow doubled, with flow rate eventually reaching up to six times the control. The change in measured lymph flow is similar in magnitude to the calculated changes in volume flow in our previous study (Benoit et al., 1989). Similarly ejection fraction and frequency of contractions increased resulting in a large change in fractional pump flow. Despite statistically insignificant changes in average vessel diameter, small changes in diastolic and systolic diameters caused the ejection fraction to increase during fast infusion and one minute post infusion thereby affecting fractional pump flow. This variable clearly demonstrated the change in lymphatic contractility to accommodate fluid volume load and is similar in direction to what we previously observed (Benoit et al., 1989). Notably, changes in lymph pump frequency and fractional pump flow were significant during the fast saline infusion (indicative of the acute pump activation) while changes in lymph velocity and flow rate were increasing throughout the infusion periods and achieves significance after the fast infusion (indicative of the increasing influence of the hypotonic volume load on interstitial lymph hydrodynamics). Changes in average shear stress experienced by the lymphatic vessels were quite large reaching up to 10X the control values at 20 minutes post-infusion. This change in shear stress could provide a

strong activation of the shear-dependent activation of nitric oxide (NO) production from the lymphatic endothelium. We have previously shown that flow-induced NO plays important roles in the modulation and regulation of the active lymph pump (Gashev, 2002; Gashev et al., 2002; Gashev et al., 2004; Gashev, 2008; Gasheva et al., 2006). On the other hand, maximum wall shear stress was highest during fast infusion and one minute post-infusion, again indicative of the increased lymph pump pulse diameter during these time periods.

Based on Starling's law, saline infusion via the femoral vein causes an increase in lymph volume at the interstitial level thereby eliciting changes in pressure and shear on the initial lymphatics (Levick, 2003; Renkin, 1986). This results in greater lymph formation. Given that the initial lymphatics lack smooth muscle cells, the collecting lymphangions must adapt to transport this excess fluid. We postulate that the increase in pressure and shear stress due to fluid volume regulates lymphatic contractility. As seen by our data, the lymphatics experience relatively low levels of wall shear stresses, less than 0.5 dynes/cm^2 on average. However, immediately upon administration of the fast saline infusion, the average shear stress significantly increases and maximum shear stress rises to 20 dynes/cm^2. The vessels seem to respond to these altered lymph pressure and shear stress by increasing contraction frequency and ejection fraction, which translate to increased pumping. Once pumping has been activated by the changes in shear, there is a corresponding increase in flow rate. Despite the small changes in vessel diameter, the lymphatic vessels sustain high values of lymph flow rate and shear stress at 20 minutes post-infusion. This supports the idea that lymph vessels appear to

have great sensitivities to changes in their mechanical environment (i.e. shear stress, pressure and flow rate) and tend to maintain diameters in situ within a reasonably controlled range, while modulating contraction frequency and pumping efficiency to handle increased loads. A number of ex vivo studies have shown that lymphatic contractility is affected by pressure and/or shear (Bohlen et al., 2009; Cox et al., 2008; Davis et al., 2011; Dixon et al., 2006; Gashev, 2002; Gashev, 2008; Zawieja et al., 1993; Zawieja, 2009; Zawieja et al., 2011). We believe that this study further highlights the importance of pressure and shear-regulated mechanisms in lymphatic pumping in vivo. The lack of significant increases in vessel diameter is likely due to the highly non-linear character of their pressure-diameter and pressure-volume curves (Davis et al., 2011; Venugopal et al., 2010). These vessels are typically highly compliant up to a pressure of approximately 5 cmH_2O, where they reach a maximum diameter that remains constant even at much higher pressures as illustrated by Davis et al. (2011). Presumably, this is to limit the amount of lymph that is stored in these conduit vessels (Quick et al., 2007). Differences between the modest diameter responses observed in this study versus those we have previously seen by Benoit et al. (1989) may also be due to the apparent selection of larger lymphatics in this study (average diastolic diameter ~117 μm) compared to those published by them (average diastolic diameter ~77 μm). Previous work by Benoit (1991) has also shown that the larger rat mesenteric lymphatics were less sensitive to the effects of hemodilution/volume loading than the smaller mesenteric lymphatics.

One limitation of this experimental setup is that we did not measure pressure during our experiments due to the complexity of the animal setup. Likewise, we did not want to make it more invasive as that would put the animal at a greater risk of inflammation. Despite this, we believe that pressure did increase at the interstitial tissue space and this is further supported by the work published by Benoit et al. (1989) and Cox et al. (2008). Another limitation is that in calculating wall shear stress, we assumed Poiseuille flow for simplicity. However we have recently shown that the uncertainty associated with the Poiseuille assumption is < 4% (Rahbar and Moore, 2011). Lastly, we were unable to implement Fourier transform techniques to determine the frequency data due to irregular contractile behavior of the lymphatics. Therefore the frequency presented in this paper is based on the number of contractions observed during acquisition divided by time, providing an "average" value for frequency.

In conclusion, we were able to show that healthy lymphatic vessels in the rat mesentery could sense changes in fluid volume load and quickly accommodated to these conditions to transport the excess fluid. We observed significant increases in the lymph pump contraction frequency, lymph flow rate, and average lymphatic wall shear stress, while diameter changes remained relatively modest. These results are highly suggestive that lymphatic vessels are extremely sensitive to mechanical stimuli, which allows them to regulate their ability to adapt to altered fluid conditions.

CHAPTER III

ASSESSMENT OF MICROPARTICLES FOR FLOW TRACKING IN ISOLATED LYMPHATIC VESSELS

Overview

Isolated lymphatic preparations are commonly used because of the ability to control each variable (input and/or output conditions) and parameters of interest – something impossible to do *in vivo*. There have been numerous reports on isolated lymphatic vessels from bovine and rat models investigating the effects of pressure and shear stress on pumping and contractile behavior. However, none of these reports have documented lymph velocities through the lymphangion and valve in these isolated experiments. This is mostly due to the lack of appropriate flow tracers available. In this section, we aim to develop neutrally buoyant particles that will serve as lymph flow trackers in isolated rat mesenteric lymphatics. Lymph flow will be evaluated at favorable and adverse pressure gradients. The particles will allow us to estimate lymph velocities throughout the lymphangion and get a better relation between pressure gradients, lymph flow, and valve resistance.

Introduction

The lymphatic system is responsible for the transport of lymph, plasma proteins, lipids and immune cells from the interstitium to the main circulation via the great veins. Lymph is formed in the interstitium when fluid and plasma proteins leak out of capillaries and are subsequently absorbed back into the lymphatics. The veins absorb

most of the fluid, transporting ~16 L/day, but the lymphatics are responsible for ~4 L/day. Without the absorption of this excess fluid, edema would develop, resulting in the swelling of localized tissue and limbs causing extreme discomfort (Rockson 2008; Rockson 2010). Lymphedema has become a growing concern due to the prevalence of secondary edema post-surgery or after radiation therapies for cancer treatment. Although lymphedema is not fatal, it impairs one's mobility and compromises their immune system. To improve edema treatments, we must first better understand the mechanisms regulating lymph formation and transport.

Once fluid accumulates in the interstitium it must enter the initial lymphatics. Pressures at the interstitial tissue beds are generally near atmospheric levels whereas, pressure within the initial lymphatics have been reported to be slightly positive indicating an unfavorable pressure gradient. Furthermore, once lymph enters the lymphatics, it must be transported "uphill" against a larger unfavorable pressure gradient. It is, therefore, crucial to understand the role of pressure gradients in regulating lymph formation and flow. Mendoza and Schmid-Schonbein (2003) have investigated pressure variations between the initial lymphatics and interstitium and have related these observations to lymph formation via the hydrostatic theory. Moreover, Galie and Spilker (2009) extended this work into a 2-D model for the primary valves in the initial lymphatics. Pressure measurements *in vivo* are extremely difficult but have been performed by a few groups (Benoit et al., 1989). These groups have shown changes in pressure to affect flow rates and contraction frequencies. Benoit et al. (1989) revealed a 10-fold increase in lymph propulsion via changes in diameter, frequency and pressure

post-volume infusion of saline in the rat mesentery. Furthermore, the work presented in the previous chapter illustrated the effects of increased flow on contractility and the lymph pump. It is therefore, without a doubt that pressure, volume loads and lymphatic valves regulate lymph flow.

Given the relationship between pressure and flow, many have also investigated the role of shear stress in regulating lymphatic contractility (Bohlen et al., 2009; Cox et al., 2008; Davis et al., 2011; Dixon et al., 2006; Gashev, 2002; Gashev, 2008; Zawieja et al., 1993; Zawieja, 2009; Zawieja et al., 2011). In particular, Bohlen et al. (2009) measured nitric oxide (NO) concentration in lymphatic vessels in situ and observed elevated levels of NO in the valve area. Nitric oxide is a common vasodilator that plays a role in relaxing the smooth muscle cells during periods of high flow, allowing the vessel to dilate and accommodate the larger flow. This accommodation in lymph flow was also observed in the collecting lymphatic vessels of the rat mesentery *in vivo* when subjected to increased volume loads, as shown in Chapter II. However, pressure was not measured from these *in vivo* experiments. Moreover, designing an *in vivo* experiment to fully characterize the relationship between pressure, flow and shear stress on lymphatic contractility and transport is no trivial task. Ex vivo experiments with isolated lymphatic vessels are much more feasible for such investigations. Some investigators have attempted to measure lymph flow rates with radio labeled or fluorescently tagged particles or proteins such as, gold and albumin (Kwon and Sevick-Muraca, 2007; Rasmussen et al., 2010; Reed and Wiig, 1983). These experiments, however, failed to provide accurate estimates for flow and did not provide any information on lymphatic

contractility. This is due to the indirect measurement of lymph flow. The radioactive or fluorescent techniques adopted by these groups can only provide a weak estimate of flow rates or change in volume. They lack the spatial resolution needed to investigate specific flow patterns. Thus, we need to develop tools to accurately track velocity in small lymphatic vessels.

Digital particle image velocimetry (DPIV) techniques are commonly used to quantify blood flow (Karri and Vlachos, 2010). Specifically, laser Doppler velocimetry (LDV) relies on the scattering of laser light by the particles seeded into the fluid; where velocity is calculated by measuring the Doppler frequency-shift of the scattered light (Briers, 2001; Humeau et al., 2007). These techniques are generally performed on larger vessels (on the order of millimeters in diameter) and therefore use particles greater than 50-100 μm in diameter. Furthermore, given that blood flow is being measured, polystyrene beads can be easily used since their density matches blood density (1.05 g/cm^3) and thereby negates any buoyancy or sinking effects. However, these large particles cannot be used to provide accurate estimates of lymph flow in 100μm-sized vessels. Additionally, lymph density is lower than blood density, approximately 1 g/cm^3, so we must adjust the experimental lymph fluid to match the particle density of 1.05 g/cm^3. Our goal is to develop neutrally buoyant microparticles to serve as flow tracers for isolated lymphatic vessels from the rat mesentery. These microspheres will be valuable tools for all isolated lymphatic vessel preparations/experiments to better correlate pressure, flow and shear stress stimuli on lymphatic behavior.

Materials & Methods

Flow Tracers: Polystyrene microspheres ranging from 1-15 μm in diameter with a density of 1.05 g/cm^3 were purchased from PolySciences, Inc. (Warrington, PA). In order to make the microspheres neutrally buoyant, we modified the composition of our albumin physiologic saline solution (APSS) to match densities. Isolated red blood cells (RBCs) were also tested as flow tracers. Red blood cells were collected from the rat heart immediately post-euthanization and placed in a heparinized tube in a 4:1 dilution.

Albumin Saline Solutions: Our original APSS recipe (in mM: 145.00 NaCl, 4.7 KCl, 2.0 $CaCl_2$, 1.17 $MgSO_4$, 1.2NaH_2PO_4 , 5.0 dextrose, 2.0 sodium pyruvate, 0.02 EDTA, 3.0 MOPS, and 10 g/L bovine serum albumin) has a density of 0.99 (~1g/cm^3) . We increased the density to 1.05 g/cm^3 by adjusting the concentration of bovine serum albumin (MW 66,776 Daltons), dextrose (MW 180.16) and adding Dextran-40 (MW 40,000 Daltons), dextran sulfate (MW >500,000 Daltons), and glycerin (MW 92.0542). All of these additives were chosen due to large molecular weight and their use in previous bench and *in vivo* experiments of the blood vasculature (Bond and Levitt, 1979; Katz et al., 1971; Kowallik et al., 1991; Modi et al., 2007; Roberts and Olbricht, 2006). A total of seven solutions were tested with the polystyrene microspheres in isolated rat mesenteric lymphatic vessels, as recorded in Table 3.1. All solutions were brought to a pH of 7.4 at 37°C before testing them on a live isolated lymphatic vessel.

Isolated Vessels & Testing: Male Sprague-Dawley rats were anesthetized with intramuscular injections of fentanyl-droperidol (0.3 mL/kg) and diazepam (2.5 mg/kg). A midline incision was made and a loop of the mesentery was exteriorized. Lymphatic

vessels were isolated and harvested from the rat mesentery and placed in physiologic buffered saline (PBS) for testing. The vessels were cannulated and pressurized in 1% albumin APSS (normal concentration) and recorded to ensure that normal contractile behavior was observed. Once spontaneous contractions were observed, the chamber bath was replaced with the pre-warmed modified APSS solution. Video was captured for up to 30-45 minutes in the new solution. This procedure was repeated for every solution with a new vessel.

Viscosity Measurements: To assess the effects of the additives on viscosity, all modified APSS solutions were measured using a rheometer (Physica MCR Series, Anton Paar). Samples were tested in duplicates and average percent change in viscosity compared to normal APSS is reported in Table 3.1.

Table 3.1. Summary of solutions tested to achieve neutral buoyancy of microparticles.

Albumin Concentration	Additive Concentration	Density (g/cm^3)	% Change in Viscosity	Outcome
1%	8-10% Dextran-40	1.047	+5.18%	Weak contractions
1%	8-10% dextrose	1.04	+15.94%	No contractions
1%	8-10% dextran sulfate	1.05	+88.92%	No contractions
1%	22% glycerin	1.05	+94.64%	No contractions
3%	4% dextrose	1.04	N/A	No contractions
3%	6% dextrose	1.05	N/A	No contractions
1%	4:1 dilution of RBCs (*used as flow tracers*)	1 g/cm^3	N/A	Contractions and Flow

Results

All modified APSS solutions impaired lymphatic contractility. The modified solutions that had the least effect on contractility were the 8-10% Dextran-40, which exhibited weak contractions after 30 minutes of incubation time. Dextran40 also exhibited the smallest increase in viscosity, approximately 5% on average. The dextrose, dextran sulfate and glycerin-based solutions inhibited all contractions up to 45 minutes of incubation time. While all solutions had densities between 1.046-1.05 g/cm^3, their viscosities differed, as illustrated in Table 3.1. Glycerin and 8-10% dextran sulfate exhibited the largest increase in shear viscosity, up to 95% increase. These changes in viscous behavior are further illustrated in Figure 3.1. We speculate that this significant change in viscosity affected the shear stress experienced by the vessel, which consequently could prevent the vessel to contract.

The only solution that allowed successful flow tracking was the RBCs suspended in normal APSS (1% albumin). The RBCs were 4-5 μm in diameter and flowed easily through the center of the lymphangion, as illustrated in Figure 3.2. Considering the suspended RBCs in normal APSS, we attempted to track the RBCs for lymphocyte velocity measurement as shown in Figure 3.3. We were limited by the camera's slow acquisition speed (28-30 fps) and thus could only track up to 2 mm/s. It should be noted that the presence of RBCs and 5 μm microspheres did not have a significant effect on the fluid's viscosity.

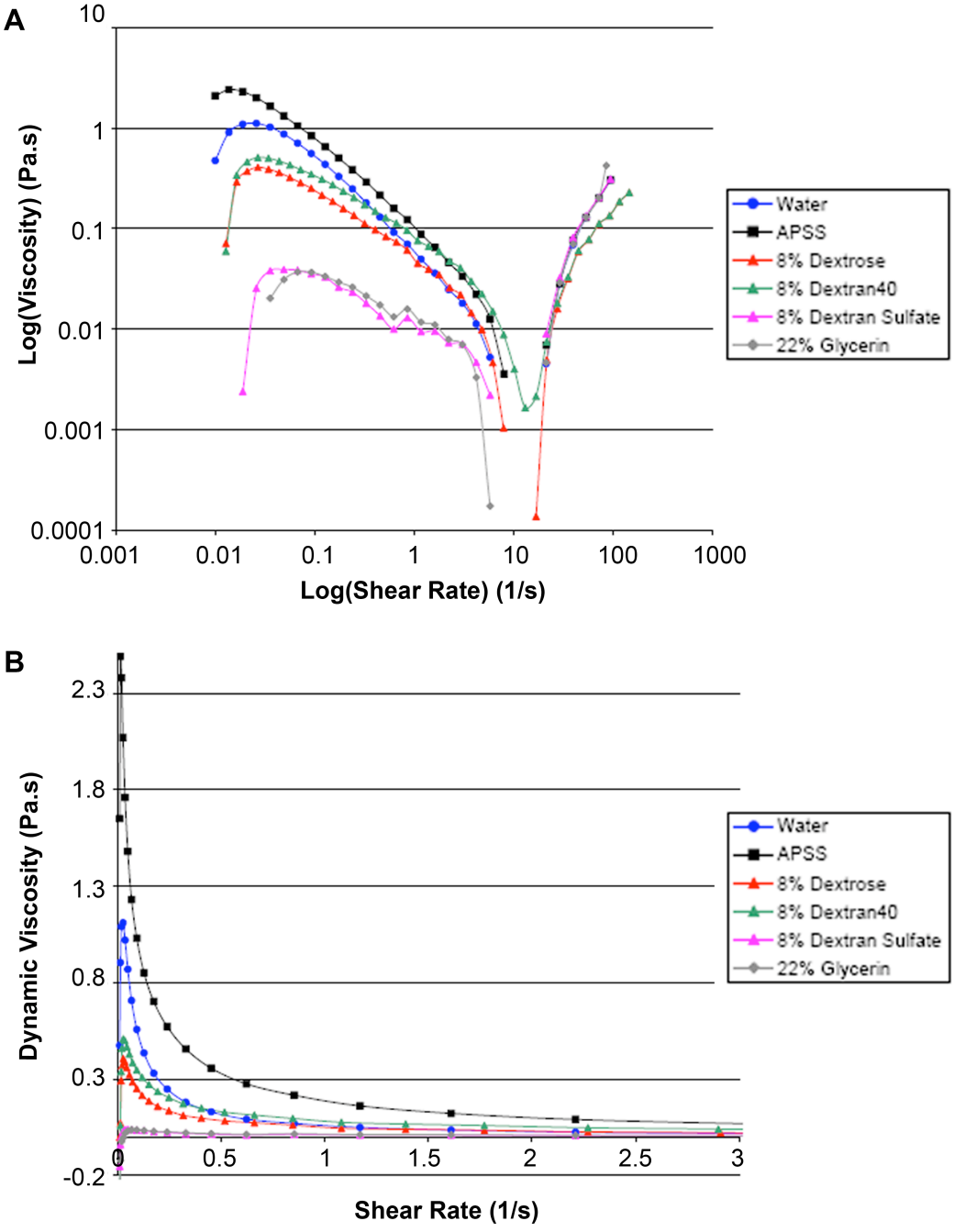

Figure 3.1. Viscosity measurements of modified APSS solutions. (A) Logarithmic plot of viscosity. (B) Dynamic viscosity vs. shear rate.

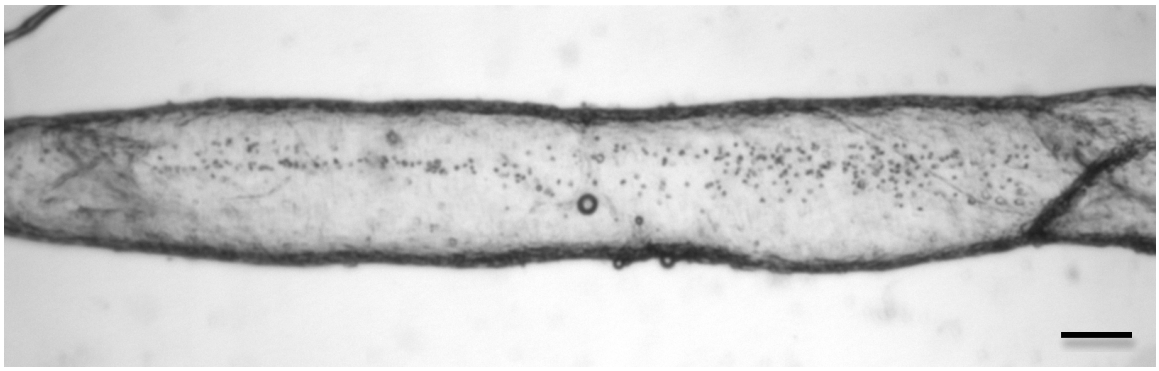

Figure 3.2. Lymphangion seeded with RBCs as flow tracers. RBCs flowed through the center of the lymphangion. (frame 1000 from 356.2 avi). Image resolution: 1624x510 pixels (~1 pixel=1 µm), 3.2x objective. Scale bar ~100 µm.

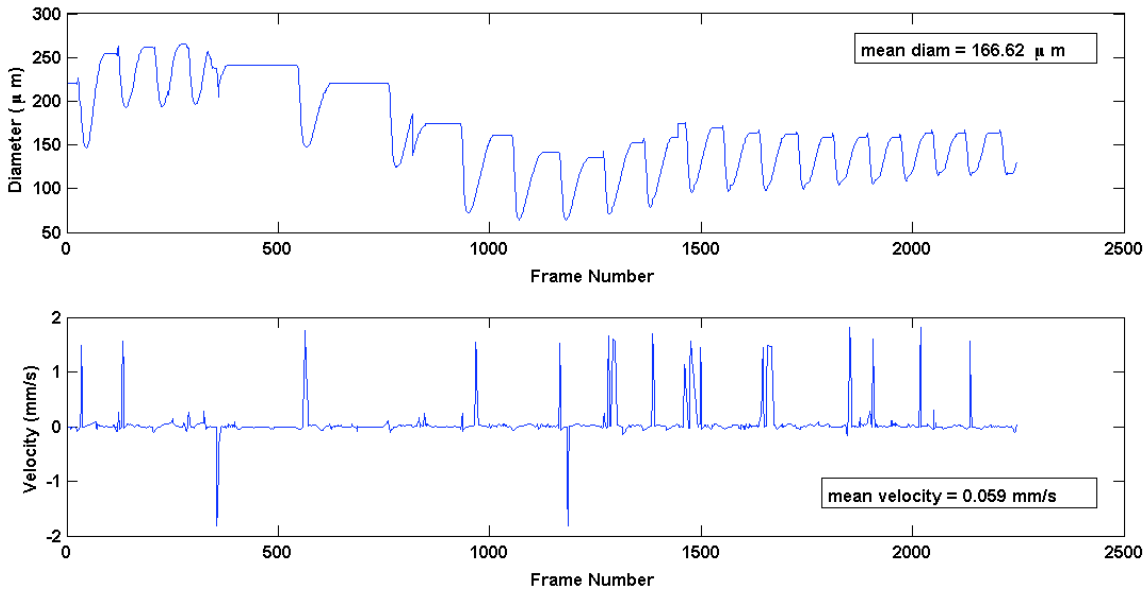

Figure 3.3. Diameter and velocity measurements from tracking RBCs. Note that due to the camera acquisition speed of 28 frames per second, we were only able to accurately capture velocities between -2 and +2 mm/s.

Discussion

Our original goal was to evaluate the effects of pressure gradients on lymph flow in an isolated lymphatic vessel. However, since we were unable to prepare a solution that would provide neutral buoyancy for the particles and leave lymphatic contractility unaffected, we decided to evaluate the reasoning for this impairment. In all of the modified APSS solutions, albumin and dextrose concentrations remained below plasma levels. Despite these relatively low concentrations, these modified solutions were not suitable for lymphatic experiments. It is important to note that success with these solutions have been recorded in the analysis of blood flow (Bond and Levitt, 1979; Katz et al., 1971; Kowallik et al., 1991). Blood has a density of 1.05 g/cm^3 and given that the field of cardiovascular research is more popular, microspheres have been designed for blood flow studies. Although one may suppose that the difference between 1.05 and 1.0 is not significant, we have shown that this 5% change in density greatly affects the lymphatic environment. The 5% increase in density created up to 95% increase in viscosity, which, we believe, greatly affected the shear environment of the lymphangion. A recent report from Tsai et al. (2005) illustrated the effects of elevated plasma viscosity and observed an increase in nitric oxide production, which consequently increased microvascular perfusion. This perfusion could potentially explain the reason for no observed contractions with our modified solutions; the lymphangion must have sensed the increase in viscosity and remained in its diastolic configuration.

Furthermore, increasing dextrose revealed that lymphatic contractility is sensitive to glucose concentration. This is in agreement with studies that correlate the prevalence

of lymphatic disorders with diabetes and metabolic syndromes (Moriguchi et al., 2005; Chakraborty et al., 2010). The data presented here, further suggests that the disease may be detrimental to lymphatic function and/or increase the likelihood of such individuals to develop lymphatic problems. The pathway in which contractility is impaired remains unknown. We speculate that increases in dextrose concentration is inhibiting and/or blocking the pacemaker capability of the vessel. Similarly, another study observed elevated gene expressions of Glut-1 (regulates glucose transport) in the lymphatics and correlated this with lymph node metastasis (in breast cancer, head and neck cancer) (Zhou et al. 2008). These findings strongly motivate further research into the interaction of diabetes, glucose uptake and transport within the lymphatic system.

While using RBCs as flow tracers was mildly successful, in terms of particle tracking (Figures 3.2 and 3.3), we must admit that administering RBCs into a lymphangion is non-physiologic. Generally, lymphocytes, dendritic cells, and macrophages are the only particles flowing through a lymphangion and the presence of RBCs indicates tissue damage (wound-healing) and/or inflammation. Both wound and inflammatory conditions have been shown to significantly affect lymph flow and lymphatic contractility (Semaeva et al., 2010). Additionally, work by Elias et al. (1990) revealed the inhibitory effects of hemoglobin on the lymphatic pump. While no change in lymphatic contractility was observed during our experiment, using RBCs is not preferred as it increases the risk of inducing inflammatory and/or wound-healing responses. The only problem we encountered with RBCs was the collection of cells in the downstream glass cannula (pipette). This accumulation of cells eventually caused a

significant backflow of particles, approximately 30 minutes from the beginning of the experiment.

We have two solid recommendations for future development of flow tracers. First, we can avoid the problem of neutral-buoyancy if we use sub-micron (<1 μm) particles due to the random Brownian motion of these small sized particles. However, if this approach is taken, regular light microscopy cannot be used because of the limitations of the optics. Even with our high-resolution camera, 1 pixel is approximately 0.5-1μm in size, so fluorescence microscopy is necessary. There are a number of sub-micron fluorescent particles available from various companies, such as Invitrogen and PolySciences Inc, and these methods have been successfully used in measuring retinal blood flow (diameter 300-500 μm) (Lynn and Ahmed, 2006; Wang et al., 2007). It is important to note that if this approach is taken, one must have a high-speed intensifier and camera to be able to image the particles flowing in the lymphatic vessel; at a rate of 300 fps (minimum) is recommended. The second alternative is to develop hollow polystyrene microspheres which have a density of ~1g/cm^3 (Kim et al., 2009). In this manner, we can use regular APSS with these hollow microspheres (~5 μm in diameter) and given the larger size, we can implement regular light microscopy optics. However, one must be aware that since these are relatively larger particles, one can still encounter problems with clogging/agglomerating of particles at the glass pipette or other areas of the flow loop.

In conclusion, we have reported our failed attempts at developing flow tracers for isolated lymphatic vessel ex vivo (in vitro) experiments. In the process, however, we

have revealed an interesting relation between fluid viscosity, glucose concentration and lymphatic contractility. These results highly motivate further investigation on the mechano-sensitivity of lymphatic endothelium and regulatory pathways for lymphatic contractility. The development of new flow tracers will greatly benefit the lymphatic research field by allowing one to perform experiments to link mechanical stimuli to biological signals and regulatory pathways.

CHAPTER IV

DYNAMIC MODELING OF LYMPH FLOW USING A SIMPLE CYLINDRICAL GEOMETRY*

Overview

The lymphatic system is an extensive vascular network featuring valves and contractile walls that pump interstitial fluid and plasma proteins back to the main circulation. Immune function also relies on the lymphatic system's ability to transport white blood cells. Failure to drain and pump this excess fluid results in edema characterized by fluid retention and swelling of limbs. It is, therefore, important to understand the mechanisms of fluid transport and pumping of lymphatic vessels. Unfortunately, there are very few studies in this area, most of which assume Poiseuille flow conditions. *In vivo* observations reveal that these vessels contract strongly, with diameter changes of the order of magnitude of the diameter itself over a cycle that lasts typically 2-3 seconds. The radial velocity of the contracting vessel is on the order of the axial fluid velocity, suggesting that modeling flow in these vessels with a Poiseuille model is inappropriate. In this paper, we describe a model of a radially expanding and contracting lymphatic vessel and investigate the validity of assuming Poiseuille flow to estimate wall shear stress, which is presumably important for lymphatic endothelial cell mechanotransduction. Three different wall motions; periodic sinusoidal, skewed sinusoi-

---

*Reprinted with permission from "A model of a radially expanding and contracting lymphangion" by Rahbar E, Moore JE Jr., 2011. Journal of Biomechanics, 44(6):1001-1007, 2011 by Elsevier.

-dal and physiologic wall motions, were investigated with steady and unsteady parabolic inlet velocities. Despite high radial velocities resulting from the wall motion, wall shear stress values were within 4% of quasi-static Poiseuille values. Therefore, Poiseuille flow is valid for the estimation of wall shear stress for the majority of the lymphangion contractile cycle.

Introduction

The lymphatic system is an extensive vascular network collecting fluid from the interstitial spaces and transporting it back to the venous circulation. Together with the presence of valves and contractile walls, fluid is pumped from essentially zero pressure tissue beds throughout the body back to the subclavian veins in the shoulder region. In addition to the transport of fluid, the lymphatic system is crucial for protein balance and immune function. The dysfunction of a lymphatic vessel can lead to a number of pathologies. Lymphedema, for example, is characterized by fluid retention usually caused by the removal of nodes or vessels during surgery or damage to the vessel and results in swelling, pain, incapacity and reduced immunity (Rockson, 2006; Stanton et al., 2009). Edema has become a greater concern with the prevalence of breast cancer; up to 75% of women develop arm lymphedema within 2 years, and 90% within 3 years of breast cancer surgery and therapy (Rockson, 2006; Stanton et al., 2009). There is no cure for lymphedema, in part because knowledge of the system's pumping characteristics is lacking.

Lymph transport has been shown to rely on two pumping mechanisms, namely the intrinsic and extrinsic pump to transport fluid. The intrinsic pump refers to the

vessel's ability to contract phasically due to the presence of smooth muscle cells in its wall, whereas the extrinsic pump is the compression of the lymphatic vessel by adjacent tissue forces and tonic constrictions. Unlike arterioles, whose smooth muscle cells contract or relax very slowly to control local blood flow, lymphatic vessels undergo large, swift contractions. Dixon et al. (2006) reported up to 39% reduction in diameter during contractions with a typical period of 2-3 seconds, resulting in contraction velocities of 0.04 mm/s, on average, in rat mesenteric lymphatic vessels. In addition to measuring vessel diameter and contraction frequencies, Dixon et al. (2006) estimated lymphocyte velocity and wall shear stress. Lymphocyte velocities ranged from -3 to 10 mm/s with average velocities of 5 mm/s. This corresponded to an average wall shear stress of 0.64 dynes/cm^2 (range = 0-12 dynes/cm^2). Flow remained in the laminar regime with Reynolds number less than 5. It was further noted that velocity and wall shear stress values were out of phase compared to the diameter tracings; suggesting that contractions were shear-regulated.

Obtaining reliable wall shear stress values requires accurate estimation of wall shear rate, which is difficult to measure due to the small size of lymphatic vessels, wall motion and slow lymph velocities. This implies the use of fluid flow modeling that can be used to estimate wall shear stress from measurements of quantities such as pressure drop, flow rate and/or diameter. Only a few have attempted to model lymphatic vessel behavior. Reddy et al. (1975) were the first to develop a model for the lymphatic system. Their model assumed 1-D laminar flow through a succession of 35 lymphangions representing the thoracic duct, connected by valves, which were modeled by a fixed

resistance to flow. Volumetric flow rate (Q), pressure (p) and radius (r) of the vessel were the variables of interest and shear stress (τ) was calculated assuming Poiseuille flow. Among their findings were weak dependences of overall flow rate on the filling and contraction flow rates, individually. Meanwhile, others have taken a different approach to modeling lymph flow. Recent work by Quick et al. (2007) use a circuit-theory analog of the system to provide important insights on the propagation of contractions. Quick et al. (2007) and Venugopal et al. (2009) show that lymphangion contractile coordination minimally affects lymph flow. Similarly, Macdonald et al. (2008) refined the Reddy model by incorporating compliant walls and increasing the number of computational nodes to investigate wave propagations of the contractions in a single lymphangion. Lymphangions were found to pump most efficiently when all sections of the wall contracted simultaneously, and there were minimal differences between forward and reverse propagating contractile waves. At a larger scale, Bertram et al. (2011) showed that sequential contractions in a short series chain of 5 lymphangions were more efficient than synchronized ones.

While these models provide a first-order approximation of lymphatic pumping and flow patterns, a major concern is the assumption of Poiseuille flow (i.e. steady flow in a straight, rigid tube). The work by Dixon et al. (2006) clearly shows that lymphatic vessels are highly dynamic and wall motion is significant; reporting values for the ratio of radial to axial velocities greater than 1. This behavior is usually seen during periods of flow reversal or rapid dilation, when axial velocities are low and radial velocities are high. Given this dynamic behavior, using Poiseuille flow, which assumes rigidity, may

not be always accurate. In particular, the high ratio of radial to axial velocity means that terms that are eliminated in the derivation of Poiseuille flow (e.g., convective acceleration) may in fact be significant (Dixon et al., 2006).

Our general goal is to construct physiologically relevant models of lymphatic pumping that include wall shear stress mediated cellular actions. This study specifically addresses the validity of assuming Poiseuille flow as an appropriate model for estimating wall shear stress from flow rate and diameter data. We generate a 3-D computational model of a radially expanding and contracting lymphangion and analyze lymph shear stress and flux relations in simple dynamic geometries throughout a contractile cycle.

Materials & Methods

Construction of Flow Model: The lymphangion model was constructed as a straight cylindrical tube with a contracting segment flanked by static inlet and outlet sections using Solidworks (SP3 2009). A smooth spline curve was added between the contracting segment and the upstream and downstream sections. These transition regions were 5 times the mean radius of the tube in length to ensure negligible effects on the flow in the region of interest (taken to be the center plane of the contracting segment, as illustrated Figure 4.1b). Nominal dimensions of the lymphangion model are illustrated in Figure 4.1. It should be noted that we assumed a constant radius around the circumference of the cylinder. The lymphangion geometry was imported into StarCCM+ (v4.02.011, CD-Adapco) and the surface remesher tool was used to generate a hexahedral mesh. The trimmer cell mesher was then implemented to generate the volume mesh due to its robustness in producing a high quality grid for the contracting segment. Specifically, the

trimmer mesh is a trimmed hexahedral cell shape based core mesh, which allows for more movement than the traditional hexahedral and polyhedral meshes. The computational mesh was refined to achieve wall shear stress convergence; it was refined until the change in shear stress was less than 2%, resulting in 10 μm cells with a 15 μm prism layer thickness and 2531 cells in the contracting segment (Figure 4.1).

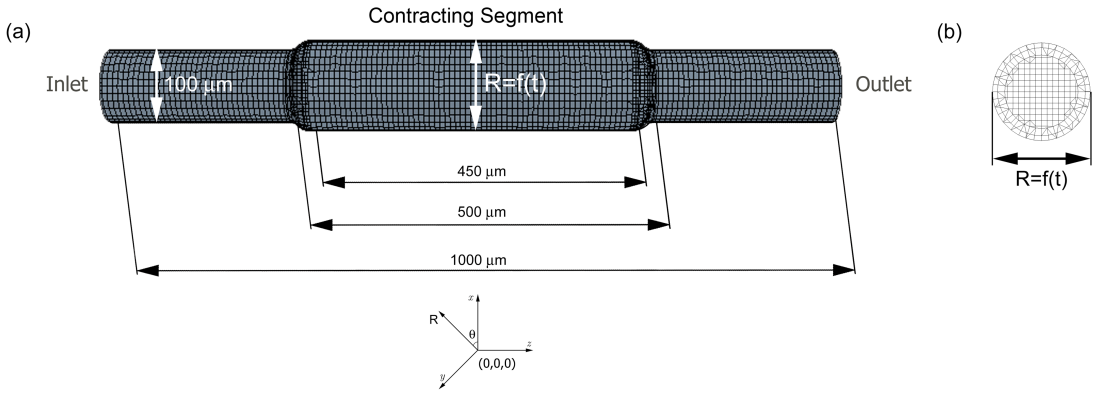

Figure 4.1. Illustration of geometry used for CFD model. (a) Illustration of radially expanding and contracting lymphangion model. The contracting segment has a prescribed motion such that the radius varies with time. The radius of this region varied from 40-120 μm for our simulations. (b) Cross-sectional view of the center of the contracting segment. A trimmed hexahedral mesh was used to accommodate the wall motion, with cell sizes of 10μm and prism layer thickness of 15 μm.

Initial and Boundary Conditions: Flow was assumed to be laminar and lymph was assumed to be an incompressible single component Newtonian fluid with a density of 0.997 g/cm^3 and dynamic viscosity of 0.9 cP. Three types of prescribed wall motions were applied to the central moving segment; periodic sinusoidal functions, skewed sinusoidal functions and physiological wall motion from *in situ* experiments. A parabolic velocity profile was defined at the inlet (both steady and time-varying) and a

static pressure condition at the outlet. The inlet velocity for the physiologic case (see figure on pg. 65) was estimated using conservation of mass and the *in situ* data for axial velocity. Specifically, the velocity waveform from the *in situ* experiment, which was taken at an unknown axial position relative to the inlet to the lymphangion, was used to determine the appropriate inlet condition by adding the mass gain/loss from the expansion/contraction of the tube segment between the inlet and the mid-point of the contracting segment of the computational fluid dynamics (CFD) model. Note that the wall motion was imposed as a boundary condition, i.e., no fluid-solid interaction (FSI) modeling was performed. A total of 15 simulations were performed investigating various inlet velocity and wall motion combinations. Reynolds (Re) and Womersley (α) numbers were very low for all simulations ($Re<1$, $\alpha<0.15$).

Simulations: We used a commercial CFD package (StarCCM+ 4.02.011, CD-Adapco) to run all simulations. This finite volume software employs an arbitrary Lagrangian-Eulerian formulation to allow for mesh movement (morpher solver) and a 2^{nd} order segregated implicit flow model for the fluid. Specifically, an AMG SIMPLE solver with an under-relaxation factor of 0.7 and 0.3 was used to calculate velocity and pressure, respectively. The variables of interest were fluid velocity and wall shear stress. Due to the axisymmetric nature of our geometry, wall shear stress was averaged around the circumference of the center plane of the contracting segment (i.e. 500 μm from inlet). All simulations were run for 16.2 seconds, corresponding to 5 contraction cycles. All initial and transient flow effects were minimal by the 3^{rd} cycle and therefore data was processed from the 4^{th} cycle (i.e. 10-13.2 seconds). Wall shear stress (τ_w) was calculated

for every cell using the equations below:

$$\mathbf{T} = \mu \left[\nabla \mathbf{v} + \nabla \mathbf{v}^{\mathrm{T}} - \frac{2}{3} (\nabla \cdot \mathbf{v}) \mathbf{I} \right] \quad \text{(Equation 4.1)}$$

$$\vec{\tau}_w = -\mathbf{T} \cdot \frac{\mathbf{a}}{|\mathbf{a}|} \quad \text{(Equation 4.2)}$$

where **a** is the axial face area vector, **v** is the velocity vector, μ is the dynamic viscosity and **T** is the stress tensor. The corresponding Poiseuille value for wall shear stress was calculated using the following equation:

$$\tau_{poiseuille} = \frac{4\mu\bar{\mathbf{v}}}{r} \quad \text{(Equation 4.3)}$$

where $\bar{\mathbf{v}}$ is the spatially averaged axial velocity at a given axial location and r is the vessel radius. It should be noted that the shear stress at the transient regions between the inlet and moving boundary are strongly affected by the boundary conditions and therefore not relevant. Thus, we focused on the center plane of the contracting segment and evaluated the axial component of wall shear stress due to the primarily axial nature of the flow. The lymphangion model was tested over a range of 0-60 μm change in radii. The static case (i.e. when $\partial r/\partial t=0$) was used to ensure that Poiseuille values matched the calculated shear stress values from the CFD model.

Results

Periodic Sinusoidal Wall Motion with Steady Inlet: When the inlet flow was steady, the shear stresses calculated in the sinusoidally expanding tubes were within 1% of the quasi-static Poiseuille values (Table 4.1). The ratios of radial to axial velocities (Vr/Va) in the high inlet velocity simulations were fairly low ($0.0036 < Vr/Va < 0.0454$), so we

investigated the smallest and largest radially changing ($\Delta R=20$, 60, respectively) simulations at a lower steady inlet velocity to increase the Vr/Va ratio (Table 4.2). Despite the order of magnitude increase in Vr/Va ratio ($0.0159 < Vr/Va < 0.540$), wall shear stress values from the dynamic simulations remained within 1% of the quasi-static Poiseuille estimation. The distribution of wall shear stress along the axial length of the contracting segment exhibited slight monotonic variations. These increases or decreases in wall shear stress are illustrated in Figure 4.2 for the $\Delta R=60$ case at four time points: the minimum ($R=60\mu m$), maximum ($R=120\mu m$) and average vessel diameters ($R=90\mu m$), both when the vessel was contracting and expanding. The monotonic variations amounted to at most 5% in this case.

Table 4.1. Results from simulations with periodic sinusoidal wall motion (T=3.2 s) and fast steady inlet condition. (Average axial velocity at inlet = 5.91 mm/s). The table compares wall shear stress values to the quasi-static Poiseuille values for shear and presents the average and maximum percent difference.

Radius Range (μm)	Axial Wall Shear Stress (dynes/cm^2)	Poiseuille Shear Stress (dynes/cm^2)	Max. |Vr/Va| Ratio	Avg. % Diff WSS	Max. % Diff WSS
$40 < R < 60$	$2.37 < \tau_w < 8.06$	$2.38 < \tau_{poiseuille} < 8.08$	0.0036	0.4%	0.5%
$60 < R < 70$	$1.52 < \tau_w < 2.44$	$1.53 < \tau_{poiseuille} < 2.45$	0.0027	0.5%	0.5%
$60 < R < 80$	$1.01 < \tau_w < 2.46$	$1.02 < \tau_{poiseuille} < 2.47$	0.0067	0.5%	0.6%
$60 < R < 100$	$0.50 < \tau_w < 2.50$	$0.51 < \tau_{poiseuille} < 2.51$	0.0204	0.6%	1.1%
$60 < R < 120$	$0.28 < \tau_w < 2.54$	$0.28 < \tau_{poiseuille} < 2.55$	0.0454	0.8%	2.7%

Table 4.2. Results from simulations with periodic sinusoidal wall motion (T=3.2 s) and slow steady inlet condition. (Average axial velocity at inlet = 1.48 mm/s). The table compares wall shear stress values to the quasi-static Poiseuille values for shear and presents the average and maximum percent difference.

Radius Range (μm)	Axial Wall Shear Stress (dynes/cm^2)	Poiseuille Shear Stress (dynes/cm^2)	Max. |Vr/Va| Ratio	Avg. % Diff WSS	Max. % Diff WSS
$40 < R < 60$	$0.57 < \tau_w < 2.08$	$0.57 < \tau_{poiseuille} < 2.08$	0.0159	0.4%	0.4%
$60 < R < 120$	$0.03 < \tau_w < 0.71$	$0.03 < \tau_{poiseuille} < 0.71$	0.5450	0.6%	1.5%

Skewed Sinusoidal Wall Motion with Steady Inlet: The skewed wall motion was constructed to emulate a rapid contraction followed by gradual diastolic filling of the vessel (Figure 4.3a). We evaluated this wall motion, with radius range of 40-60μm, at three steady parabolic inlet velocities ($\bar{v}$ = 5.91, 1.48 and 0.0591 mm/s). Axial velocity and wall shear stress values were much higher than the corresponding periodic wall motion case; suggesting that the increase in rate of contraction affects the maximum velocity. Furthermore the rate of dilation followed by the contraction caused backflow, as commonly observed *in vivo* (Dixon et al., 2006; Zawieja, 2009). Despite the changes seen in velocity, wall shear stress values were still accurately estimated by Poiseuille (within 1%). The skewed wall motion simulation with the slowest inlet velocity ($\bar{v}$= 0.0591 mm/s, Figure 3a) exhibited the highest Vr/Va ratio of 1.3, but this did not affect the accuracy of the Poiseuille estimate (Figure 4.2b). Wall shear stress along the axis of the contracting segment varied only during the transient period of contraction, amounting to at most a 15% monotonic increase for the slowest inlet velocity case ($\bar{v}$ = 0.0591 mm/s).

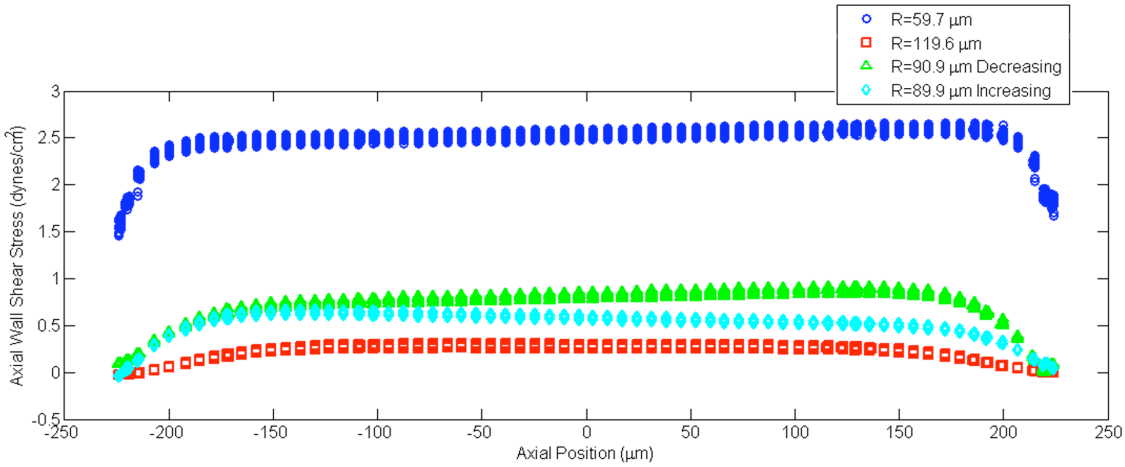

Figure 4.2. Distribution of axial wall shear stress versus axial position of the contracting segment. Results are shown for instantaneous wall shear stress values at the minimum (60 µm), maximum (120µm) and average vessel radius (90 µm) for the periodic sinusoidal wall motion with a steady inlet case (the last case presented in Table 1a). Note that both time points the vessel is at its average size of 90 µm are plotted (i.e. as the vessel contracts "decreasing" and as the vessel dilates, "increasing"). The slight changes in wall shear stress along the axial length of the contracting segment are due to the monotonic changes in velocity, which thereby affect our wall shear stress calculation.

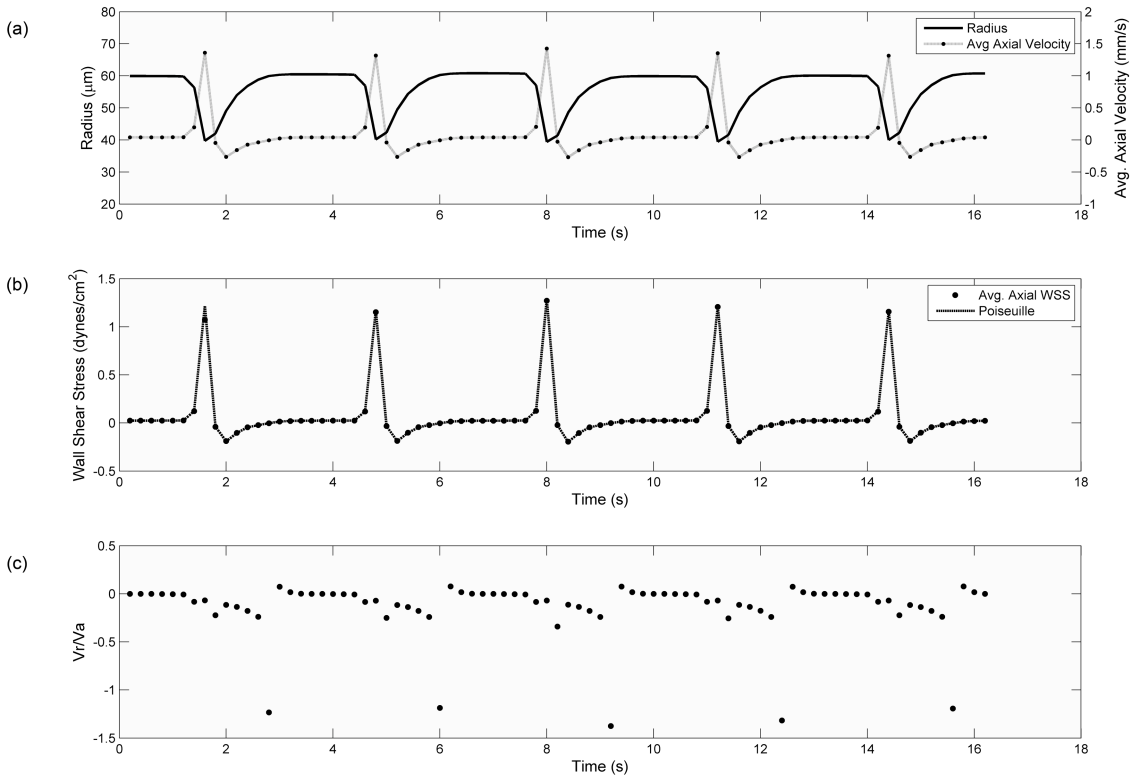

Figure 4.3. Results from skewed sinusoidal wall motion (T=3.2s) with a steady parabolic inlet velocity. (Average axial velocity at inlet = 0.0591 mm/s) a) Vessel radius (line) and axial velocity values (dotted line) at the center of the contracting segment, b) Average axial wall shear stress (dot) and quasi-static Poiseuille (dotted line) values, c) Radial to axial velocity ratio. Highest ratio observed during vessel dilation after rapid contraction.

Periodic Sinusoidal Wall Motion with Unsteady Inlet: An unsteady parabolic velocity profile was applied at the inlet of the lymphangion model such that the minimum inlet velocity would coincide with the maximum diameter and vice versa. Three different unsteady inlet velocity amplitudes (±1.9, ±7.5, ±15 mm/s) were investigated and this allowed for negative axial velocities (i.e. backflow). Velocity and wall shear stress values for the ±7.5 mm/s unsteady inlet case were similar to the steady inlet condition (v_{inlet} = 5.91 mm/s), as shown in Figure 4.4. However, the Vr/Va ratio was much higher in the unsteady case. Regardless, Poiseuille estimates for shear stress were still within 2% (Table 4.3). The increase in wall shear stress along the axis of the contracting segment was <20%, achieving its maximum value during strongest vessel contraction.

Skewed Sinusoidal Wall Motion with Unsteady Inlet: Applying the lowest amplitude unsteady parabolic velocity profile (±1.9 mm/s) at the inlet with the skewed sinusoidal wall motion created more backflow ($-1.34 < v_{axial} < 3.76$ mm/s) and consequently larger values of shear ($-0.80 < \tau_w < 3.34$ dynes/cm^2) than the corresponding steady case. However, this did not affect the accuracy of the Poiseuille assumption (Table 4.3). In fact, the average percent difference between Poiseuille and CFD shear values was almost half of the corresponding steady inlet case (0.22% vs. 0.46%) as shown in Table 4.2. Similar to the periodic wall motion with unsteady inlet, wall shear stress values increased along the axis of the contracting segment by <20%.

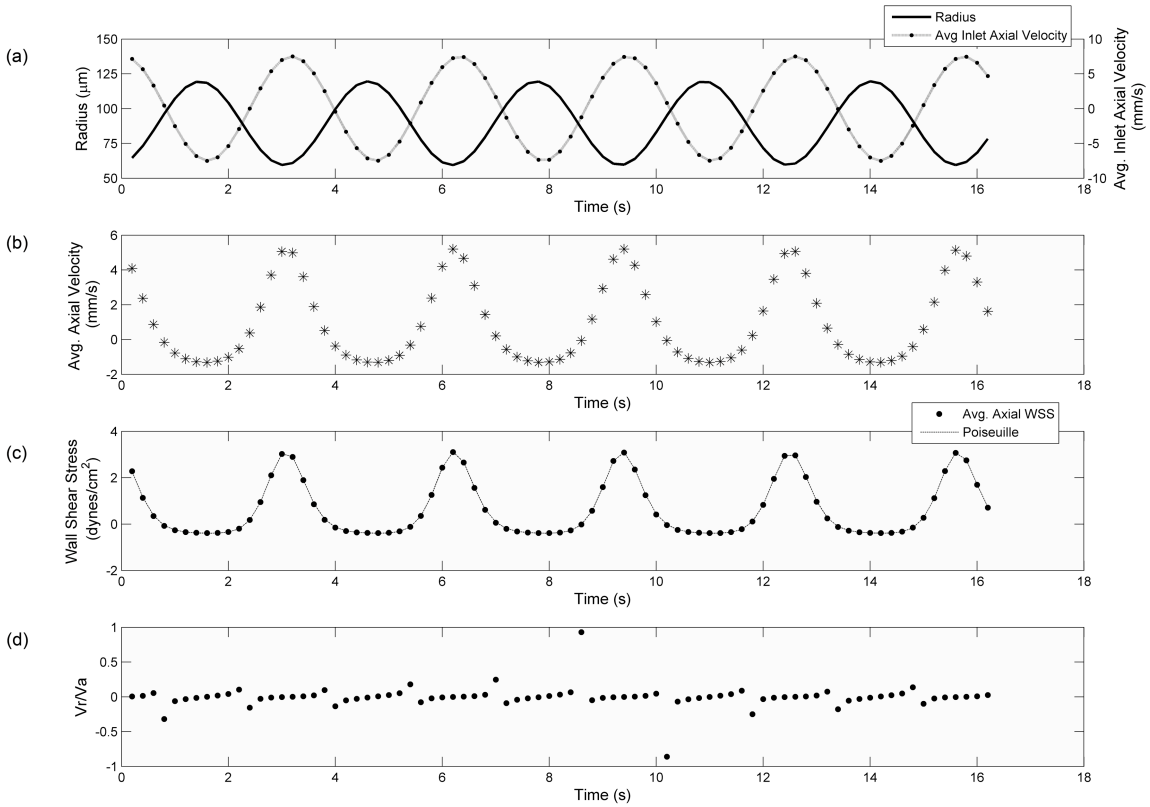

Figure 4.4. Results from periodic sinusoidal wall motion (T=3.2s) with an unsteady parabolic inlet velocity ($-7.5 < v_{inlet} < 7.5$ mm/s). a) Vessel radius (line) and inlet axial velocity (dotted line) values used as boundary conditions, b) Resulting average axial velocity in contracting segment, c) Average axial wall shear stress (dot) and quasi-static Poiseuille (dotted line) values, d) Radial to axial velocity ratio.

Table 4.3. Results from simulations with periodic and skewed sinusoidal wall motion and unsteady inlet velocities. Periodic wall motion ($60 < R < 120$) and skewed wall motion ($40 < R < 60$) had the same time period (T=3.2 s) and unsteady inlet velocities. Differences between axial wall shear stress and Poiseuille were averaged over time for these unsteady cases.

Wall Motion	Inlet Velocity (mm/s)	Axial Wall Shear Stress (dynes/cm^2)	Poiseuille Shear Stress (dynes/cm^2)	Max. |Vr/Va| Ratio	Avg. % Diff WSS	Max. % Diff WSS
Periodic $60 < R < 120$	$-1.9 < v_{inlet} < 1.9$	$-0.12 < \tau_w < 0.81$	$-0.12 < \tau_{poiseuille} < 0.81$	1.36	0.4%	1.4%
Periodic $60 < R < 120$	$-7.5 < v_{inlet} < 7.5$	$-0.38 < \tau_w < 2.96$	$-0.39 < \tau_{poiseuille} < 2.97$	0.86	0.7%	2.0%
Periodic $60 < R < 120$	$-15 < v_{inlet} < 15$	$-0.80 < \tau_w < 5.94$	$-0.81 < \tau_{poiseuille} < 5.97$	0.58	0.8%	2.0%
Skewed $40 < R < 60$	$-1.9 < V_{inlet} < 1.9$	$-0.80 < \tau_w < 3.34$	$-0.80 < \tau_{poiseuille} < 3.35$	0.095	0.2%	0.5%

Simulations with In Situ Diameter and Inlet Velocity Values: To investigate how well our radially expanding and contracting tube emulated physiological conditions, we used data from *in situ* experiments as boundary conditions for the CFD model. The inlet velocity and diameter waveform applied as boundary conditions are shown in Figure 4.5a. The resulting axial velocity calculated by the model was compared to the axial velocity measured *in situ* (Figure 4.5b). The general shape of the velocity waveform was reconstructed by the CFD model, but there remained some regions with larger discrepancies. These regions did not correlate to the times where the Vr/Va ratio was high (Figure 4.5d), but instead correlated to periods of rapid contraction/expansion (i.e. Vr was relatively high, but Va was not low). Note that contraction caused the CFD and

Poiseuille estimates of wall shear stress to be too high, while expansion caused them to be too low. At other time points, the wall shear stress estimates were within 4% of the quasi-static Poiseuille values.

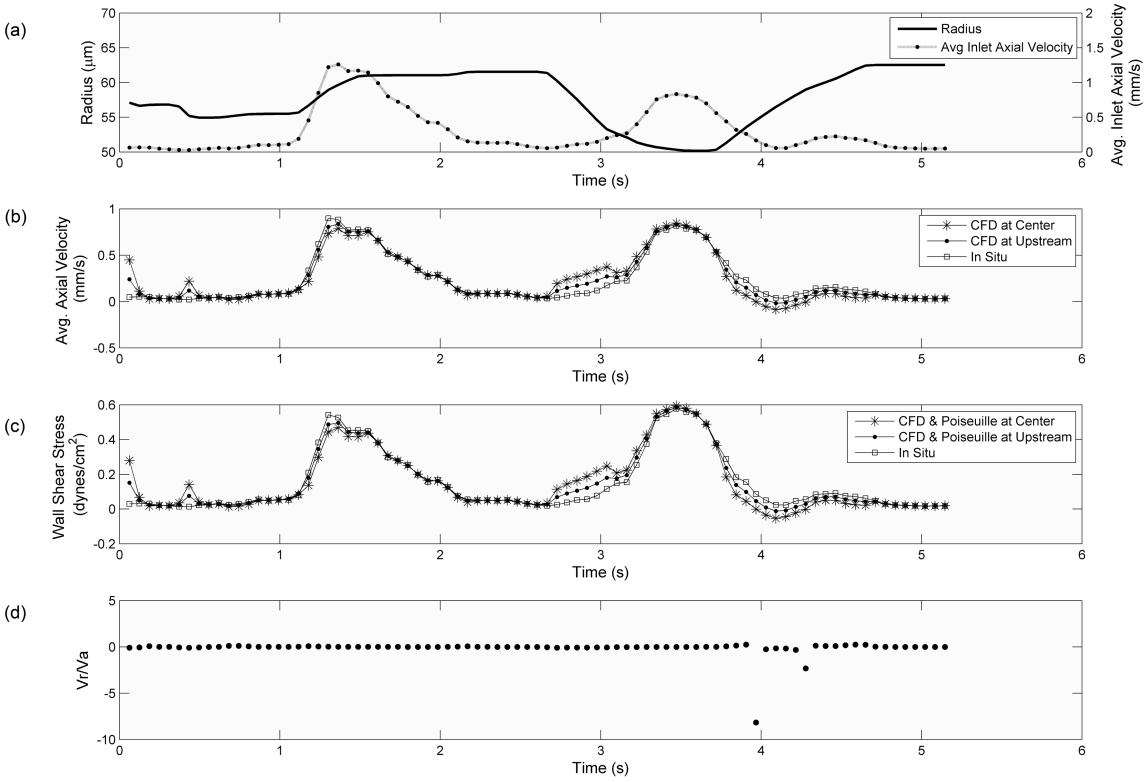

Figure 4.5. Results from physiological wall motion and inlet velocities obtained from *in situ* experiments. a) Vessel radius (line) and inlet axial velocity (dotted line) values ($0.028 < v_{inlet} < 1.28$ mm/s) applied as boundary conditions, b) Average axial velocity in contracting segment at the center (asterisks) and upstream locations (dots) compared to *in situ* velocity (square) values, c) Average axial wall shear stress values from CFD model at the center (asterisks) and upstream (dot) locations, corresponding quasi-static Poiseuille (line) values, and wall shear stress estimated from *in situ* data (squares) d) Radial to axial velocity ratio. The CFD result deviates from *in situ* result at times of rapid contraction or expansion. These deviations are due to our estimate of inlet velocity. It appears that the *in situ* data was taken at a location further upstream of the contracting segment (i.e. closer to the inlet).

To verify if Poiseuille flow conditions persisted during the periods of significant wall motion (i.e. high radial velocities) we investigated the velocity profiles at four time points during the physiologic simulation (Figure 4.6); with positive and negative radial velocities (Vr =+10, +14 and -20 μm/s). Velocity profiles were evaluated at three axial locations from the contracting segment, namely the center, upstream and downstream planes. The upstream and downstream planes were located 125 μm from the center plane. The velocity profiles at all locations and time points were parabolic in nature and had quadratic curve fits with $R^2 > 0.99$. This supports that Poiseuille flow conditions are maintained during the entire lymphangion contractile cycle.

Discussion

The investigation of flow patterns through natural and implanted conduits is commonly pursued because of the substantial evidence linking fluid dynamics to cellular response. Most previous models of lymph flow are one-dimensional and only provide information on flow and pressure through a lymphangion. This is the first 3D model of lymph flow that solves for velocity and wall shear stress throughout the contractile cycle. Our results strongly support the use of Poiseuille for wall shear stress calculations, since these estimations will be within 4% of the value calculated in a fully dynamically expanding tube under typical lymphatic flow conditions. Our results further show that the Vr/Va ratio, though high at times during the contractile cycle, does not invalidate the Poiseuille assumption. This is likely due to the low Reynolds numbers associated with lymphatic flow.

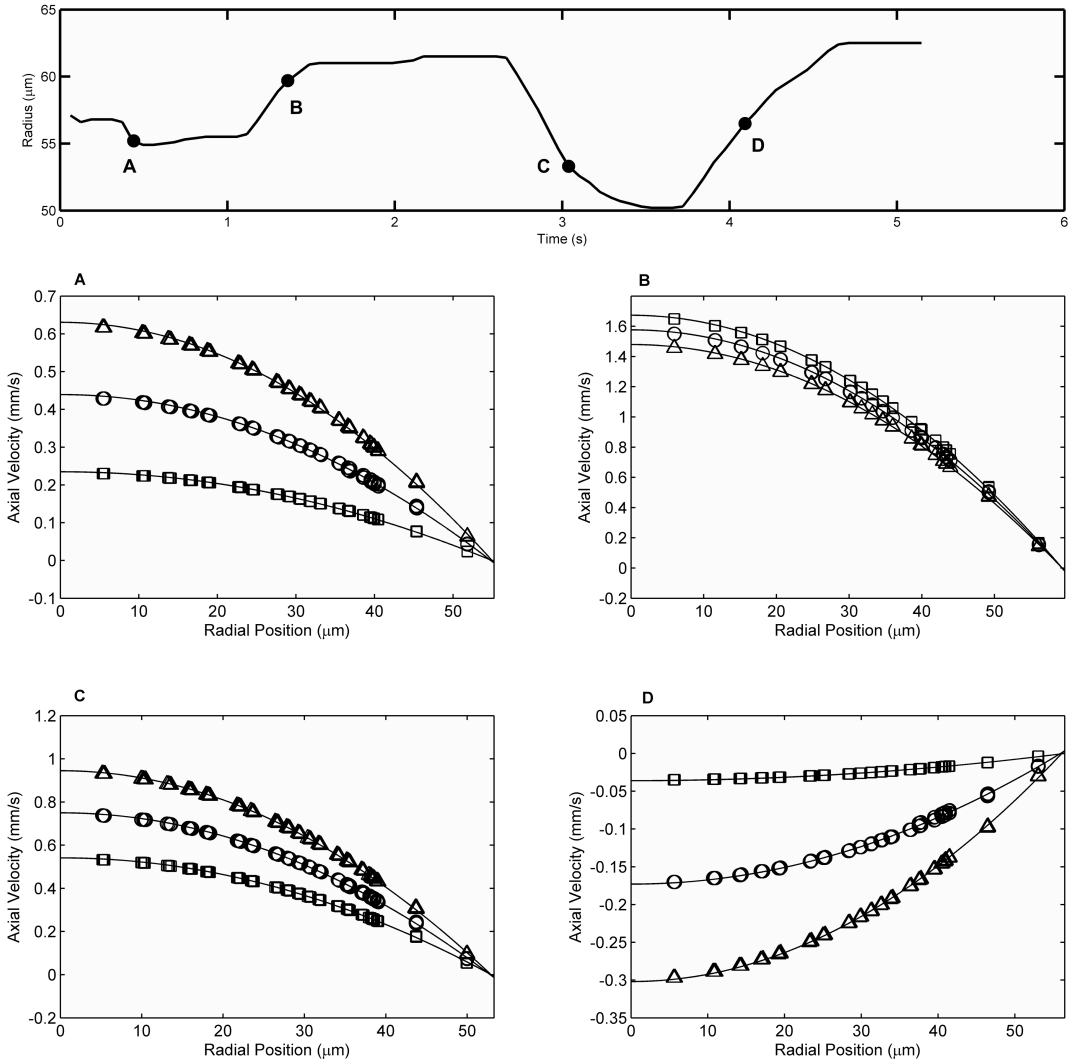

Figure 4.6. Velocity profiles for the physiologic case at four time points experiencing high wall motion. The radius plot for the physiologic case is shown with the 4 time points labeled A, B, C, and D. Velocity profiles where taken from the upstream (squares), center (circles) and downstream (triangles) planes in the contracting segment and fit with a quadratic curve (solid line). Upstream and downstream planes were 125 μm from the center plane. (A) time = 0.44 s, R = 55.2 μm, Vr = -20 μm/s (B) time = 1.36 s, R = 59.7 μm, Vr = +10 μm/s (C) time = 3.04 s, R = 53.3 μm, Vr = -20 μm/s (D) time = 4.09 s, R = 56.5 μm, Vr = +14 μm/s. All curve fits resulted in R^2>0.99. This illustrates that the velocity profile remains parabolic throughout the simulation, even during periods of severe wall motion. Hence, the Poiseuille assumption remains valid along the axial length of the contracting segment.

The simulations presented in this paper illustrate the differences between steady and unsteady inlet conditions and different types of wall motion. The CFD results closely matched Poiseuille values for velocity and wall shear stress for all simulations except the one with *in situ* boundary conditions. We believe that the discrepancies observed between the CFD result and *in situ* velocity values were due to the applied inlet velocity boundary condition. Given that we had to estimate the inlet velocity from the *in situ* data without knowing the actual lymphangion length may have caused some error. It can be difficult to determine the exact relative axial position or lymphangion length of the *in situ* measurements, as the field of view generally does not contain both valves. Upon closer investigation, it is evident that the results from the center plane do not correspond as precisely to the *in vivo* velocity and shear stress values during rapid dilation and contraction. Showing shear stress estimates from the center plane of the contracting segment facilitates the internal comparison to the Poiseuille estimation, but not necessarily to the *in situ* measurements. To verify this, we analyzed a region 125 μm upstream from the center of the lymphangion. The velocity and shear stress values at this upstream location were much closer to the *in situ* result, suggesting that the *in situ* experiment was taken at an axial location closer to the inlet of the lymphangion, as shown in Figure 4.5. Poiseuille values remained to be a good estimate for wall shear stress (<4% error) at this upstream location. Furthermore, the verification of parabolic velocity profiles at the upstream, center and downstream planes during periods of significant wall motion strongly suggests the presence of Poiseuille flow during the entire lymphangion contractile cycle (Figure 4.6). It is important to note that an error in

diameter or flow rate measurements could lead to much greater errors in wall shear stress (>20%). The errors presented in this paper from the simulations are much smaller; hence, Poiseuille is a fair estimate for wall shear stress in non-valvular regions of the lymphangion.

The work by many investigators (Bohlen et al., 2009; Dixon et al., 2006; Quick et al., 2007; Zawieja, 2009), including us, has demonstrated that wall shear stress likely plays a large role in regulating lymphatic contractility through its actions on the endothelium. As seen by the simulations, wall shear stress values were highest when vessel diameter was at a minimum and lowest during vessel dilation. Although our wall motion was defined as a function of time only, future work could incorporate wall motions that are dependent on pressure, shear stress and time. Such simulations could provide better insights on how wall motion is linked to changes in shear stress and consequently nitric oxide production as illustrated by Bohlen et al. (2009).

It is important to note that our model has a few limitations. Lymph was modeled with the same viscosity and density as water, as is commonly assumed. While lymph may be slightly more viscous, our results would not change by much due to flow remaining in the strongly laminar regime (very low Reynolds and Womersley numbers) and not in the realm of transitional flow. Furthermore, our CFD model does not account for non-uniform contractions as they may occur in vivo. In terms of geometry, lymphatic vessels are predominantly straight and cylindrical with the exception of the valve areas. Therefore, our model is not appropriate for studying flow near lymphatic valves, nor did we include valves in our single lymphangion. We also neglected the potential effects of

lymphocytes and other cells suspended in lymph. Inclusion of low volume fractions of suspended cells (typical of lymph) would not be expected to affect the conclusions of this study.

In summary, our results show that a simple radially expanding and contracting cylindrical tube can emulate lymphatic contractions and lymph flow rates observed experimentally and that Poiseuille flow provides a reasonable estimate for wall shear stress, within 4%.

CHAPTER V

CHARACTERIZATION OF THE PASSIVE PRESSURE-DIAMETER RELATIONSHIP OF A LYMPHANGION

Overview

Lymphatic vessels are distensible vessels with the ability to contract intrinsically to propel fluid towards the systemic blood circulation. In general, lymph flow depends on both the rate of lymph production by tissues and organs and the passive and active driving forces of the pump. The passive driving forces can be generated by deformations of adjacent tissues such as respiratory movements, arterial pulsations and skeletal muscle contractions. The passive properties of lymphangion walls and the ability of valves to prevent reflux are closely related to lymph flow driven by extrinsic forces. We therefore aim to characterize the passive mechanical properties of a lymphangion in both mid-lymphangion and valve segments. Passive pressure-diameter relations of lymphangions will be evaluated and supplemented by images of the structural composition of the vessel wall using nonlinear optical microscopy techniques. These experimental results will then be used to develop a model for the passive properties of lymphangions, which will greatly enhance our knowledge of lymphatic vessel behavior.

Introduction

The lymphatic system is responsible for the transport of fluid, proteins, lipids and immune cells throughout the body. Fluid transport begins at the interstitium where lymph enters the initial lymphatics and is further propelled by collecting lymphatic

vessels via intrinsic and extrinsic pumping mechanisms, together with valves to prevent retrograde flow. Intrinsic pumping refers to the ability of the vessels to contract independently due to the presence of muscle cells in the vascular wall. These muscle cells tend to possess characteristics of smooth and cardiac muscle cells. Extrinsic pumping, on the other hand, relies on the compression of lymphatic vessels due to pulsations of blood vessels or contractions of surrounding tissues. Most studies have illustrated fluid transport by the intrinsic pump from the rat mesentery, thoracic and cervical areas. (Gashev, 2008; Zawieja et al., 2011). They further characterize the intrinsic pump to be a combination of phasic (rapid) and tonic (slow, long-lasting) contractions (Zawieja et al., 2011). On the other hand, lymphatic vessels from skeletal tissue beds rely more on the extrinsic pump than lymphatic vessels from other tissue beds (Skalak et al., 1984). It is without question that these pumping mechanisms are crucial to the transport of lymph. However, there remain many unanswered questions on the exact mechanisms of autoregulation of lymph flow.

Collecting lymphatic vessels typically experience 40-60% changes in diameter through a single contractile cycle (Dixon et al., 2006). Given this dynamic and compliant nature of the vessels, it is important to characterize these cyclic mechanical deformations of the wall and the intrinsic mechanical properties of a lymphangion. These mechanical properties are essential factors influencing the distribution of lymph volume. To date, constructive modeling of the lymphatic vasculature has been difficult because of the complexity of performing experiments on lymphatic vessels. First, these vessels are very small, on the order of 100 μm, and they are nearly transparent. Moreover, they are thin

walled and usually in deep tissue and hard to isolate. Recent reports have illustrated the non-homogenous distribution of muscle cells within the vessel wall (Gashev, 2002; Gashev, 2008; Zawieja, 2009; Zawieja et al., 2011). It is assumed that collagen and elastin are the other dominant components of the vessel wall but there are no reports of their contribution to vessel properties. Therefore, there is a need to determine the structure of lymphatic vessels and better characterize their passive mechanical properties.

Ohhashi et al. (1980) studied the active and passive mechanical properties of bovine mesenteric lymphatics (vessel diameter ~3 mm) via a series of pressure-volume and pressure-radius relations. Their findings suggested that smooth muscle cells play a role in the elastic behavior of the lymphangion. They even further state that spontaneous activity of lymphatic smooth muscle is regulated by not only stretch but also the rate of deformation. However, their analysis lacked computational modeling techniques to characterize this behavior. Venugopal et al. (2010), on the other hand, described a mathematical model illustrating the nonlinear pressure-volume relation of lymphatic vessels with a piecewise-function. While this is a good first attempt, better models – particularly those using "continuous" functions are more suitable for mechanical characterization. Numerous studies and models have been developed for arterial microcirculation and the roles of myogenic, shear and metabolic responses on autoregulation of blood flow (Carlson and Secomb, 2005; Carlson et al., 2008; Zulliger et al., 2004). However, none of these have been adapted to describe lymphatic microcirculatory autoregulation.

In this section, we aim to develop a theoretical model to characterize the passive properties of the lymphatic wall at the valve and the two adjacent straight segments (i.e. upstream and downstream of the valve) along the axial length of a lymphangion. Furthermore, we will examine the distribution of collagen and elastin at these three regions of interest to better correlate the vascular properties with the mechanics of the lymphangion.

Materials & Methods

Vessel Isolation: Male Sprague-Dawley rats (150-300 g) were anesthetized with an intraperitoneal (IP) injection of sodium pentobarbital (60 mg/kg) and a loop of intestine was exteriorized. Lymphatic vessels (80-180 mm) were dissected from the mesentery and placed in albumin physiological saline solution (APSS) at room temperature. APSS contained (in mM): 145.0 NaCl, 4.7 KCl, 2.0 $CaCl_2$, 1.2 $MgSO_4$, 1.2 NaH_2PO_4, 0.02 EDTA, 5.0 glucose, 2.0 sodium pyruvate, 3.0 3-(*N*-morpholino) propanesulfonic acid and 0.5 g/100 ml purified bovine serum albumin (pH = 7.4 at 37^{o}C). All chemicals were obtained from Sigma (St. Louis, MO) except albumin (Product #10856, U.S. Biochemicals, Cleveland, OH). A venule and arteriole of comparable size were also isolated to serve as a point of reference for comparison. Animals were subsequently euthanized with Nembutal (120 mg/kg). All animal protocols were approved by the University of Missouri Animal Care and Use Committee and conformed to the Public Health Service Policy for the Humane Care and Use of Laboratory Animals (PHS Policy, 1996).

Isolated lymphatic segments with one valve were cannulated at each end with a glass micropipette, filled with APSS (~3 mL chamber) and held in a Lucite holder mounted on a Burg-style V-track system (Duling et al., 1981). The entire apparatus was then transferred to the stage of an inverted microscope (Inverted Zeiss ACM equipped with Zeiss 3.2x and 6.3x objectives). Input and output pressures (P_{in} and P_{out}, respectively) were initially set from standing reservoirs and the axial length of the vessel was adjusted so that there was no slack in the vessel with P_{in} and P_{out} temporarily set to ~13 cmH_2O; this ensured no buckling of the vessel at higher pressures. A continuous flow of heated APSS (2 ml/min) prevented changes in osmolarity associated with evaporation.

Pressure-Diameter Protocol: An in-house LabVIEW (version 2010, National Instruments, Austin, TX) program was used to acquire high-resolution video of the entire pressure-diameter experiment including measurements of internal vessel diameter, inlet and outlet pressures (Davis, 2005). The vessel image was digitized with a high-resolution (0.5-1 μm/pixel; 1624x510 pixels) firewire camera (Basler AG, model A641FM; Ahrensburg, Germany) at 28-30 Hz. P_{in} and P_{out} were measured using low-pressure transducers (CyberSense model 104; Nicholsville, KY) and digitized in synchrony with diameter data at 60 Hz using an A-D card (model PCI 6030e; National Instruments, Austin, TX). Each lymphatic vessel was allowed to equilibrate and exhibit spontaneous contractions at 37°C before the start of experimentation to ensure normal behavior. The chamber bath was flushed and replaced with Ca^{2+}-free physiologic saline (replaced $CaCl_2$ with 3 mM EDTA). P_{in} and P_{out} were then ramped at a constant rate of

~4 cmH_2O/minute from 0-20 cmH2O, resulting in the passive pressure-diameter curve. A total of 9 mesenteric lymphatic vessels were tested.

Video Post-Processing: The video images from all experiments were recorded in an AVI file along with embedded pressure and diameter data, so that all the measured parameters could be replayed and reprocessed offline at three sites along the vessel: upstream of the valve, valve sinus, and downstream of the valve. The video was compressed (5:1) without degrading the image quality using a lossless Lagarith video codec. Internal diameters were normalized with respect to each region's respective maximum passive diameter (at pressure = 20 cmH_2O) and plotted against pressure.

Modeling Passive Response: Passive pressure-diameter relations were modeled using the following function, shown below:

$$P_{passive}(D) = P_0\left(\exp\left[S_p\left(D/D_0 - 1\right)\right] - 0.001\left(D/D_0\right)^{-3} + 0.05\right) \quad \text{(Equation 5.1)}$$

where P_o is the passive pressure parameter, S_p is the passive sensitivity parameter of the vessel, D is vessel diameter normalized to D_o, which is the maximum passive diameter observed experimentally (i.e. at pressure = 20 cmH_2O). The exponential term represents the passive response at higher pressures and the cubic term models the collapsible behavior at low pressures (i.e. "tube law"). A nonlinear least squares regression analysis was performed in Matlab (version 2010b, MathWorks Inc., Natick, MA) to obtain the "best fit" coefficients for each region of interest; P_o and S_p were bounded so that their values remained positive. Parameter values were then compared for each region (upstream, valve, downstream) to determine if there was any regional variation.

Fixed Vessel Preparation: Lymphatic vessels were isolated from the rat mesentery and pressure fixed at low and high pressures (2 and 7 cmH_2O, respectively) with formalin and/or formaldehyde and then stored in physiologic saline solution (PSS) at 4°C until imaging. The vessels were mounted on 2.4% agarose wells, such that the vessel was straight and valve could be easily viewed. Efforts were made to mount the vessels at the same level of axial stretch. The vessels were submerged in PSS while imaging at room temperature.

Nonlinear Optical Microscopy: The custom built-NLOM system has been previously described by Larson and Yeh (2006). Briefly, sub-10-fs pulses (800 nm, 133-nm full width at half maximum) from a Kerr lens mode-locked Ti:Al2O3 oscillator (Femtosource, Femtolasers, Cambridge, MA) pumped by a frequency-doubled Nd:YVO4 solid-state laser (Verdi, Coherent, Santa Clara, CA) were coupled into an epifluorescence port of an upright microscope (Axioskop2 MAT, Carl Zeiss, Thornwood, NY) via dual-axis galvanometer-driven mirrors (Cambridge Technology, Lexington, MA). The laser beam was directed to the microscope objective (20x Achroplan, numerical aperture: 1.0, water immersion, Carl Zeiss) by a short-pass dichroic mirror (635dcspxruv3p, Chroma, Rockingham, VT). Nonlinear optical signals were directed by the objective through one of two accessory ports on the binocular head to a custom-built dual-channel detector housing two dichroic mirrors and band-pass filters (Chroma), focusing lenses (31 2321, Linos Photonics, Milford, MA), and a pair of photon-counting photomultipliers tubes (R7400P, Hamamatsu, Bridgewater, NJ). Second harmonic generation (SHG) and two photon fluorescence (TPF) signals were

separated with a long-pass dichroic mirror (430dcxru, Chroma) and band-pass filters (HQ405/40 and HQ480/40, respectively, Chroma). Photomultiplier tubes were connected to a pre-amplifier/discriminator (F-100T, Advanced Research Instruments, Golden, CO), which thresholds signal current and converts it to transistor-transistor logic pulses for photon counting. The entire NLOM system was placed on a vibration-isolated optical table. We imaged each vessel at three locations: upstream of the valve (250-300 μm from valve), the valve sinus and downstream of the valve (250-300 μm from valve) with a 0.5 μm step size in the z-direction (i.e. z-step). SHG and TPF signal components were imaged and segmented simultaneously to obtain images of fibrillar collagen (types I and III) and elastin, respectively.

Image Processing: Matlab (version 2010b, MathWorks Inc., Natick, MA) and ImageJ (NIH) were used to process the image stacks obtained from the nonlinear optical microscope. Images were converted from 16 to 8 bit and the signals from the SHG and TPF were isolated to represent the collagen and elastin components, respectively. Median and Gaussian filters were used to remove noise and the image stacks were normalized to allow for appropriate comparisons. Mean SHG and TPF signals were used to calculate collagen to elastin ratios (C:E ratio) from individual slices. Full width half maximum calculations of each signal were performed to obtain collagen and elastin layer thickness through the wall.

Statistical Analysis: The coefficients obtained from the "best fits" were recorded and presented in Table 5.1 as the mean ± standard error (SE). We evaluated differences between coefficients from the 3 areas (valve sinus, upstream and downstream) for

statistical differences using a paired student t-test with Bonferroni correction (95% confidence level).

Results

Lymphatic vessels exhibited a highly nonlinear pressure-diameter response at very low pressures compared to arterioles and venules of comparable size (Figure 5.1). Lymphatic vessels would experience a sharp transition around 5 cmH_2O, whereas venules would experience this more gradually between 10 and 15 cmH_2O; arterioles did not illustrate such behavior within the pressure range shown here (Figure 5.1).

The passive properties of the lymphangions were modeled with a two-parameter equation, described in the Methods section (Equation 5.1). The mean values for P_o and S_p across all regions were 17.68 ± 0.629 cmH_2O and 22.17 ± 2.56, respectively. The parameter values for each region are listed in Table 5.1. There is a slight increase in the mean value of S_p as you move from the upstream to downstream regions of the vessel. However, statistical analysis did not reveal any significant differences between regions (p-value > 0.05). The curve fits obtained with the model had $R^2 > 0.9$; representative images of the curve fits for one vessel are shown in Figure 5.2.

Images from the nonlinear optical microscope revealed a predominantly elastin valve leaflet with collagen and elastin embedded throughout the rest of the vessel wall in a distinct outer/inner layer arrangement. The valve leaflets were bicuspid in nature and had collagen bands oriented in the axial direction at the insertion points and buttresses (i.e. locations where the valve meets the vessel wall). This suggests that the collagen fibers provide additional support to prevent valve inversion. Collagen fiber structures in

vessels fixed at low pressure (2 cmH_2O) were more undulated than at high pressures (7 cmH_2O), as was expected (Figures 5.3-5.8). Collagen layer thickness was 7.4 μm, on average, and we could not detect a significant change with increasing pressure. Elastin layer thickness, however, decreased from 11.1 μm in low pressure fixed vessels to 8.2 μm in high pressure fixed vessels, on average (Table 5.2). This decrease in elastin layer thickness follows from the incompressible nature of the vessel. Collagen to elastin ratios (C:E) were estimated using the mean signal from a single slice in the central plane of the lymphangion. The C:E ratio was larger in the low pressure-fixed vessels (0.9 compared to 0.7), but we believe that this is not a true indication of C:E content. Our results did not indicate a significant difference between collagen and elastin compositions between the three regions (i.e. upstream, valve, downstream) of the lymphangion.

Table 5.1. Best-fit parameters for passive pressure-diameter model. Results are reported as mean ± standard error.

	P_o (cmH_2O)	S_p
Upstream	18.00 ± 0.57	20.42 ± 5.25
Valve	17.28 ± 0.74	21.74 ± 2.89
Downstream	18.09 ± 0.72	24.58 ± 2.49

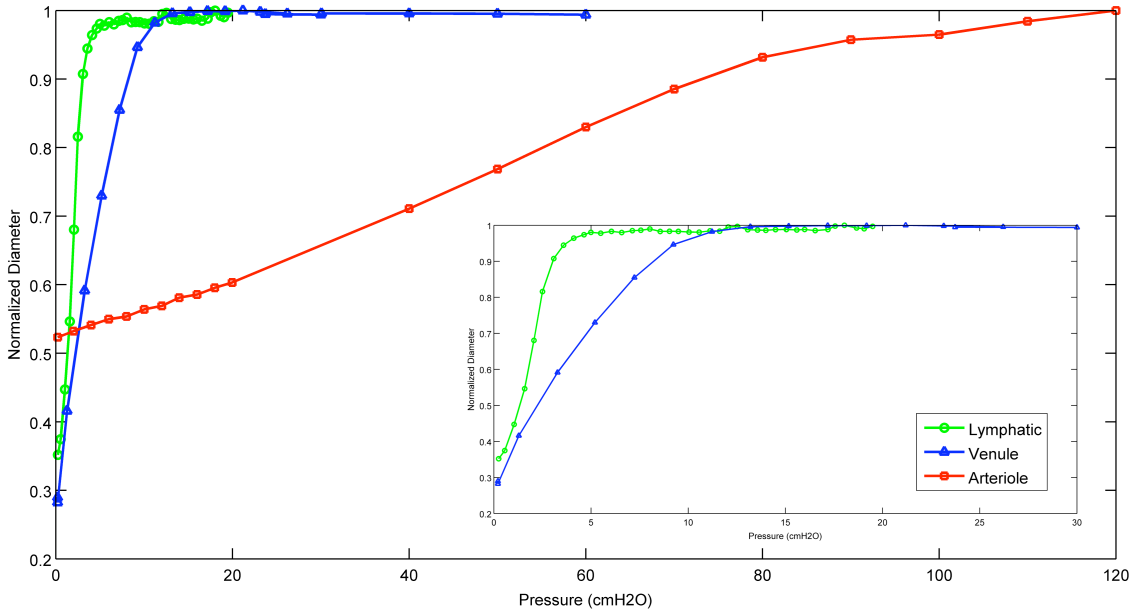

Figure 5.1. Pressure-diameter relations of the vasculature. Lymphatic vessel (green circles), venule (blue triangles), and arteriole (red squares) of comparable size (d~180-280 μm) were isolated from the rat. The lymphatic vessel operates at the lowest pressure range (0-5 cmH_2O), approximately 1/3 of the venule pressure range, and exhibits the sharpest transition from low to higher pressures, clearly seen in the inset (zoomed in to pressure values of 0-30 cmH_2O). The sharp nonlinear transition is not observed in venules and arterioles.

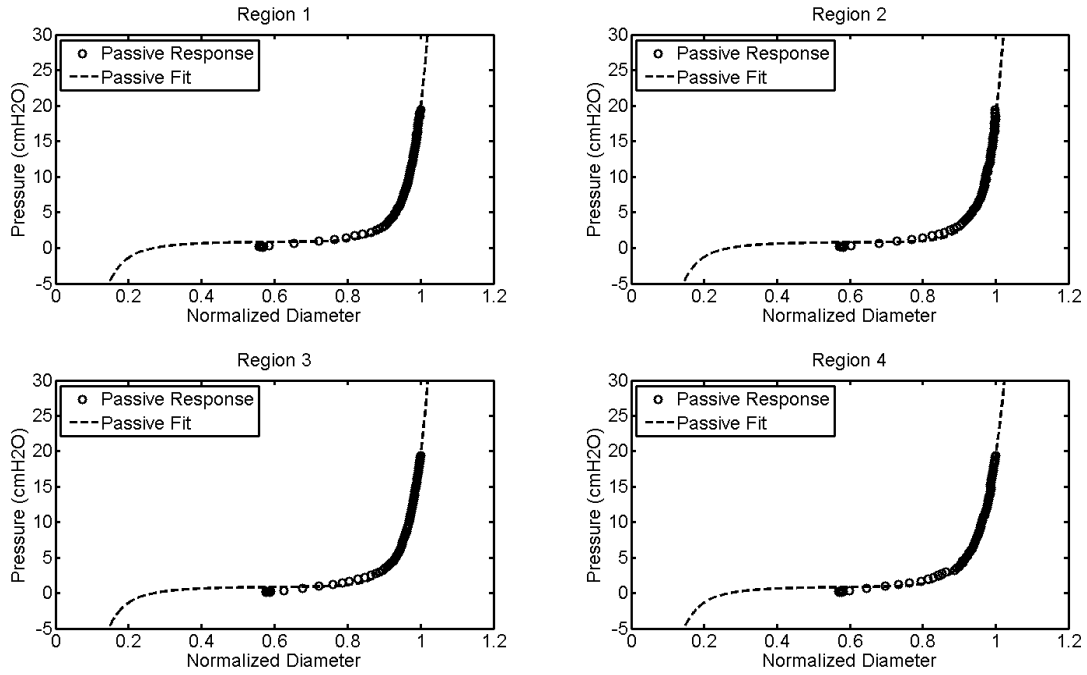

Figure 5.2. Passive curve fits at four regions along a lymphangion. Regions 1 and 2 correspond to upstream locations (260 µm and 170 µm from valve, respectively), Region 3 is at the valve site and Region 4 is 200 µm downstream of the valve.

Table 5.2. Summary of collagen and elastin layer thicknesses and C:E ratio.

	Pressure = 2 cmH_2O			**Pressure = 7 cmH_2O**		
	Collagen Thickness (µm)	**Elastin Thickness (µm)**	**C:E Ratio**	**Collagen thickness (µm)**	**Elastin thickness (µm)**	**C:E Ratio**
Upstream	7.36	10.71	0.69	7.01	6.79	0.92
Valve	7.62	11.36	0.77	5.99	8.99	0.82
Downstream	7.24	11.32	0.73	9.38	9.03	0.98
Average	7.40	11.13	0.73	7.46	8.27	0.91

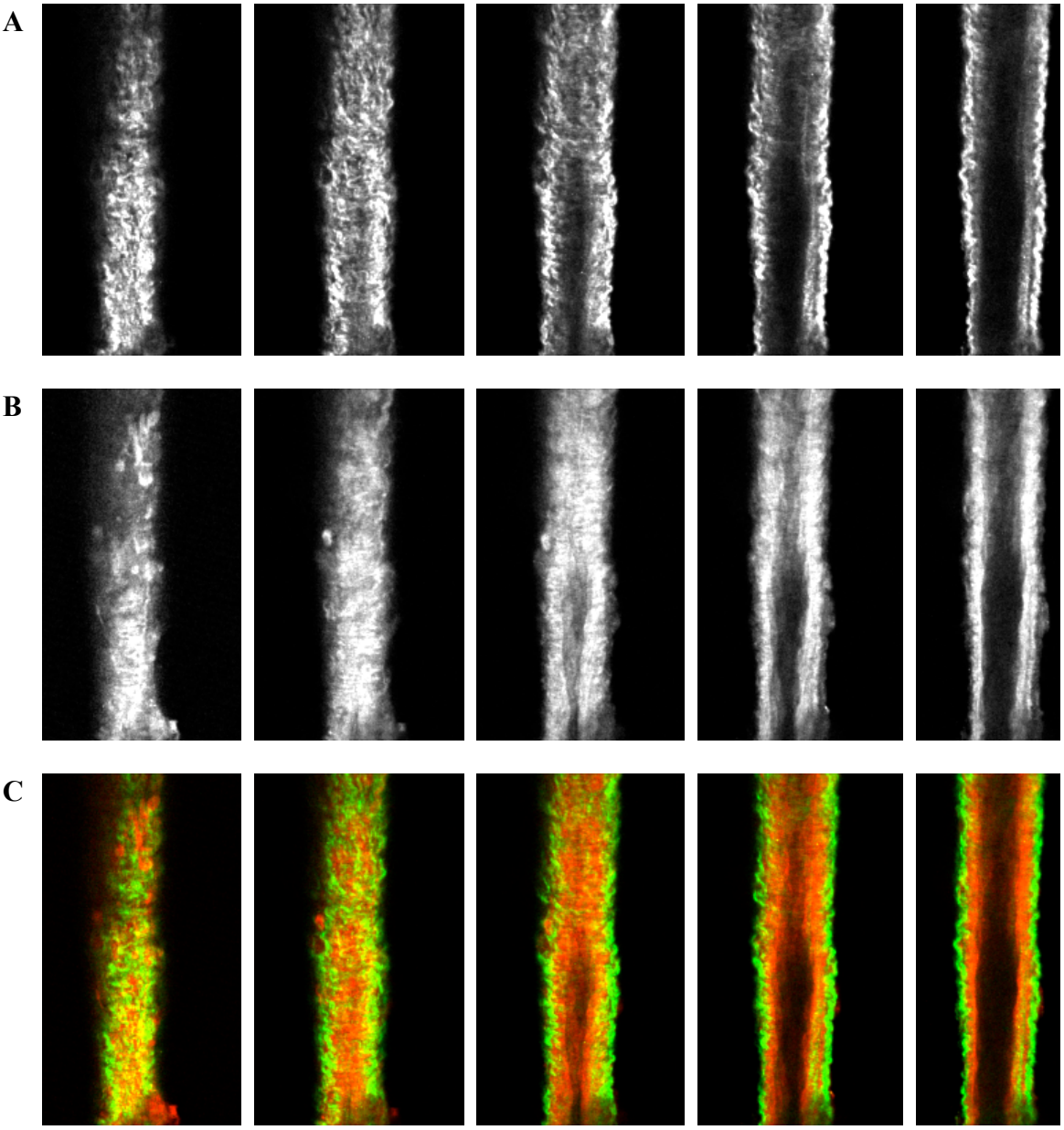

Figure 5.3. NLOM images of upstream segment at low pressures. The vessel pressure fixed at 2cmH_2O was imaged 250µm upstream of valve. (A) SHG signal representing collagen structure, (B) TPF signal representing elastin, and (C) Overlayed images of SHG and TPF signals (Collagen in green, Elastin in red). Each slice is ~7µm apart and vessel diameter ~ 90 µm.

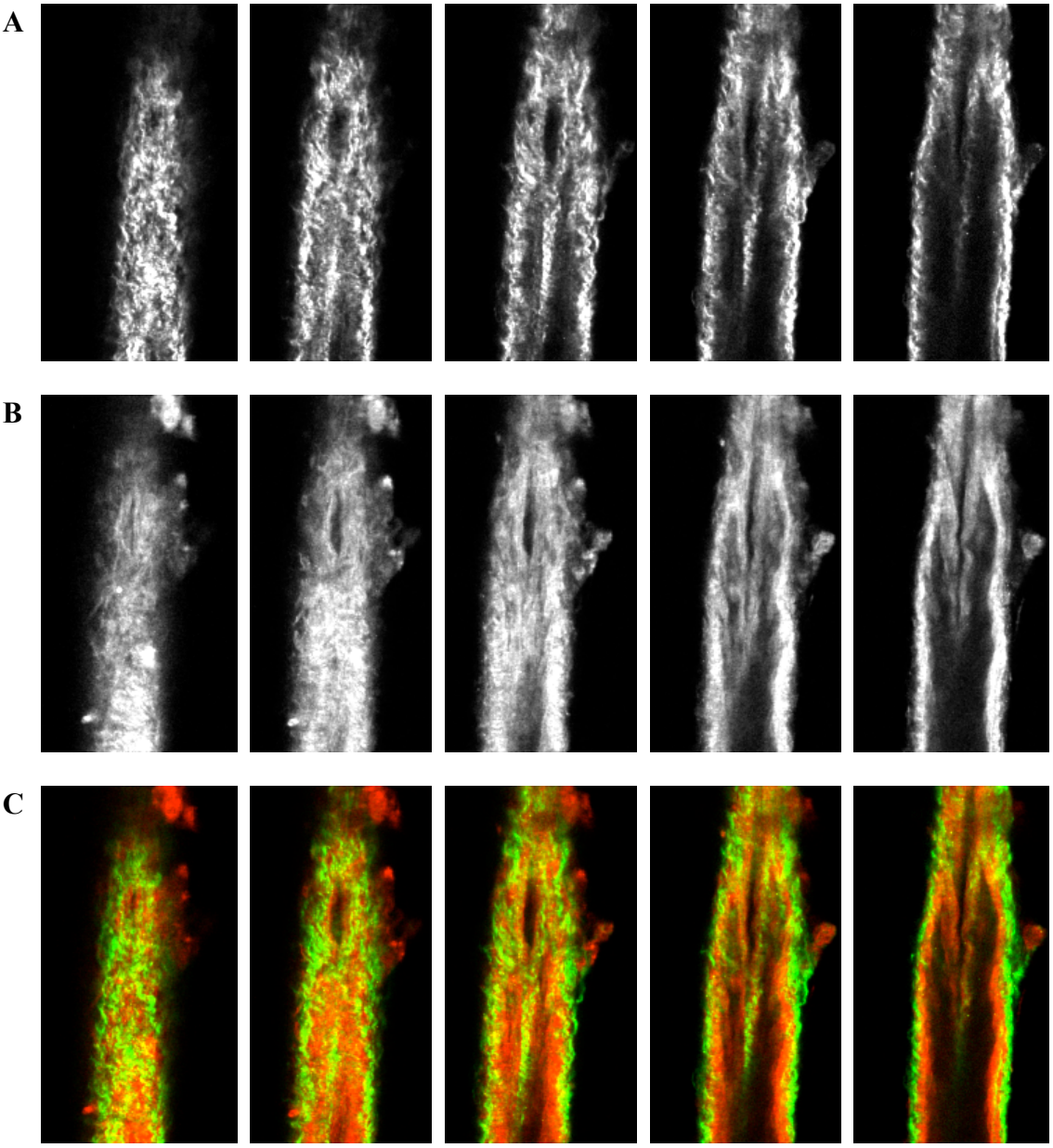

Figure 5.4. NLOM images of valve segment at low pressures. The vessel pressure fixed at 2cmH_2O was imaged at the valve. (A) SHG signal representing collagen structure, (B) TPF signal representing elastin, and (C) Overlayed images of SHG and TPF signals (Collagen in green, Elastin in red). Each slice is ~7µm apart and vessel diameter ~ 110 µm.

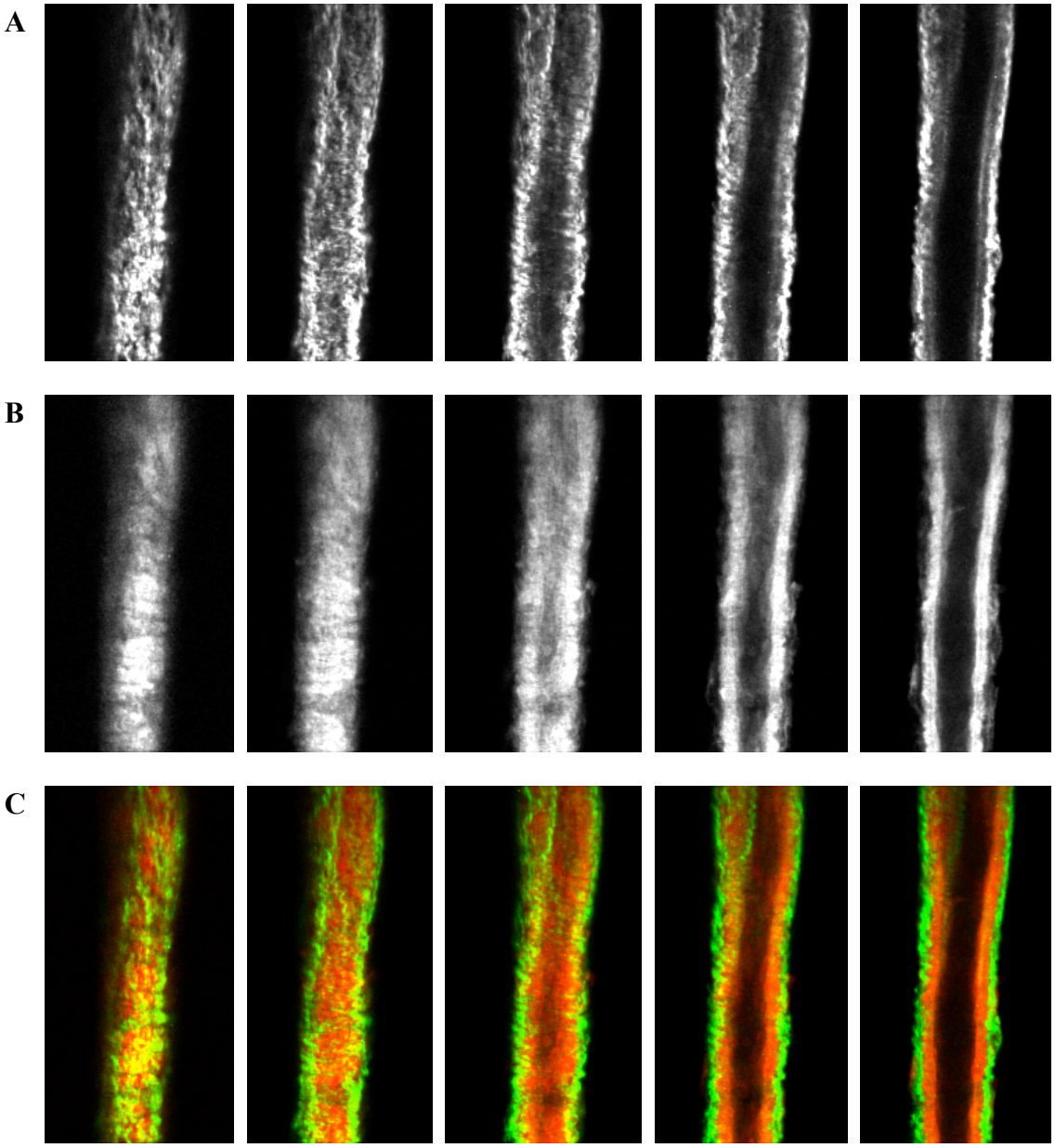

Figure 5.5. NLOM images of downstream segment at low pressures. The vessel pressure fixed at 2cmH_2O was imaged 250 µm downstream of the valve. (A) SHG signal representing collagen structure, (B) TPF signal representing elastin, and (C) Overlayed images of SHG and TPF signals (Collagen in green, Elastin in red). Each slice is ~7µm apart and vessel diameter ~ 90 µm.

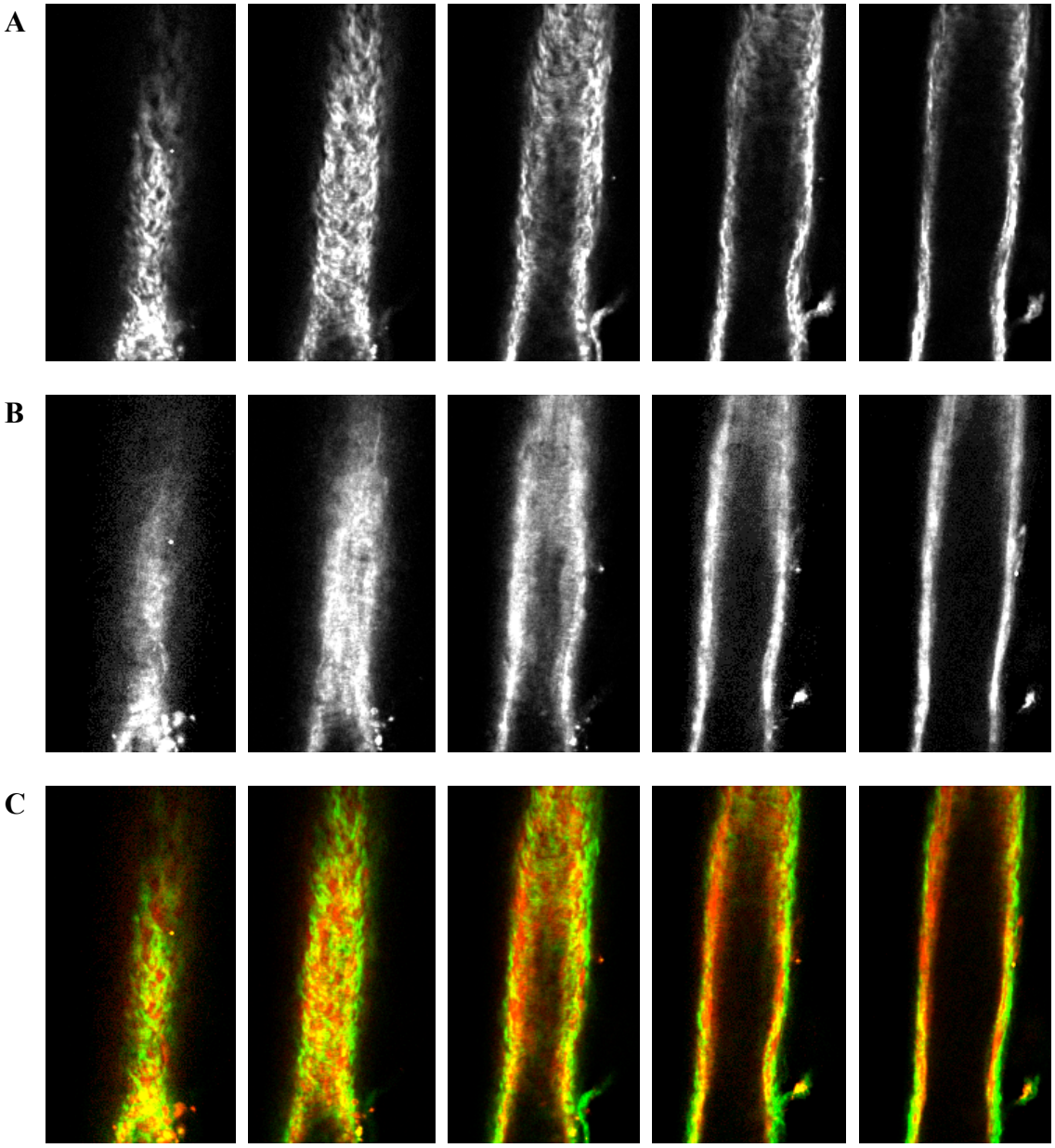

Figure 5.6. NLOM images of upstream segment at high pressures. The vessel pressure fixed at 7cmH_2O was imaged 275 µm upstream from the valve. (A) SHG signal representing collagen structure, (B) TPF signal representing elastin, and (C) Overlayed images of SHG and TPF signals (Collagen in green, Elastin in red). Each slice is ~7µm apart and vessel diameter ~ 110 µm.

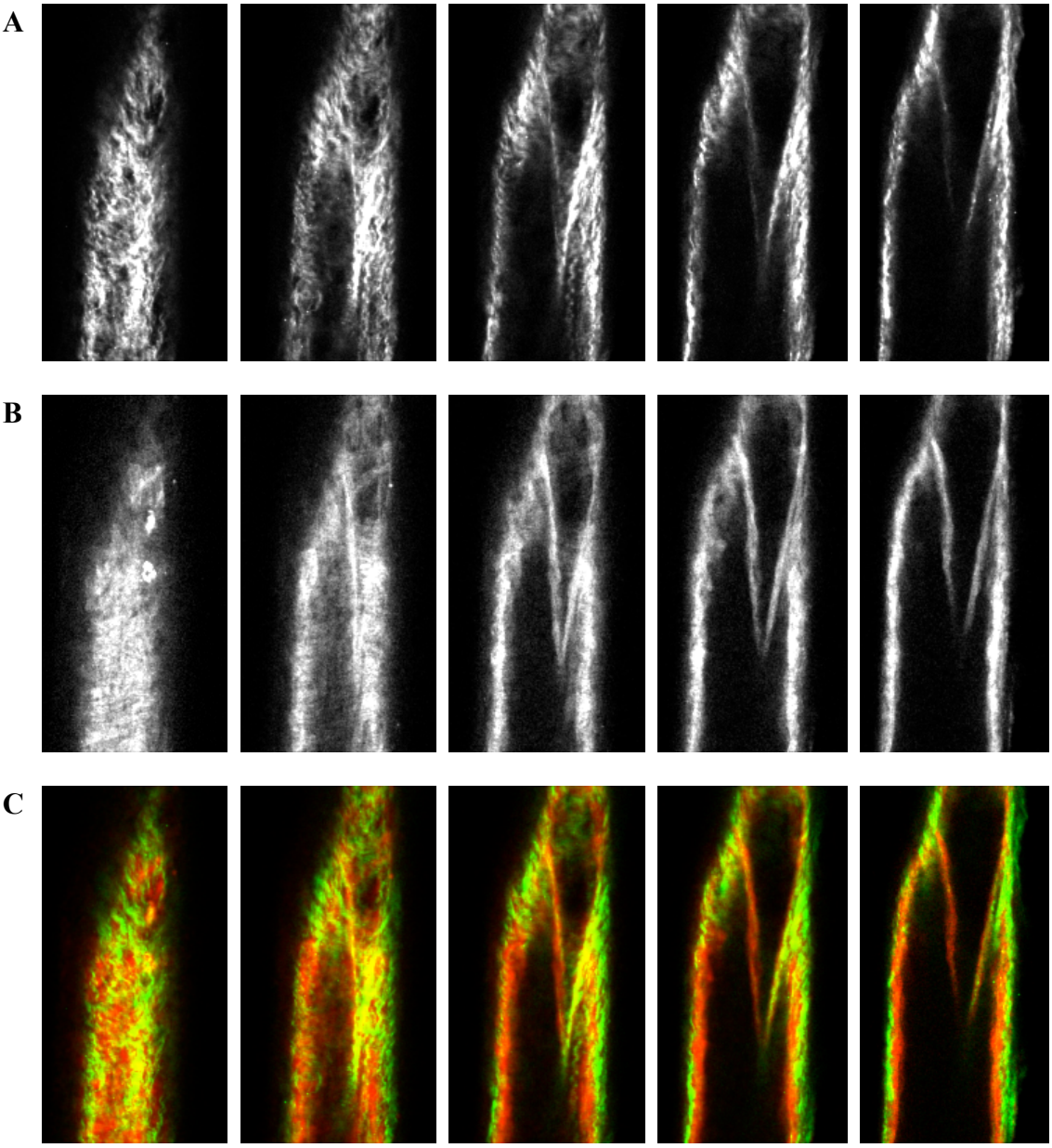

Figure 5.7. NLOM images of valve segment at high pressures. The vessel pressure fixed at 7cmH_2O was imaged at the valve. (A) SHG signal representing collagen structure, (B) TPF signal representing elastin, and (C) Overlayed images of SHG and TPF signals (Collagen in green, Elastin in red). Each slice is ~7µm apart and vessel diameter ~ 110 µm.

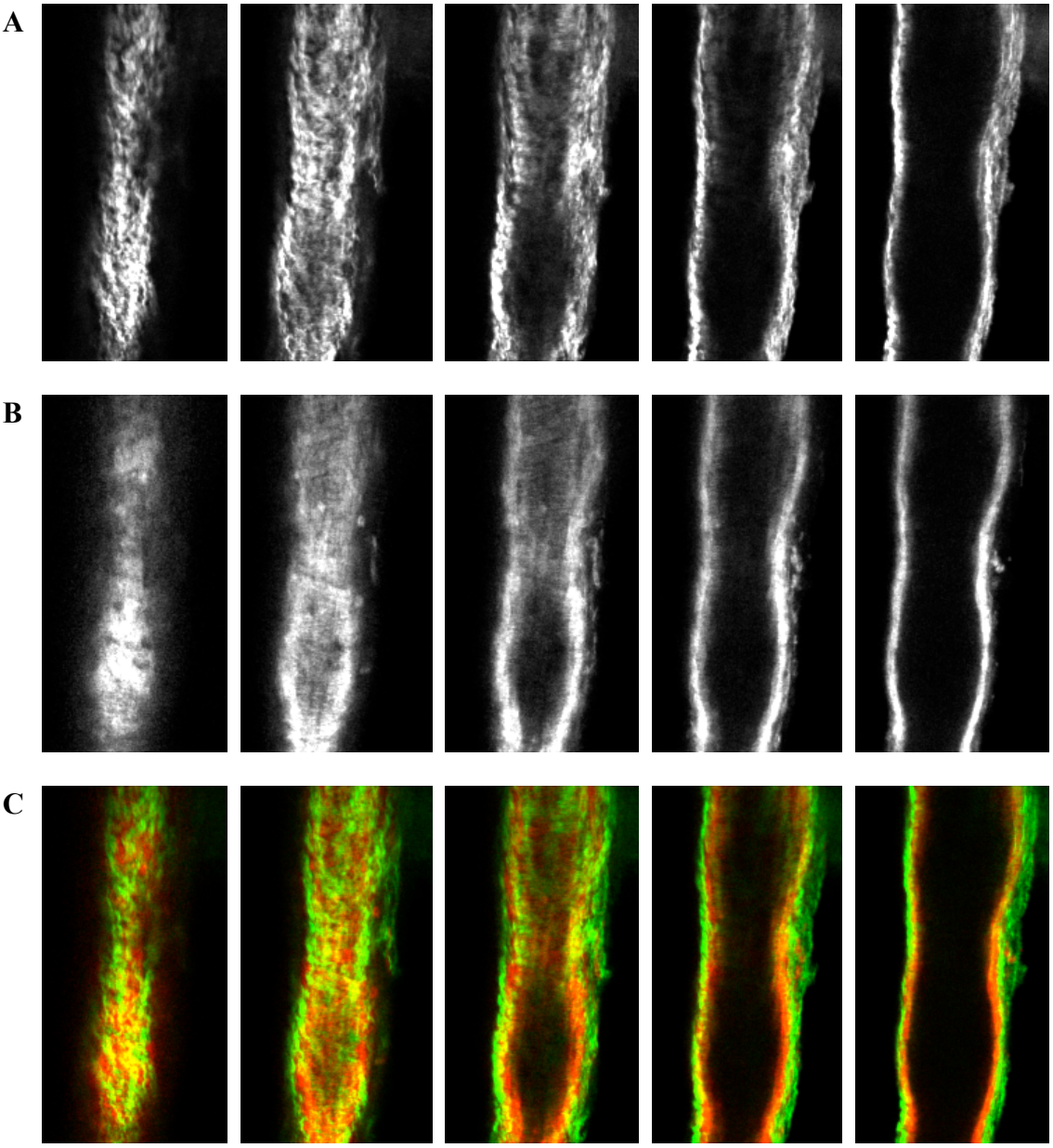

Figure 5.8. NLOM images of downstream segment at high pressures. The vessel pressure fixed at 7cmH_2O was imaged 250µm downstream of the valve. (A) SHG signal representing collagen structure, (B) TPF signal representing elastin, and (C) Overlayed images of SHG and TPF signals (Collagen in green, Elastin in red). Each slice is ~7µm apart and vessel diameter ~ 112 µm.

Discussion

Expanding our knowledge of basic mechanical characteristics of a lymphangion is essential for elucidating modes of regulation of lymph transport. There have only been a few attempts at characterizing the mechanical properties of lymphangions, where most of these have been in larger vessels (0.5-3 mm in diameter) and analysis has been more qualitative (Ohhashi et al., 1980). None have developed constitutive models or correlated the mechanics to structural components. This is mainly due to the difficulty in performing mechanical tests and histology on such small, thin-walled vessels. In this study, we successfully imaged collagen and elastin fiber structure of rat mesenteric lymphatic vessels using NLOM and performed pressure-diameter tests to develop a model characterizing the passive properties of a lymphangion.

For the first time, we showed that lymphatic valves were composed of elastin and almost devoid of collagen. Collagen was only observed in the insertion points and buttresses of the valves and the outer wall of the vessel, suggesting its role in providing structural support for the valves and vessel. The buttresses are believed to provide support to the leaflets, allowing rapid and complete closure of the valve during retrograde flow and preventing valve inversion (Mazzoni et al., 1987). Previous studies on lymphatic valve structure illustrated only an endothelial layer on the valve leaflets and no elastin (Takada, 1971, Bloom and Fawcett 1968). In fact, Skalak et al. (1984) showed that valves had collagen on both sides along with endothelial cells. Further, Albertine et al. (1982) only observed connective tissue components (i.e. collagen fibrils and fibroblasts) in canine lymphatic valves. They detected no smooth muscle cells, nerve

fibers or elastin in the valves. We believe that this may be attributed to the weakness of the methods used in these studies (e.g. histological sectioning, light microscopy, scanning electron microscopy and transmission electron microscopy) and the levels of elastin being too minute to detect. NLOM allows for the imaging of a live and/or fixed vessel without any staining and hence, is advantageous for evaluating collagen and elastin structure in fully intact lymphatic vessels. One limitation of this technique is the need to fix the vessel due to the long scanning times involved (on the order of hours).

Using blood vasculature terminology, the lymphangion wall can be described as a three-layer vessel, with an endothelial cell intimal lining, a thick elastin media layer and an adventitial layer of collagen fibers. This is in agreement with previous studies, which showed a thick, continuous elastic lamina beneath the endothelium followed by several thin layers of muscle cells within the elastic lamina (Bannykh et al., 1995). Although we did not stain smooth muscle cells in this study, numerous reports from Zawieja et al. (2011) have illustrated the circumferential distribution of smooth muscle cells within the lymphatic wall. They further report fewer smooth muscle cells in the valve sinus region compared to upstream and downstream segments (Zawieja, 2009; Zawieja et al., 2011). We, however, observed no significant changes in the average collagen or elastin layer thickness or distribution within the walls of the varying regions of the lymphangion. Based on our results, we describe lymphatic vessels as cylindrical tubes composed of an inner elastin layer and outer collagen mesh.

In addition to characterizing the structural organization of lymphatic vessels, we developed a two-parameter model for the passive mechanical response of lymphatic

vessels. Unlike previously established models for arteriole passive response (Carlson and Secomb, 2004; Carlson et al., 2008), our model incorporates a cubic term, which recovers "tube law" behavior. This is important for describing the collapsible nature of the vessel at low and negative pressures. We feel that this makes the model much more physiologic since lymphatic vessels are more prone to experience negative pressure levels than arterioles.

Our experimental results were similar to the findings of Ohhashi et al. (1980), who performed pressure-radius and pressure-volume tests on bovine mesenteric lymphatics, and observed higher distensibility at lower luminal pressures. The pressure-diameter curves suggest that normal operating pressures for a lymphatic vessel are between 0-5 cmH_2O and lymphatic vessels become "conduit-like" at pressures greater than 5 cmH_2O. This observation is consistent with the findings of Venugopal and Quick et al. (2010) who described a piecewise function for the pressure-volume relationship of a lymphangion. We believe that our model is superior in that it is a continuous function (i.e. easily differentiable) and can easily be implemented into further models investigating lymph flow.

Results from our model further illustrate that passive properties of lymphatic vessels do not significantly vary with region. This result correlates to the relatively homogenous distribution of collagen and elastin observed from the NLOM images. However, given the non-homogenous distribution of muscle cells in a lymphangion, there could be regional differences in the active response of the vessel. Assessing the effects of muscle tone on lymphatic properties would provide crucial information to

develop an active model for the autoregulation of lymph flow.

In conclusion, we developed the first two-parameter computational model characterizing the passive pressure-diameter response of a lymphatic vessel. We show that lymphatic vessels respond nonlinearly at very low pressures, unlike arterioles and venules of similar size. Additionally, lymphatic valve leaflets were shown to be composed of elastin and not collagen, for the first time. This work clearly illustrates the compliant nature of lymphatic vessels and provides a solid foundation for further lymphatic modeling. Future work includes modeling the effects of muscle tone to obtain an active and total response for lymphatic vessels.

CHAPTER VI

SUMMARY, RECOMMENDATIONS AND FUTURE DIRECTIONS

Summary

The goal of this dissertation was to characterize and investigate lymphatic behavior both experimentally and computationally. *In situ* experiments were performed to investigate the effects of edema on lymph flow and lymphatic contractility (Chapter II). Significant increases in flow rate, contraction frequency and wall shear stress were observed. These results strongly suggested the role of mechanics on the regulation of lymph flow and contractile events. Similarly, the negative results from developing neutrally buoyant particles for lymph flow visualization highlighted the effects of viscosity and the sensitivity of lymphatic vessels to altered solutions, specifically changes in protein and/or sugar concentration (Chapter III). Together, these experiments led to the development of the first 3-D computational flow model for a single lymphangion (Chapter IV). The Poiseuille assumption was validated for a complete contractile cycle, proving to be accurate within 4% mainly due to the viscous nature of lymph flow. Lastly, passive mechanical properties of lymphatic vessels were modeled and correlated with their collagen and elastin fiber structure (Chapter V). Valve leaflets were shown to be predominantly composed of elastin for the first time. In summation, these studies greatly enhanced our understanding of the lymphatic system and the role of mechanics on the regulation of lymph flow and lymphatic contractility.

Recommendations

The field of lymphatic vascular research has been understudied compared to blood vessel research. It is, therefore, of no surprise that our knowledge of the lymphatic system is extremely basic. Moreover, the delicate and dynamic nature of these vessels makes them harder to handle for experiments. In fact, the aims of this dissertation were modified due to the failed experimental design and techniques. For example, we originally wanted to develop a 3-D computational flow model using realistic lymphangion geometries. Fast scan confocal microscopy was employed to obtain stacks of dynamic lymphangion geometries. Successful acquisition was estimated at 3 stacks per second (i.e. ~300 fps) to ensure a complete dynamic stack. However, the current fast scan confocal microscope software limited the transfer time between the high speed camera and the computer, slowing down the capture time. This problem could be corrected by investing in a faster camera, computer and/or potentially writing an in-house acquisition program to minimize the delay in image acquisition.

Furthermore, the fast scan confocal microscope is capable of fast 2-D streaming which would be extremely beneficial for lymph flow measurements. Given that the polystyrene microspheres did not work well as flow tracers in isolated lymphatic vessels, efforts must be made to develop new flow particles. Based on recent in vitro studies of the microcirculation, there is a strong motivation for the use of fluorescent nanoparticles and/or quantum dots to seed APSS in isolated lymphatic vessel experiments. These fluorescent particles have the advantage of being small and yet bright allowing for easy tracking. Quantum dots, for example do not photobleach (i.e. do not lose fluorescence)

and could be easily used for time-lapse studies of lymph flow. Moreover, the use of multi-fluorescent imaging allows one to investigate various protein and/or cell signaling pathways in conjunction with observing changes in the fluid mechanical environment. There is a need for developing novel tools to facilitate lymphatic research and expand our understanding of the system. We must exploit technology to accelerate our learning curve towards the lymphatic system.

Future Directions

A common misnomer is that lymphatic disorders are rare. While this may be true in developed countries, millions of individuals suffer from pathologies that could be lymphatic based. For example, lymphatics are responsible for lipid transport, fluid transport and immune cell trafficking. Therefore, they play an important role in wound healing, inflammation, metabolic syndromes and cancer. With the prevalence of cancer and type II diabetes on the rise, I foresee a boom in lymphatics research within the next decade. In particular, efforts must be made to understand the cause for these disease pathologies, in terms of cell signaling and mechanical stimuli. Together, the field will grow in two specific areas: (1) developing computational models for the lymphatic system, and (2) developing therapeutic regimens for lymphatic disorders.

Until recently, lymphatic research has been predominantly biology and physiology based. In general, most groups investigate lymphangiogenesis, vascular development and cancer metastasis rather than studying lymph transport and mechanics. While both are important, as an engineer, I feel that characterizing the mechanics will lead to a better understanding of the lymphatic vasculature and potentially a new treatment for

edema. Lymph transport and lymphatic contractility are an exciting and new area for biomedical engineers, primarily those interested in biomechanics. The current literature has illustrated the extreme sensitivity of lymphatic vessels, ranging from 10-80 fold, to changes in pressure/stretch and shear/flow. A number of in vitro, in vivo and computational projects can be developed to investigate the role of mechanical stimuli on lymphatic vessels, which can be then implemented towards building new devices and/or therapies for lymphatic pathologies.

The results from this dissertation have provided a solid foundation for further computational analysis. We have combined basic biological experiments with fluid and solid mechanics to better characterize lymphatic function. Future work would entail developing an active model for lymphatic vessels (i.e. assessing the effects of muscle tone on lymphatic response) and extending this model to a network of lymphangions connected in series and/or in parallel. There is also a need to characterize lymphatic valve behavior. Although not included in my dissertation, I did have the opportunity to collaborate with Dr. Davis from Columbia, MO on a valve gating paper, which investigated the role of pressure in valve opening and valve closing with respect to vessel distention (Davis et al., 2011). This project was the first paper to describe lymph valve closure. We observed that valves have a normal tendency to stay open to facilitate lymph transport and close when there is a significant unfavorable pressure gradient. More investigations are necessary to develop models for valve behavior. From preliminary examination, we anticipate valve resistance to be a function of pressure and diameter (i.e. vessel distensibility).

With improved experimental techniques and implementation of new technology, novel computational models can be developed to fully characterize lymph flow throughout the network and provide insights into valve resistance and mechanisms modulating wall tension in lymphatic vessels, such as shear-induced pathways. These models will aid in developing new treatments for lymphatic pathologies; such as discovering a method to recover lymphatic function via mechanical or biochemical means. Lymphatic research is, undoubtedly, just beginning and will continue to attract the attention of new researchers in the years to come.

REFERENCES

Akl, T., Rahbar, E., Zawieja, D., Gashev, A., Moore, J., Coté, G., 2010. Fast imaging system and algorithm for monitoring microlymphatics. Optical Diagnostics and Sensing X: Toward Point-of-Care Diagnostics. In Proceedings of the SPIE 7572, 75720K-75720K-6, San Francisco, California, USA.

Albertine, K.H., Fox, L.M., O'Morchoe, C.C., 1982. The morphology of canine lymphatic valves. Anatomical Record 202, 453-461.

Aselli, G., 1627. De Lacteibus sive Lacteis Venis, Quarto Vasorum Mesarai corum Genere novo invento. Mediolani, Milano.

Azzali, G., Arcari, M.L., 2000. Ultrastructural and three dimensional aspects of the lymphatic vessels of the absorbing peripheral lymphatic apparatus in Peyer's patches of the rabbit. Anatomical Record 258, 71-79.

Bannykh, S., Mironov Jr, A., Bannykh, G., Mironov, A., 1995. The morphology of valves and valve-like structures in the canine and feline thoracic duct. Anatomy and Embryology 192, 265-274.

Barrowman, J.A., 1978. Physiology of the gastro-intestinal lymphatic system. Monographs of the Physiological Society, 9-11, 1-312.

Benoit, J., 1991 Relationships between lymphatic pump flow and total lymph flow in the small intestine. American Journal of Physiology 261, H1970-H1978.

Benoit, J.N., Zawieja, D.C., Goodman, A.H., Granger, H.J., 1989. Characterization of intact mesenteric lymphatic pump and its responsiveness to acute edemagenic stress. American Journal of Physiology 257, H2059-H2069.

Bertram, C.D., Macaskill, C., Moore, J.E., 2011. Simulation of a chain of collapsible contracting lymphangions with progressive valve closure. Journal of Biomechanical Engineering 133, 011008.

Blyth, M., Hall, P., Papageorgiou, D., 2003. Chaotic flows in pulsating cylindrical tubes: A class of exact Navier-Stokes solutions. Journal of Fluid Mechanics 481, 187-213.

Bohlen, H.G., Wang, W., Gashev, A., Gasheva, O., Zawieja, D., 2009. Phasic contractions of rat mesenteric lymphatics increase basal and phasic nitric oxide generation in vivo. American Journal of Physiology-Heart and Circulatory Physiology 297, H1319-H1328.

Bond, J.H., Levitt, M.D., 1979. Use of microspheres to measure small intestinal villus blood flow in the dog. American Journal of Physiology 236, E577-E583.

Briers, J.D., 2001. Laser Doppler, speckle and related techniques for blood perfusion mapping and imaging. Physiological Measurement 22, R35-R66.

Brown, P., 2005. Lymphatic system: Unlocking the drains. Nature 436, 456-458.

Carlson, B.E., Arciero, J.C., Secomb, T.W., 2008. Theoretical model of blood flow autoregulation: Roles of myogenic, shear-dependent, and metabolic responses. American Journal of Physiology-Heart and Circulatory Physiology 295, H1572-H1579.

Carlson, B.E., Secomb, T.W., 2005. A theoretical model for the myogenic response based on the length-tension characteristics of vascular smooth muscle. Microcirculation 12, 327-338.

Casley-Smith, J.R., 1968. How the lymphatic system works. Lymphology 1, 77-80.

Casley-Smith, J.R., 1972. The role of the endothelial intercellular junctions in the functioning of the initial lymphatics. Angiologica 9, 106 –131.

Casley-Smith, J.R., Florey, H.W., 1961. The structure of normal small lymphatics. Quarterly Journal of Experimental Physiology and Cognate Medical Sciences 46, 101-106.

Chakraborty, S., Zawieja, S., Wang, W., Zawieja, D.C., Muthuchamy, M., 2010. Lymphatic system: A vital link between metabolic syndrome and inflammation. Annals of the New York Academy of Sciences 1207, E94-E102.

Cox Jr, C.S., Radhakrishnan, R., Villarrubia, L., Xue, H., Uray, K., Gill, B.S., Stewart, R. H., Laine, G. A., 2008. Hypertonic saline modulation of intestinal tissue stress and fluid balance. Shock 29, 598-602.

Davis, M.J., 2005. An improved, computer-based method to automatically track internal and external diameter of isolated microvessels. Microcirculation 12, 361-372.

Davis, M.J., Rahbar, E., Gashev, A.A., Zawieja, D.C., Moore, J.E., 2011. Determinants of valve gating in collecting lymphatic vessels from rat mesentery. American Journal of Physiology -Heart and Circulatory Physiology , accepted March 29, 2011.

Dixon, J.B., Greiner, S.T., Gashev, A.A., Cote, G.L., Moore, J.E., Zawieja, D.C., 2006. Lymph flow, shear stress, and lymphocyte velocity in rat mesenteric prenodal lymphatics. Microcirculation 13, 597-610.

Duling, B.R., Gore, R.W., Dacey Jr, R.G., Damon, D.N., 1981. Methods for isolation, cannulation, and in vitro study of single microvessels. American Journal of Physiology 241, H108-H116.

Elias, R.M., Wandolo, G., Ranadive, N.S., Eisenhoffer, J., Johnston M.G., 1990. Lymphatic pumping in response to changes in transmural pressure is modulated by erythrolysate/hemoglobin. Circulation Research 67, 1097-1106.

Galie, P., Spilker, R.L., 2009. A two-dimensional computational model of lymph transport across primary lymphatic valves. Journal of Biomechanical Engineering 131, 111004.

Gashev, A.A., 2002. Physiologic aspects of lymphatic contractile function: Current perspectives. Annals of the New York Academy of Sciences 979, 178-196.

Gashev, A.A., 2008. Lymphatic vessels: Pressure- and flow-dependent regulatory reactions. Annals of the New York Academy of Sciences 1131, 100-109.

Gashev, A.A., Davis, M.J., Zawieja, D.C., 2002. Inhibition of the active lymph pump by flow in rat mesenteric lymphatics and thoracic duct. Journal of Physiology 540, 1023-1037.

Gashev, A.A., Davis, M.J., Delp, M.D., Zawieja, D.C., 2004. Regional variations of contractile activity in isolated rat lymphatics. Microcirculation 11, 477-492.

Gashev, A.A., Wang, W., Laine, G.A., Stewart, R.H., Zawieja, D.C., 2007. Characteristics of the active lymph pump in bovine prenodal mesenteric lymphatics. Lymphatic Research and Biology 5, 71-79.

Gasheva, O.Y., Zawieja, D.C., Gashev, A.A., 2006. Contraction-initiated NO-dependent lymphatic relaxation: A self-regulatory mechanism in rat thoracic duct. Journal of Physiology 575, 821-832.

Grotberg, J., Jensen, O., 2004. Biofluid mechanics in flexible tubes. Annual Review of Fluid Mechanics 36, 121-147.

Hagendoorn, J., Padera, T.P., Kashiwagi, S., Isaka, N., Noda, F., Lin, M.I., Huang, P.L., Sessa, W.C., Fukumura, D., Jain, R.K., 2004. Endothelial nitric oxide synthase regulates microlymphatic flow via collecting lymphatics. Circulation Research 95, 204-209.

Humeau, A., Steenbergen, W., Nilsson, H., Strömberg, T., 2007. Laser Doppler perfusion monitoring and imaging: Novel approaches. Medical & Biological Engineering & Computing 45, 421-435.

Hunter, J., 1837 Experiments on absorption by veins. In: Palmer, J.F. (Ed.), The works of John Hunter Volume 4. Longman, London, pp. 299-314.

Huntington, G.S., McClure, C.F.W., 1910. The anatomy and development of the jugular lymph sac in the domestic cat (Felis domestica). American Journal of Anatomy 10, 177–311.

Johnson, G.A., Borovetz, H.S., Anderson, J.L., 1992. A model of pulsatile flow in a uniform deformable vessel. Journal of Biomechanics 25, 91-100.

Karri, S., Vlachos, P.P., 2010. Time-resolved DPIV investigation of pulsatile flow in symmetric stenotic arteries-effects of phase angle. Journal of Biomechanical Engineering 132, 031010.

Katz, M., Blantz, R., Rector, F., Seldin, D., 1971. Measurement of intrarenal blood flow 1. Analysis of microsphere method. American Journal of Physiology 220, 1903-1913.

Kim, G.B., Lim, N.Y., Lee, S.J., 2009. Hollow microcapsules for sensing micro-scale flow motion in x-ray imaging method. Microfluidics and Nanofluidics 6, 419-424.

Kowallik, P., Schulz, R., Guth, B.D., Schade, A., Paffhausen, W., Gross, R., Heusch, G., 1991. Measurement of regional myocardial blood flow with multiple colored microspheres. Circulation 83, 974-982.

Kwon, S., Sevick-Muraca, E.M., 2007. Noninvasive quantitative imaging of lymph function in mice. Lymphatic Research and Biology 5, 219-231.

Larson, A.M., Yeh, A.T., 2006. Ex vivo characterization of sub-10-fs pulses. Optics Letters 31, 1681-1683.

Levick, J.R., 2003. Circulation of fluid between plasma, interstitium and lymph. In: Levick, J.R. (Ed.) An introduction to cardiovascular physiology 4th edition, Hodder Arnold, London, pp.171-198.

Lynn, C.N., Ahmed, J., 2006. A technique for tracking intravascular fluorescent microspheres for the determination of arteriolar blood flow in rats. Biomedical Sciences Instrumentation 42, 90-95.

Macdonald, A.J., Arkill, K.P., Tabor, G.R., McHale, N.G., Winlove, C.P., 2008. Modeling flow in collecting lymphatic vessels: One-dimensional flow through a

series of contractile elements. American Journal of Physiology-Heart and Circulatory Physiology 295, H305-H313.

Mazzoni, M.C., Skalak, T.C., Schmid-Schönbein, G.W., 1987. Structure of lymphatic valves in the spinotrapezius muscle of the rat. Blood Vessels 24, 304-312.

Mendoza, E., Schmid-Schonbein, G., 2003. A model for mechanics of primary lymphatic valves. Journal of Biomechanical Engineering-Transactions of the ASME 125, 407-414.

Modi, S., Stanton, A.W.B., Mortimer, P.S., Levick, J.R., 2007. Clinical assessment of human lymph flow using removal rate constants of interstitial macromolecules: A critical review of lymphoscintigraphy. Lymphatic Research and Biology 5, 183-202.

Moriguchi, P., Sannomiya, P., Lara, P.F., Oliveira-Filho, R.M., Greco, K.V., Sudo-Hayashi, L.S., 2005. Lymphatic system changes in diabetes mellitus: role of insulin and hyperglycemia. Diabetes/Metabolism Research and Reviews 21, 150-157.

Negrini, D., Fabbro, M.D., 1999. Subatmospheric pressure in the rabbit pleural lymphatic network. Journal of Physiology 520, 761–769.

Negrini, D., Ballard, S.T., Benoit J.N., 1994. Contribution of lymphatic myogenic activity and respiratory movements to pleural lymph flow. Journal of Applied Physiology 76, 2267 –2274.

Negrini, D., Moriondo, A., Mukenge, S., 2004. Transmural pressure during cardiogenic oscillations in rodent diaphragmatic lymphatic vessels. Lymphatic Research and Biology 2, 69–81.

Nohl-Oser, H.C., 1972. An investigation of the anatomy of the lymphatic drainage of the

lungs as shown by the lymphatic spread of bronchial carcinoma. Annals of the Royal College of Surgeons of England 51, 157-176.

Ohhashi, T., Azuma, T., Sakaguchi, M., 1980. Active and passive mechanical characteristics of bovine mesenteric lymphatics. American Journal of Physiology 239, H88-H95.

Oliver, G., 2004. Lymphatic vasculature development. Nature Reviews Immunology 4, 35-45.

Oliver, G., Alitalo, K., 2005. The lymphatic vasculature: Recent progress and paradigms. Annual Review of Cell and Developmental Biology 21, 457-483.

Olszewski, WL., 2002. Contractility patterns of normal and pathologically changed human lymphatics. Annals of the New York Academy of Sciences 979, 52-63.

Pries, A., Secomb, T., 2002. Structural adaptation of microvascular networks and development of hypertension. Microcirculation 9, 305-314.

Quick, C.M., Ngo, B.L., Venugopal, A.M., Stewart, R.H., 2009. Lymphatic pump-conduit duality: Contraction of postnodal lymphatic vessels inhibits passive flow. American Journal of Physiology-Heart and Circulatory Physiology 296, H662-H668.

Quick, C.M., Venugopal, A.M., Gashev, A.A., Zawieja, D.C., Stewart, R.H., 2007. Intrinsic pump-conduit behavior of lymphangions. American Journal of Physiology-Regulatory, Integrative and Comparative Physiology 292, R1510-R1518.

Rahbar, E., Moore, J.E., 2011. A model of a radially expanding and contracting lymphangion. Journal of Biomechanics 44, 1001-1007.

Rasmussen, J.C., Tan, I., Marshall, M.V., Adams, K.E., Kwon, S., Fife, C.E., Maus, E.A., Smith, L.A., Covington, K.R., Sevick-Muraca, E.M., 2010. Human lymphatic architecture and dynamic transport imaged using near-infrared fluorescence. Translational Oncology 3, 362-372.

Reddy, N., Krouskop, T., Newell, P., 1975. Biomechanics of a lymphatic vessel. Blood Vessels 12, 261-278.

Reddy, N.P., Krouskop, T.A., Newell Jr, P.H., 1977. A computer model of the lymphatic system. Computers in Biology and Medicine 7, 181-197.

Reed, R.K., Wiig, H., 1983. Interstitial albumin mass and transcapillary extravasation rate of albumin in DMBA-induced rat mammary tumours. Scandinavian Journal of Clinical & Laboratory Investigation 43, 503-512.

Renkin E.M., 1986. Some consequences of capillary permeability to macromolecules: Starling's hypothesis reconsidered. American Journal of Physiology 250, H706–H710.

Roberts, B.W., Olbricht, W.L., 2006. The distribution of freely suspended particles at microfluidic bifurcations. AIChE Journal 52, 199-206.

Rockson S.G., 2006. Addressing the unmet needs in lymphedema risk management. Lymphatic Research and Biology 4, 42-46.

Rockson, S.G., 2008. Diagnosis and management of lymphatic vascular disease. Journal of the American College of Cardiology 52, 799-806.

Rockson S.G., 2010. Causes and consequences of lymphatic disease. Annals of the New York Academy of Sciences 1207, E2-E6.

Sabin, F.R., 1902. On the origin of the lymphatic system from the veins, and the development of the lymph hearts and thoracic duct in the pig. American Journal of Anatomy 1, 367–389.

Sabin, F.R., 1904. On the development of the superficial lymphatic's in the skin of the pig. American Journal of Anatomy 3, 183–195.

Sabin, F.R., 1913. The origin and development of the lymphatic system. Johns Hopkins Press, Maryland, pp. 1-94.

Schmid-Schönbein G.W., 1990. Mechanisms causing initial lymphatics to expand and compress to promote lymph flow. Archives of Histology and Cytology 53, 107-114.

Semaeva, E., Tenstad, O., Skavland, J., Enger, M., Iversen, P.O., Gjertsen, B.T., Wiig, H., 2010. Access to the spleen microenvironment through lymph shows local cytokine production, increased cell flux, and altered signaling of immune cells during lipopolysaccharide-induced acute inflammation. Journal of Immunology 184, 4547-4556.

Sharma, R., Wendt, J.A., Rasmussen, J.C., Adams, K.E., Marshall, M.V., Sevick-Muraca, E.M., 2008. New horizons for imaging lymphatic function. Annals of the New York Academy of Sciences 1131, 13-36.

Skalak, T., Schmid-Schonbein, G., Zweifach, B., 1984. New morphological evidence for a mechanism of lymph formation in skeletal muscle. Microvascular Research 28, 95-112.

Stanton A.W.B., Modi S., Mellor R.H., Levick J.R., Mortimer P.S., 2009. Recent advances in breast cancer-related lymphedema of the arm: Lymphatic pump failure and predisposing factors. Lymphatic Research and Biology 7, 29-45.

Stewart, R.H., Laine, G.A., 2001. Flow in lymphatic networks: Interaction between hepatic and intestinal lymph vessels. Microcirculation 8, 221-227.

Szuba, A., Rockson, S.G., 1998. Lymphedema: Classification, diagnosis and therapy. Vascular Medicine 3, 145-156.

Tsai, A.G., Acero, C., Nance, P.R., Cabrales, P., Frangos, J.A., Buerk, D.G., Intaglietta, M., 2005. Elevated plasma viscosity in extreme hemodilution increases perivascular nitric oxide concentration and microvascular perfusion. American Journal of Physiology -Heart and Circulatory Physiology 288, H1730-H1739.

Uchida, S., Aoki, H., 1977. Unsteady flows in a semi-infinite contracting or expanding pipe. Journal of Fluid Mechanics 82, 371-387.

Venugopal, A.M., Quick, C.M., Laine, G.A., Stewart, R.H., 2009. Optimal postnodal lymphatic network structure that maximizes active propulsion of lymph. American Journal of Physiology -Heart and Circulatory Physiology 296, H303-H309.

Venugopal, A.M., Stewart, R.H., Laine, G.A., Quick, C.M., 2010. Nonlinear lymphangion pressure-volume relationship minimizes edema. American Journal of Physiology-Heart and Circulatory Physiology 299, H876-H882.

Venugopal, A.M., Stewart, R.H., Laine, G.A., Dongaonkar, R.M., Quick, C.M., 2007. Lymphangion coordination minimally affects mean flow in lymphatic vessels.

American Journal of Physiology-Heart and Circulatory Physiology 293, H1183-H1189.

Wang, L., Fortune, B., Cull, G., McElwain, K.M., Cioffi, G.A., 2007. Microspheres method for ocular blood flow measurement in rats: Size and dose optimization. Experimental Eye Research 84, 108-117.

Yoffey, J.M., Courtice, F.C., 1970. Lymphatics, lymph and the lymphomyeloid complex. Academic Press, London, pp. 1-942.

Zawieja, D.C., 2009. Contractile physiology of lymphatics. In Proceedings of a Mini-symposium: Lymphedema: An overview of the biology, diagnosis, and treatment of the disease. Lymphatic Research and Biology 7, 87-96.

Zawieja, D.C., von der Weid, P.Y., Gashev, A.A., 2011. Microlymphatic Biology. In: Comprehensive Physiology. John Wiley & Sons, New Jersey, 125–158.

Zawieja, D.C., Davis, K.L., Schuster, R., Hinds, W.M., Granger, H.J., 1993. Distribution, propagation, and coordination of contractile activity in lymphatics. American Journal of Physiology 264, H1283-H1291.

Zhou, S., Wang, S., Wu, Q., Fan, J., Wang, Q., 2008. Expression of glucose transporter-1 and -3 in the head and neck carcinoma--the correlation of the expression with the biological behaviors. Journal for Oto-Rhino-Laryngology and Its Related Specialties 70, 189-194.

Zulliger, M.A., Fridez, P., Hayashi, K., Stergiopulos, N., 2004. A strain energy function for arteries accounting for wall composition and structure. Journal of Biomechanics 37, 989-1000.

Zweifach, B.W., Intaglietta, M., 1968. Mechanics of fluid movement across single capillaries in the rabbit. Microvascular Research 1, 83-101.

VITA

Elaheh Rahbar received her Bachelor of Science degree in Materials Science and Engineering from Michigan State University in 2006. She entered the biomedical engineering department at Texas A&M University in August 2006 and received her Doctor of Philosophy degree in August 2011. Her research interests include biofluid mechanics, lymph transport and lymphatic disorders. Ms. Rahbar may be reached at Department of Biomedical Engineering, 5045 Emerging Technologies & Economic Development, 3120 TAMU, College Station, TX 77843-3120. Her email is rahbarel@tamu.edu.